THE DURABILITY OF CONCRETE USING CONCRETE PLANT WASH WATER

by

Khanh An Tran

A thesis
presented to the University of Waterloo
in fulfillment of the
thesis requirement for the degree of
Master of Applied Science
in
Civil Engineering

Waterloo, Ontario, Canada, 2007

AUTHOR'S DECLARATION

I hereby declare that I am the sole author of this thesis. This is a true copy of the thesis, including any required final revisions, as accepted by my examiners.

I understand that my thesis may be made electronically available to the public.

ABSTRACT

Hundreds of ready-mix concrete trucks are dispatched daily from ready-mix concrete plants. On average, a concrete truck has a carrying capacity ranging from 7 to 9 cubic metres of concrete, requiring about 1500 litres of water. In addition, 500 to 1300 litres of water are used to wash out the excess concrete when the truck returns. Based on these figures, it is clear that the ready-mixed concrete industry consumes large amounts of fresh water.

The purpose of this study is to determine the feasibility of using the wash water as mixing water in new concrete. The specific goal of this project is to determine the influence of the high pH and dissolved solids content of the wash water on the durability of concrete, particularly in regard to de-icing salt induced corrosion of steel reinforcement. Two types of mix designs were used in this research: a standard class N and a higher strength, structural C2 concrete. Two sets of concrete specimens were made with both mix designs: one with wash water and one with clean water. The project consists of a multi-component experimental program, beginning with wash water characterization, then pore solution and cement chemistry, followed by an evaluation of the effect of wash water on concrete workability and mechanical properties, resistance to de-icing salt scaling, and corrosion of reinforcing steel embedded in the concrete. In addition, the effect of the wash water on the effectiveness of air entraining agents (AEA) was determined using air void analysis of specimens with different AEA contents.

On the basis of the results obtained from the comparative study using wash water versus tap water, it appears that wash water can be used as mixing water for the production of concrete without compromising the durability properties related to corrosion and salt scaling performance. In addition, the mechanical and plastic properties of wash water concrete meet all standards pertaining to the use of wash water concrete and are similar to those of tap water concrete. Finally, the pore solution, thermal analyses, and water analyses of wash water and tap water showed comparable results. Overall, with regards to the tests conducted thus far, the use of wash water as mixing water in concrete poses no durability concerns.

ACKNOWLEDGEMENTS

This thesis is dedicated to my parents

who sacrificed everything for their children's education

and

those who believed in me through times when I doubted myself.

TABLE OF CONTENTS

LIST OF APENDICES

LIST OF FIGURES

LIST OF TABLES

CHAPTER 1
INTRODUCTION

1.1 GENERAL

Concrete is the most widely used construction material in the world (Mehta et al., 1993). When compared to other common construction materials such as wood and steel, which are susceptible to rotting, corrosion, or fire damage, concrete excels for its durability under hostile conditions. In addition to having excellent intrinsic properties such as durability and water resistance, concrete is relatively inexpensive and can be formed into various shapes at ambient temperature, which adds to its appeal as the ideal construction material (Hansson, 1995).

Globally, it is estimated that, in 2000, over 12.6 billion tons of concrete is consumed annually (Mehta, 2002) and this number continues to increase. Water, which is one of the components used to make concrete, constitutes 14% to 21% of the volume of concrete (Kosmatka et al., 2002). Putting these numbers in perspective, roughly 1 billion cubic metres of water are consumed by the concrete industry each year. This is enough to supply water to all Canadians for a third of a year based on a "Canadians and Water Consumption" report (Region of Peel, 2001). Although concrete is considered by many as an environmentally friendly material, its sheer consumption makes the ready-mix concrete industry the biggest consumer of natural resources in the world (Mehta and Mammohan, 2005).

Water is one of the most abundant natural resources available on this planet. It is generally thought that water covers two-third of the Earth's surface. However, of all the available water, only 3% of it is fresh water and 99.9% of that is unusable for various reasons (Gleick, 1996).

1

This leaves only 0.1% of water as useable fresh water for human consumption, as shown in Figure 1.1.
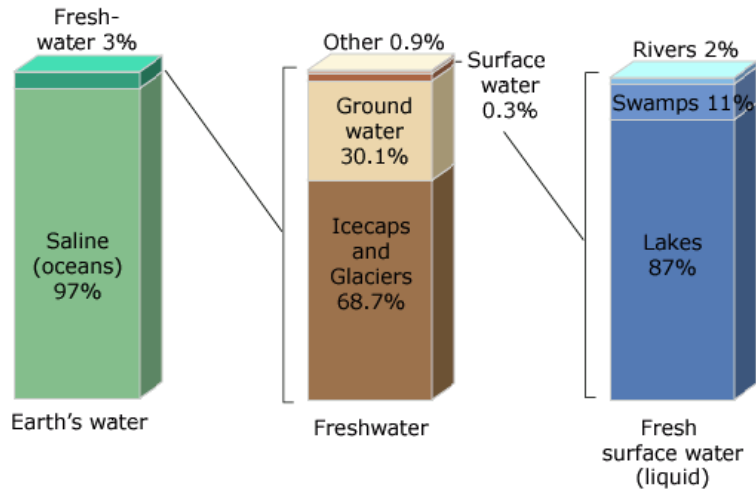
Figure 1.1: Distribution of Earth's water (USGS, 2007)

Currently, water shortage around the world is a growing crisis. In 2005, it was estimated that approximately 500 million people living on this planet were short of water, and the number is expected to reach 3 billion by 2025 (Malhotra, 2005). Since the supply of natural resources is limited, (Sakai, 2005), it is vital that sustainable development is promoted in order for future generations to survive.

In addition to the water used in the production of concrete, each truckload of concrete requires thorough rinsing to remove the remaining concrete upon return, generating a vast amount of wash water. More specifically, wash water refers to the water accumulated after equipment cleaning, particularly the washing out of residue concrete from the inside of a truck drum. The production of a typical truck load of 9 cubic metres of concrete with a water-cement ratio of 0.45 requires as much as 1000 to 1500 litres of water. In addition, 500 to 1300 litres of water are used to wash out the remaining concrete (Sandrolini and Franzoni, 2001). Wash water cannot be disposed in most municipal wastewater systems because of its high alkalinity, particulate content and possible presence of chemical admixtures. In many ready-mix concrete plants, wash water is

stored in reservoir tanks or pits, allowing the particulates to settle and the pH level to decrease to safe levels. It can then be discharged back into the municipal waste water system (Paolini et al., 1998). However, this method is not cost effective, nor is it environmentally friendly. In most urban centres, the government has made wash water disposal even more difficult due to stringent regulations limiting the use of fresh water and concerning the quality of the water that is treated before returning to the water system (Water and Wastewater Report, 2005). The idea of recycling wash water to use in the production of new concrete, thus, seems to be an attractive idea from both economical and environmental perspectives.

1.2 OBJECTIVES

Currently, wash water concrete reuse is limited to relatively low strength concrete without air entraining admixture. The use of wash water in structural reinforced concrete is generally ignored due to the lack of research regarding the durability of wash water concrete and the effect it has on steel reinforcement (Borger et al., 1994; Sandrolini and Franzoni, 2001; Su et al. 2002). Most of the existing research focuses primarily on fresh properties and strength of concrete and the long-term durability is generally ignored. Consequently, the overall objective of this research is to learn more about the effects of wash water on the durability of concrete, emphasizing the corrosion of reinforcing steel, surface scaling due to freeze-thaw damage, and plastic and hardened concrete properties.

1.3 THESIS ARRANGEMENT

Chapter 2 provides background information pertinent to concrete durability, cement chemistry and research to date on the use of wash water. Chapter 3 describes the experimental program used for this project. Chapter 4 presents the results and the discussion of the study. The applications of the findings are presented in Chapter 5. Chapter 6 presents the summary, conclusions and recommendations for further work.

CHAPTER 2

BACKGROUND AND LITERATURE REVIEW

2.1 GENERAL

Concrete durability is defined as the ability to resist weathering action, abrasion, and other deterioration mechanisms while maintaining its original form or serviceable condition (ACI 201, 2001). The most common forms of concrete deterioration are: corrosion of reinforcing steel, freezing and thawing damage, alkali-aggregate reactions, and sulphate attack. These deterioration mechanisms can lead to concrete cracking, spalling, surface scaling, and possibly premature failure. Often, these forms of deterioration can be prevented or minimized if proper concrete design, with regards to durability, is considered. The goal of this chapter is to provide the reader with enough background information on the durability design of concrete to understand the significance of the experimental program and the test results.

2.2 DURABILITY DESIGN OF CONCRETE

Concrete is a highly heterogeneous material by nature. Most other construction materials contain only a few constituents, but modern concrete has many components. The quality and performance of concrete depends on many factors, from the chemistry of the cement to the proportioning of the ingredients and the chemical admixtures used. All of these will influence the performance and durability of concrete.

2.2.1 Cement Chemistry

Concrete is a composite material comprising of cement paste and aggregate. The cement paste is produced from mixing cement with water and typically occupies about 25 to 40% of the concrete by volume. Sand and gravel, or crushed stone, are the most commonly used aggregates, and are categorized into either fine or coarse aggregate as shown in Figure 2.1. Aggregates greater than

4

4.75 mm are classified as coarse and aggregates less than 4.75 mm are classified as fine (CSA A23.1-04, 2004).
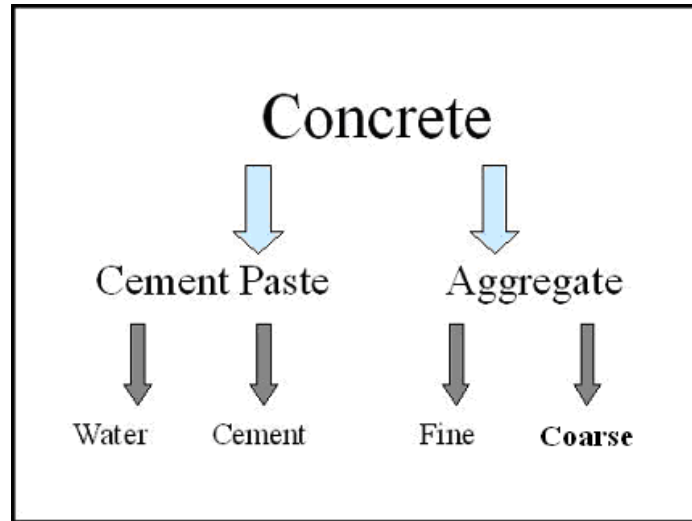
Figure 2.1: The make-up of concrete

2.2.1.1 Chemical Composition of Cement

Modern portland cement contains four major components: tricalcium silicate (C_3S), dicalcium silicate (C_2S), tricalcium aluminate (C_3A), and tetracalcium aluminoferrite (C_4AF). The composition of portland cement is based on the work of Bogue (Bogue, 1955), which estimates the weight percentages of the compositions based on CaO, SiO_2, Al_2O_3, Fe_2O_3, and SO_3 components as shown in Equation 2.1 to Equation 2.4. Table 2.1 summarized the compositions, notations, and weight distribution.

$$C_3S = 4.07(CaO) - 7.60(SiO_2) - 6.72(Al_2O_3) - 1.43(Fe_2O_3) - 2.85(SO_3)$$

Equation 2.1

$$C_2S = 8.60(SiO_2) + 5.07(Al_2O_3) + 1.1(Fe_2O_3) - 3.07(CaO)$$

Equation 2.2

$$C_3A = 2.65(Al_2O_3) - 1.69(Fe_2O_3)$$

Equation 2.3

$$C_4AF = 3.04(Fe_2O_3)$$

Equation 2.4

Table 2.1: General use portland cement compositions (ACI 225R-99, 1999)

	Chemical Formula	Shorthand Notation	Wt. %
1) Tricalcium silicate	$3CaO \cdot SiO_2$	C_3S	40-63
2) Dicalcium silicate	$2CaO \cdot SiO_2$	C_2S	9-31
3) Tricalcium aluminate	$3CaO \cdot Al_2O_3$	C_3A	6-14
4) tetracalcium aluminoferrite	$4CaO \cdot Al_2O_3 \cdot Fe_2O_3$	C_4AF	5-13

In addition to the four major compounds, there are other oxides present in cement from the manufacturing process, such as, MgO, TiO_2, Mn_2O_3, K_2O, and Na_2O (ACI 225R-99, 1999). Out of these oxides, K_2O and Na_2O are of the greatest impact because they result in a cement paste pore solution with a pH greater than 13, which allows a stable passive film to form on steel. However, they can trigger alkali-aggregate reaction (AAR). The total alkali metal oxide content is often expressed as the Na_2O equivalent, shown in Equation 2.5, and is limited to less than 1.8 kg/m^3 for concrete used in area that is at risk of AAR attack (CSA A23.2-27A, 2004).

$$Na_2O \ Equivalent = Na_2O + 0.658K_2O \qquad \text{Equation 2.5}$$

When cement mixes with water, C_3S and C_2S react to form calcium silicate hydrate gel (C-S-H = $CaO \cdot SiO_2 \cdot 4H_2O$), which is primarily responsible for strength development. C_3A is largely responsible for setting of concrete and the degree of heat generated within in the first few days and may cause premature stiffening without significant strength development (ACI 225R-99, 1999). C_4AF reacts very similar to C_3A except it produces less heat of hydration and does not cause premature stiffening (Mindess et al., 1981). Both C_3A and C_4AF are by-products of the industry's desire to reduce the cost of manufacturing cement, and their presence in cement is generally undesirable. The formation and hydration steps for portland cement are summarized in Figure 2.2.

COMPONENT ELEMENTS

O$_2$	Si	Ca	Al	Fe

CEMENT COMPONENT OXIDES

COMPONENT OXIDES

CaO	SiO$_2$	Al$_2$O$_3$	Fe$_2$O$_3$	SO$_3$

CEMENT COMPOUNDS

C$_3$S	C$_2$S	C$_3$A	C$_4$AF

PORTLAND CEMENTS

Different types of portland cement

HYDRATION PRODUCTS

Gel	Ca(OH)$_2$
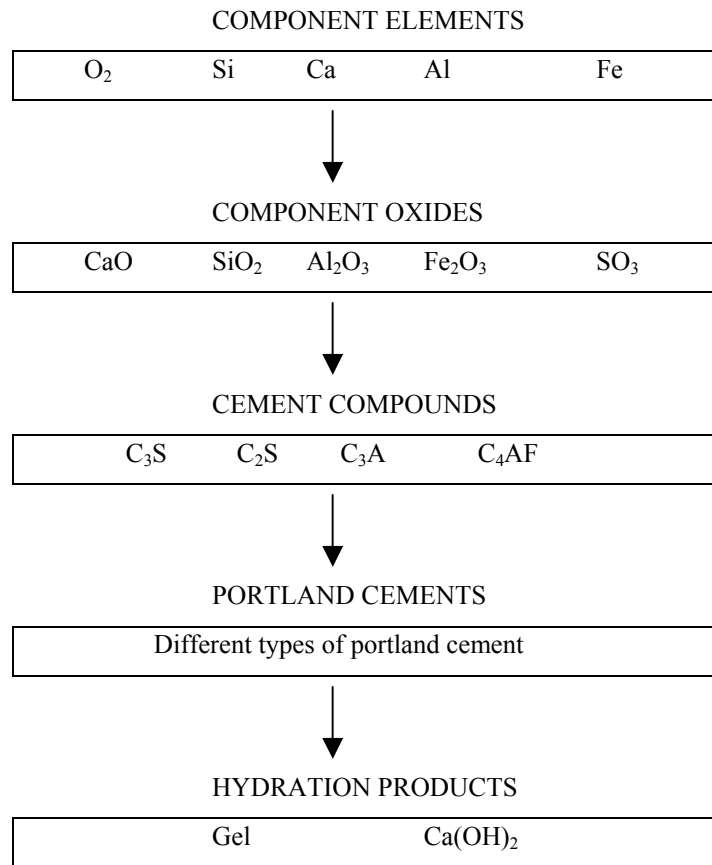
Figure 2.2: Formation and hydration of portland cement (Neville, 1981)

2.2.1.2 Cement Hydration

The hydration of cement is initiated by the presence of water. The role of cement hydration is to bind aggregates together to produce concrete. The two calcium silicates provide the driving force behind the hardening and strength development of cement and their chemical hydration reactions are shown in Equation 2.6 and Equation 2.7 (Brown, 2006).

$$3CaO \cdot SiO_2 + 5.3H_2O \rightarrow 1.7CaO \cdot SiO_2 \cdot 4H_2O + 1.3Ca(OH)_2 \qquad \text{Equation 2.6}$$

$$\quad (C_3S) \qquad (H) \qquad\qquad (C\text{-}S\text{-}H) \qquad\quad (CH)$$

$$2CaO \cdot SiO_2 + 4.3H_2O \rightarrow 1.7CaO \cdot SiO_2 \cdot 4H_2O + 0.3Ca(OH)_2 \qquad \text{Equation 2.7}$$

$$\quad (C_2S) \qquad (H) \qquad\qquad (C\text{-}S\text{-}H) \qquad\quad (CH)$$
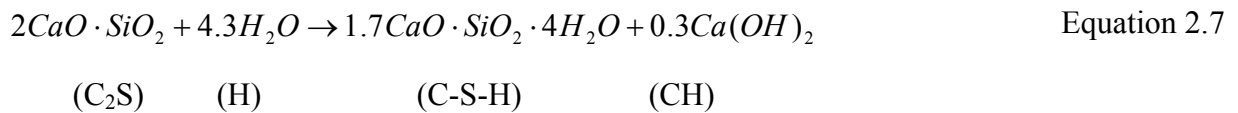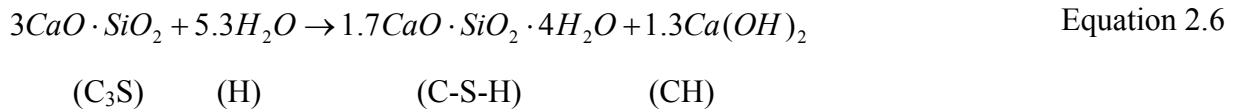
The rate of hydration of C_3S and C_2S are not equivalent, because C_3S hydration is believed to be primarily controlled by diffusion whereas the C_2S hydration is believed to be controlled by slow intrinsic reactivity (Lea, 1960). A graph of the hydration rates of major cement components can be seen in Figure 2.3. In fact, the hydration rates of the components are not linear with respect to time but rather appear to resemble a square root function. This indicates that complete hydration can, in fact, take years to achieve.
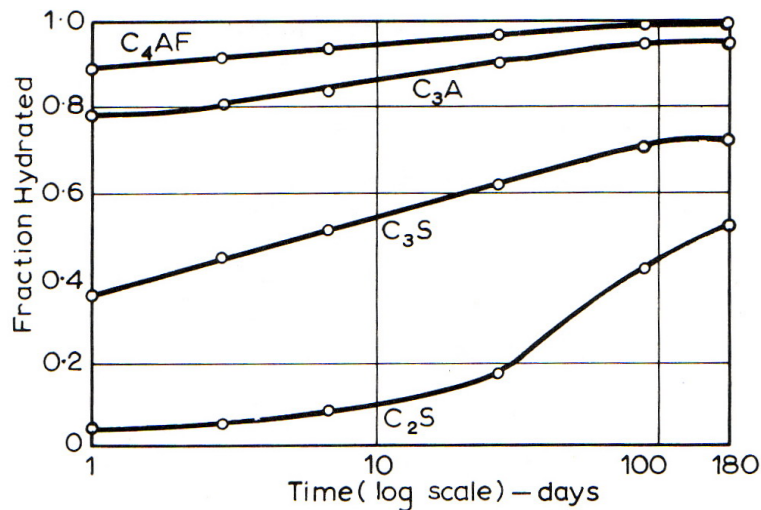
Figure 2.3: Rates of hydration of major cement components (Copeland and Bragg, 1953)

The hydration of C_3A occurs very quickly to produce calcium aluminate hydrate (C-A-H), thus leading to the rapid heat of hydration. The process consumes water quickly and can often lead to flash set, which is undesirable. Gypsum, a source of sulphate, is added or blended into the cement to reduce the rate of this reaction and prevent flash set. The addition of gypsum initiates a reaction resulting in the production of ettringite ($3CaO \cdot Al_2O_3 \cdot 3CaSO_4 \cdot 32H_2O$), as shown in Equation 2.8. The formation of ettringite is identified as being expansive, but since this occurs in the unhardened or plastic phase, it is not detrimental to the concrete. Ideally, it is desirable to have all of the C_3A converted to ettringite, which is achieved by providing a sufficient amount of gypsum in the cement. However, if there is an insufficient amount of gypsum available, the remaining un-reacted C_3A component will react with ettringite to form monosulfoaluminate, which is an unstable product. Monosufoaluminate can revert back to ettringite when exposed to

8

an external source of sulphate. This process is highly detrimental when it occurs in already hardened cement paste. The preceding phenomenon is known as sulphate attack on concrete and the reactions are given by Equation 2.9 and Equation 2.10. The exact gypsum content required in cement needs to be carefully proportioned, such that both C_3A and gypsum are used up in the early stages of hydration. Typically, the amount of gypsum blended with cement production is approximately 2.5% by weight of SO_3 for C_3A contents less than 5% and 3% by weight of SO_3 for C_3A contents greater than 5% (Neville, 1981).

$$3CaO \cdot Al_2O_3 + 3CaSO_4 \cdot 2H_2O + 26H_2O \rightarrow 3CaO \cdot Al_2O_3 \cdot 3CaSO_4 \cdot 32H_2O \qquad \text{Equation 2.8}$$

$$\text{(C}_3\text{A)} \qquad \text{(gypsum)} \qquad \text{(H)} \qquad \text{(ettringite)}$$

$$2(3CaO \cdot Al_2O_3) + 3CaO \cdot Al_2O_3 \cdot 3CaSO_4 \cdot 32H_2O + 4H_2O \rightarrow$$
$$3(3CaO \cdot Al_2O_3 \cdot CaSO_4 \cdot 12H_2O) = monosulfoa\,luminate \qquad \text{Equation 2.9}$$

$$3(3CaO \cdot Al_2O_3 \cdot CaSO_4 \cdot 12H_2O) + 2CaSO_4 \cdot 2H_2O + 16H_2O \rightarrow$$
$$3CaO \cdot Al_2O_3 \cdot 3CaSO_4 \cdot 32H_2O = ettringite \qquad \text{Equation 2.10}$$
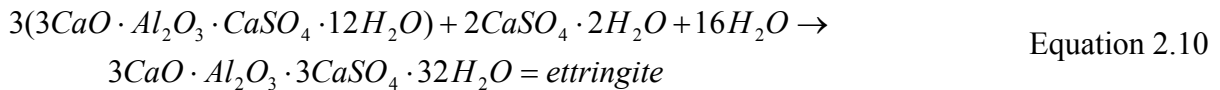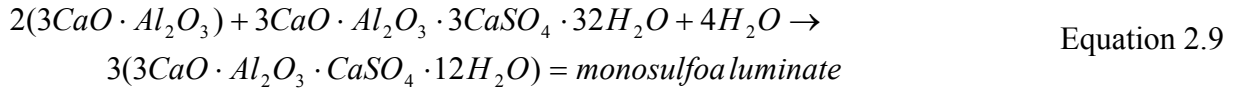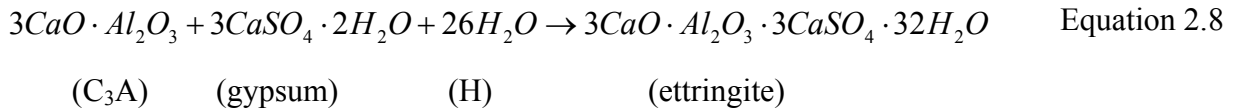
C_4AF reacts in a similar manner to C_3A, but does not consume as much water and as such, it does not result in flash set. The process also produces less heat of hydration than C_3A. The reactions involving C_4AF can be seen in Equation 2.11 (Brown, 2006).

$$3(4CaO \cdot Al_2O_3 \cdot Fe_2O_3) + 12CaSO_4 \cdot 2H_2O + 110H_2O \rightarrow \qquad \text{Equation 2.11}$$
$$4(3CaO \cdot Al_2O_3 \cdot Fe_2O_3 \cdot 3CaSO_4 \cdot 32H_2O) + 2Al_2O_3 \cdot Fe_2O_3 \cdot 3H_2O$$
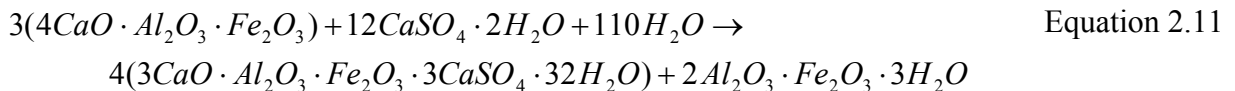
2.2.1.3 Cement Paste Setting and Heat of Hydration

Setting of cement refers to the period when the paste starts to stiffen, such that it is transforming from a fluid state to a solid state. In the setting stage, two distinct types of setting terminology are used: initial set and final set, which are graphically illustrated in Figure 2.4. Generally, cement paste set time decreases as temperature increases. However, when the temperature is above $30^\circ C$, a reverse trend has been observed (Lea, 1971).

The reaction of cement is exothermic since it demands vast amounts of energy to produce cement. The rate of heat evolution is proportional to the different stages of hydration, as summarized in the plot of heat of evolution versus time in Figure 2.5.
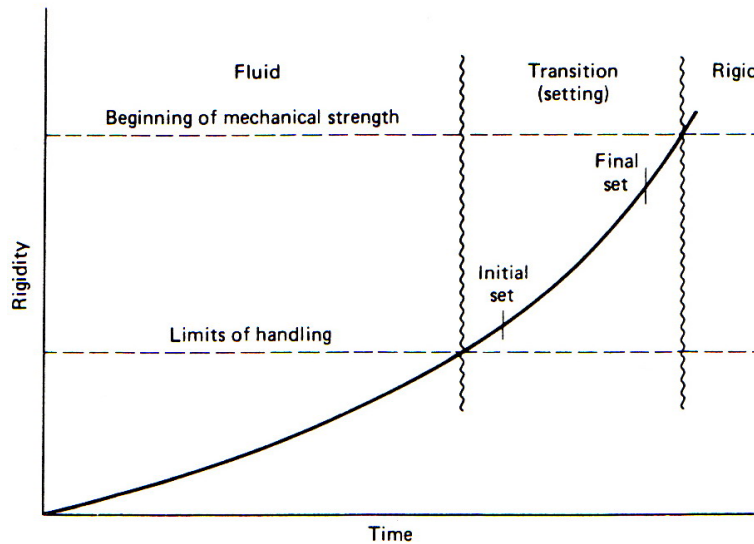
Figure 2.4: Setting time of cement paste (Mindess et al., 2003)

The heat development can be divided into five distinct stages according to Mindess and Young (1981) shown in Figure 2.5. Stage one, referred to as the initial stage, occurs within 30 minutes of contact between water and cement. The second stage is the dormant, or induction period, and occurs between 0.5 and 6 hours. There is very minimal heat of evolution or activity occurring, allowing working time for the concrete to be placed. It should be noted that initial set occurs at the end of this second stage and placed concrete cannot be re-shaped. Stage three, which occurs between 6 and 12 hours, is known as the acceleration period. Saturated levels of CH are reached and formation of C-S-H starts. At this point, the cement paste starts to show signs of stiffness and strength gain. Final set occurs at some point in this stage. Stage four, occurring between 12 and 24 hours, is known as the deceleration stage because the heat of evolution declines from its peak. At this point, the cement has already achieved final set. Stage five, which covers the time from 24 hours and beyond, signifies steady state. The cement continues to hydrate without a significant amount of heat evolution occurring.

10
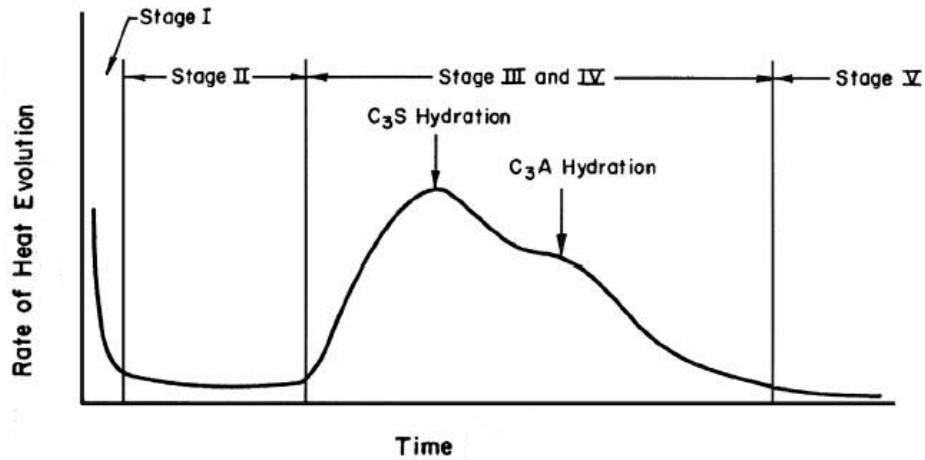
Figure 2.5: Amount of heat of evolution vs. hydration time (Kosmatka et al., 2002)

2.2.1.4 Products of Hydration

Calcium silicate hydrate is the main product of cement hydration, and occupies about 50 to 60% of the hydration volume (Mehta et al., 1993). The structure of C-S-H is still heavily debated because the exact ratio of C:S is uncertain (Neville, 1981). Regardless, C-S-H is collectively recognized as being playing a major role in the strength development of cement paste.

Another product of hydration is calcium hydroxide, which occupies approximately 10 to 25% of the hydration volume (Mehta et al., 1993). It forms when lime precipitates from C_3S, and to a lesser degree from C_2S reaction with water as describe in Equation 2.6 and 2.7. The CH structure resembles that of a relatively large crystallized hexagonal sheet and can be up to 30μm in size (Melzer and Eberhard, 1989).

Powers (1958) suggested that a w/c ratio as low as 0.38 is required for complete hydration of cement; therefore, any w/c ratio below 0.38 leads to incomplete hydration, as there is not enough water available to carry out the chemical reaction. The benefits of using low w/c ratio (less than 0.38) have been shown to have advantageous effects such as, lower porosity and the unhydrated cement may act as filler material to further hydrate in the presence of an external source of

11

moisture, producing high strength paste (Powers and Brownyard, 1946). Thus, it is common to find high performance concrete or HPC with w/c ratio less than 0.38.

2.2.1.5 Type of Pores and Water Held in Cement Paste

Capillary pores are the remnant of spaces initially occupied by water during hydration. The physical shape of capillary pores is not fully known, as its shape depends on many variables such as hydration rate and available water. Mercury intrusion porosimetry (MIP) is a popular technique to determine pore size distribution in hydrated cement paste (Winslow and Diamond, 1970), but the technique is questioned by many for the validity of the measured pore size distribution (Diamond, 2000), as the technique may damage the pore structure in the process. Capillary pores are, by far, much larger than gel pores, which are remnants of gel water, as illustrated in Figure 2.6.
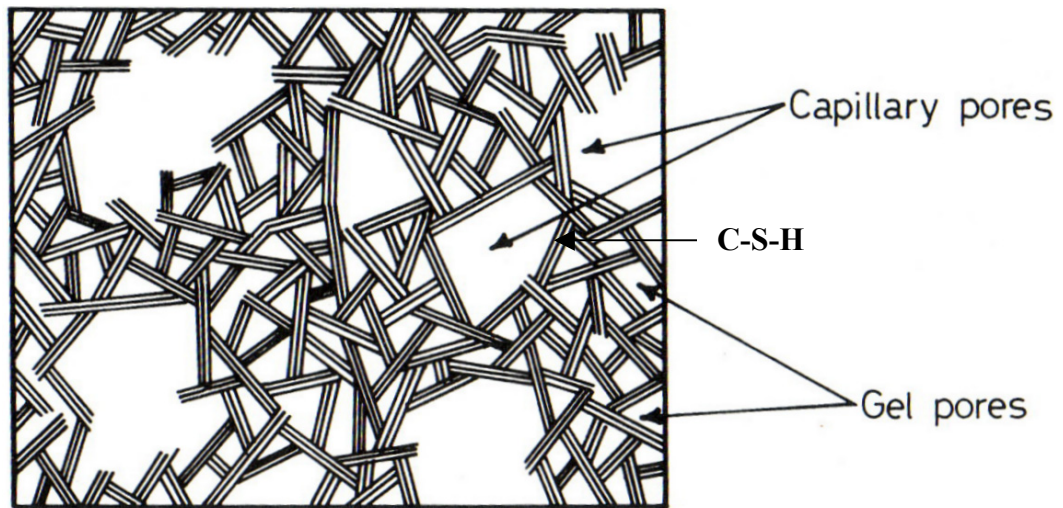
Figure 2.6: Schematic diagram of the hydration products (Soroka, 1979)

According to Fieldman et al. (1970), interlayer water and physically adsorbed water are held in between and on the surface of C-S-H structure. Gel water is physically bound to the surface of C-S-H due to surface tension forces while interlayer water is bounded between the C-S-H structure due to hydrogen bonds, as shown in Figure 2.7.
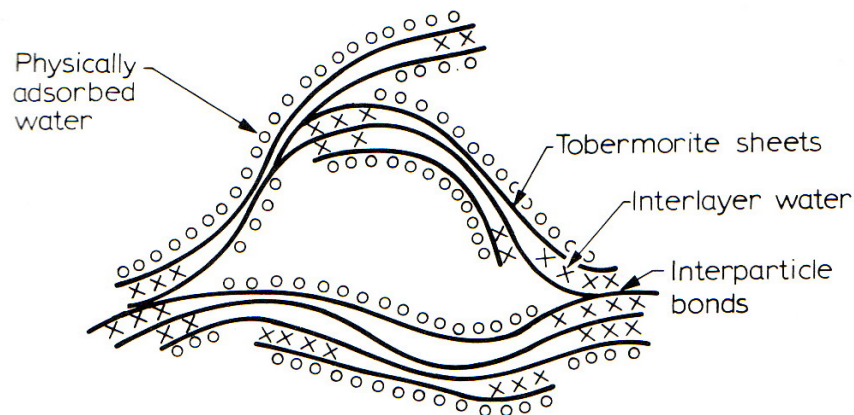
Figure 2.7: Structure of C-S-H and the interlayer water (Fieldman et al., 1970)

2.2.1.6 Types of Cement

Based on the constituents of oxides used, varying percentages of C_3S, C_2S, C_3A, C_4AF, and other minor compounds are produced in cement, creating different types of portland cement. There are six general types of portland cement commercially available based on CSA A3001 classification (2003) as shown in Table 2.2. Depending on the application of the work, a different grade of cement would be used. Aside from portland cement, there is blended cement, which uses additional or supplementary cementing materials (SCM) such as natural pozzolan, fly ash, silica fume, and ground granulated blast furnace slag blended in as partial replacement for portland cement. The compositions of each type of blended cement can vary dramatically from that of portland cement depending on the percentage replacement. As much as 60% cement replacement is allowed under the provision of CSA A3001 (2003) blended cement proportions.

Table 2.2: Portland cement types based on CSA A3001 classification

Description	Type
General use	GU
High early strength	HE
Moderate sulphate resistance	MS
High sulphate resistance	HS
Moderate heat of hydration	MH
Low heat of hydration	LH

13

2.2.1.7 Supplementary Cementing Materials (SCM) and Pozzolans

With the growing attention to sustainable development, the concrete industry is looking for alternative materials, such as mineral admixtures or pozzolans with cementing properties, to supplement the use of cement. Mineral admixtures that are commonly used as a replacement for cement and in blended cement include fly ash, silica fume, and ground granulated blast furnace slag. The use of mineral admixtures has two major benefits:

1. It reduces the use of cement, which is a cost saving effort, as most of the mineral admixtures are less expensive than cement. They are often by-products of manufacturing processes used in the silicon, coal, or metals industry.

2. It can enhance the properties of concrete; such as reduce permeability and segregation, without compromising concrete quality.

Natural pozzolan is found in volcanic ash. Pozzolans can also be obtained as a by-product from the process of burning coal for power in the form of fly ash. By itself, pozzolan possesses little, or no, cementing or binding property (ACI 116, 2000) in the presence of water. However, in the presence of water and calcium hydroxide, it reacts to produce calcium silicate hydrate and calcium aluminate hydrates, which are similar to the products of portland cement hydration. The pozzolanic reaction requires CH from a C_3S and C_2S reaction to activate it, thus, its reactivity is slow compared to the cement reaction.

Ground granulated blast-furnace slag (GGBFS), or slag, is a by-product from the production of iron. Slag appearance is white in colour and typically ground to less than 45µm (ASTM C989, 2006), which is in the same order of magnitude as cement. The reaction of slag is slow, as the slag particle initially forms an impervious layer when it first contacts water; therefore, cement containing slag replacement initially hydrates slower than cement alone (Taylor, 1990). With the help of an alkali activator such as NaOH, KOH, or $Ca(OH)_2$ the hydroxyl ions help break the impervious glassy layer and therefore increase the hydration rate (ACI 233, 2003).

Subsequently, in cement containing slag the replacement set-time is slightly retarded, as the total C_3S content is less, resulting in a longer curing time and lower heat of hydration compared to using pure cement. In addition, the use of slag demands slightly less water for the same consistency than cement without slag replacement (Meusel and Rose, 1983).

2.2.1.8 Air Entraining Agent

Air entraining agent is a chemical admixture employed during the batching process of concrete to produce a system of entrained air in the cement paste. Entrained air is noticeably different from entrapped air, which is trapped in the cement paste due to mixing action. Entrained air is very small, usually between 0.01 to 0.1mm in diameter (ACI 212, 2004), whereas entrapped air is typically visible to the unaided eye. The air entraining mechanism employs ionic repulsion forces at the molecular level. Lea (1971) suggests that air entraining surfactants operate at the air-water and the solid-water interface, as shown in Figure 2.8. At the air-water interface, the agent helps by reducing surface tension, which promotes dispersion and bubble formation. At the solid-water interface, the surfactant adsorbs on the cement particle to produce a hydrophobic surface, which facilitates the attachment of small air voids to the cement particles (Lea, 1971).
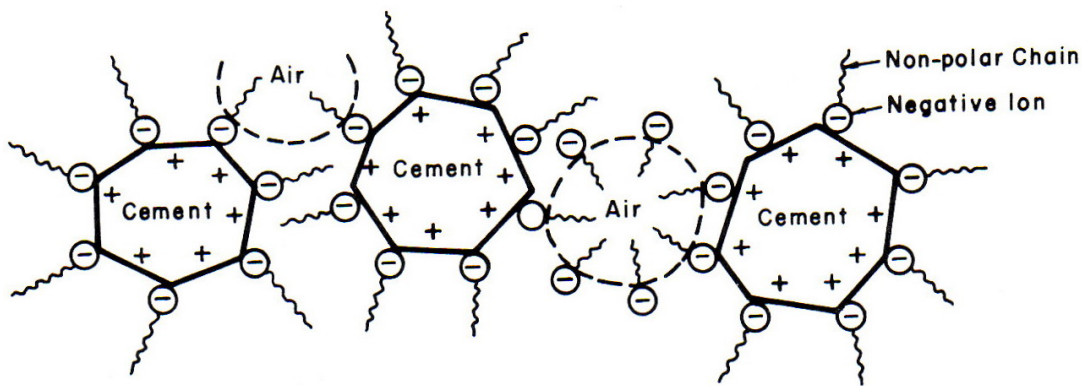
Figure 2.8: Mechanism of air entraining agent (Mehta et al., 1993)

The primary purpose of entraining air in cement paste is to prevent freeze-thaw damage. Freeze-thaw damage in cement paste is a physical form of deterioration and there are multiple theories

as to the mechanism that causes the damage (ACI 201, 2001). Powers (1945) suggested that water expands 9% by volume during freezing. When capillary pore volume is saturated with 91% or more with water, it will cause expansive tensile forces. When expansive force exceeds the tensile strength of the cement paste, frost damage occurs in the form of surface scaling and cracking. Another theory suggests that as dissolved alkali solution becomes trapped in capillary pores and freezes, it will produce an osmotic potential. This occurs because pure water is likely to freeze first, creating an alkali concentration gradient (Powers, 1956; Helmuth, 1960). The concentration gradient would, in turn, draw more water from adjacent capillary pores to the freezing site in an attempt to neutralize the gradient. This continues until the pore is full and the process starts over again at a new site. Regardless of the mechanism that causes freeze-thaw damage, entrained air is believed to help alleviate the pressure caused by the freezing and thawing action, so long as the entrained air void system contains pores of adequate size and which are evenly distributed throughout the paste.

2.2.2 Properties of Concrete

The properties of concrete involve the interaction between the cement paste and the aggregates. The role of the cement paste and sand as mortar is to bind coarse aggregate together. The adhesion of the mortar to the coarse aggregate is a function of its shapes and sizes. Therefore, mixture proportion of the components used in concrete will have an impact on its properties.

2.2.2.1 Water to Cement Ratio

Water-to-cement (w/c) ratio is the ratio of water to cement by mass. Cement content includes the use of fly ash, silica fume, slag, pozzolan, and other supplementary cementing materials. Typically, w/c ratio ranges from 0.35 to 0.65 in the concrete construction industry, depending on the application. The actual w/c ratio used in concrete is often dictated by the strength and workability requirements, rather than just meeting the minimum w/c ratio required for cement hydration. The role of w/c ratio is important to achieving the desired fresh and hardened properties, which will ultimately influence the durability properties.

2.2.2.2 Fresh Properties of Concrete

The fresh properties of concrete refer to the characteristics of the concrete when it is in the unhardened state. Workability of concrete is often used to describe the handling condition of the concrete mixture, which includes the ease of mixing, placing, and finishing. Since workability is a loosely coined terminology used to describe many parameters in the concrete industry, no single test is currently available to determine the workability of concrete. Consistency of a concrete mix for a given mixture design is important to achieving uniformity. A standard practice used to measure the consistency of concrete is to measure the concrete slump using a slump cone test (CSA A23.2-5C, 2004). Generally, the slump is greater when the concrete is more fluid and wet. A slump of 25 to 100 mm (ACI 211, 1997) is typically acceptable depending on the application of the concrete, as shown in Table 2.3.

The air content in concrete refers to the total air content, which includes entrained, entrapped, and air voids measured in fresh concrete and is given as a volume percentage. Standard practice used to measure the air content of fresh concrete employs a pressure-type meter in accordance with CSA A23.2-4C (2004). It is recommended that an air content between 5 to 8 % should be used (CSA A23.1, 2004) in freeze-thaw susceptible areas. Aside from minimizing freeze-thaw damage, entrained air can provide additional benefits such as improved workability for the same concrete mixture design. The tiny entrained air bubbles act as fine spherical particles with minimal surface friction (Neville, 1983), which prevents coalescence of cement particles when mixed with water. Another benefit to using entrained air is the stabilization given by the tiny bubbles dispersed throughout the cement paste. Within freshly placed concrete, it controls the movement of water rising, known as bleeding, and coarse aggregate falling, known as segregation (Kosmatka et al., 2002).

An alternative to using the pressure-type method to measure the air content in concrete is the volumetric technique (CSA A23.2-7C, 2004). The idea is to displace the air content in cement paste and measure the percentage of displaced air, which is then compared to the initial volume

17

of the paste content. The displacement of total air content in concrete is achieved by using isopropyl alcohol in a known volume of cement paste or mortar by using the Chace indicator (AASHTO T199, 2000). The total air content in concrete can be estimated based on the known paste content and displaced volume of air.

Table 2.3: Recommended slumps for various constructions (ACI 211, 1997)

Concrete construction	Slump, mm	
	Maximum	Minimum
Reinforced foundation walls and footings	75	25
Plain footings, caissons, and substructure walls	75	25
Beams and reinforced walls	100	25
Building columns	100	25
Pavements and slabs	75	25
Mass concrete	50	25

2.2.2.3 Strength of Concrete

The strength of concrete is the most emphasized property of concrete. Less attention is often paid to the durability properties such as resistance to freeze-thaw damage, which is frequently more important than strength requirements. Standard compressive strength of concrete is typically measured at 28 days (f_c') on a 100 x 200 mm cylinder. Concrete is cured after cast to prevent moisture loss by placement in a humidity room or by covering the specimens with burlap and plastic sheet. The concrete is cured to promote further hydration, as water is required in the hydration of C_3S and C_2S to achieve maximum strength, as shown in Figure 2.9. Thus, concrete will continue to hydrate and gain strength if there is water present.

Water-cement ratio plays a major role on influencing the compressive strength of concrete. Water that is not used for hydration initially occupies space in its liquid phase and eventually evaporates, leaving capillary voids behind. As a result, high w/c concrete is porous and hollow

and it follows that concrete containing a high w/c ratio leads to low strength, as predicted by Abram (1918) using Abram's water/cement ratio equation (Equation 2.12). Therefore, w/c ratio greatly influences the strength of concrete given that the concrete is properly compacted, as shown in Figure 2.10.

$$f_c = \frac{k_1}{k_2^{w/c}}$$

Equation 2.12

Tensile strength of concrete can be obtained through three types of testing: direct tensile, splitting cylinder (ASTM C496, 2004) or flexural tests (ASTM C78, 2002). Flexural strengths are obtained in a 3- or 4-point bending test. The flexural strength from bending test is referred to as the modulus of rupture. The tensile and compressive strength is proportional to one another, as shown in the relationship given by Equation 2.13 from CSA A23.3-04 (2004) Concrete Design Handbook. Generally, concrete with a high compressive strength will have a high tensile strength.

$$f_r = 0.6\sqrt{f_c'}$$

Equation 2.13
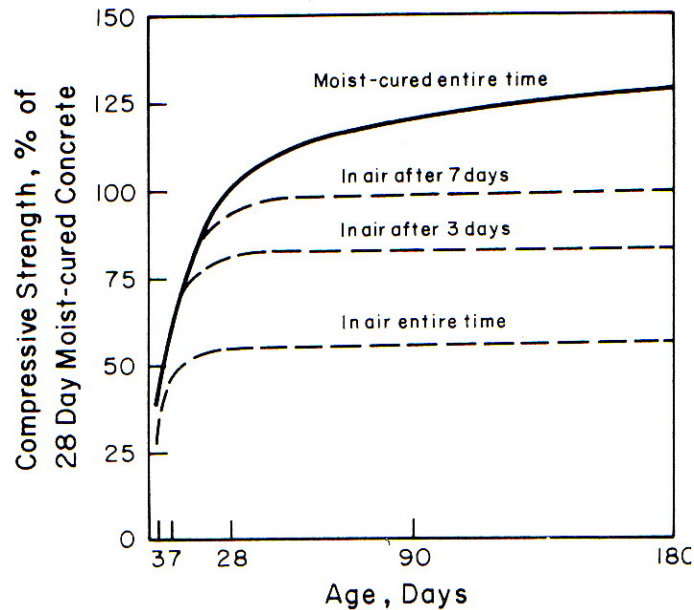
Figure 2.9: Compressive strength vs. types of curing regime (Concrete Manual, 1981)
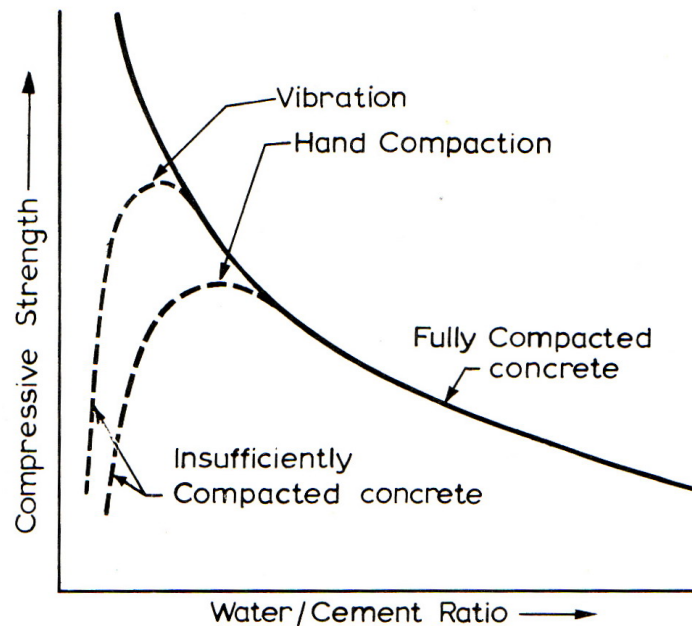
Figure 2.10: The influence of w/c ratio on compressive strength (Neville, 1981)

2.2.2.4 Permeability of Concrete

The permeability of concrete refers to the transport property of a substance through a porous solid. The permeability coefficient (K) is based on Darcy's Law for steady-state flow. Generally, porous concrete is viewed as permeable concrete, which may not always be true. Porosity in concrete comes from tiny voids dispersed throughout the paste of the concrete, but the pores are not necessary connected. Therefore, a concrete can theoretically have high porosity but a low permeability coefficient, though the two properties are often correlated. The transport of water and water vapour through concrete is of great concern as it provides a mean for deleterious agents such as chlorides, sulphates, and other alkali metals to enter, leading to other form of attack and concrete deterioration.

2.2.2.5 Concrete Properties Containing Slag

There are numerous studies on the properties of concrete containing slag and most have found slag to be more benefiting than detrimental to the overall quality. Fulton (1974) reported that the

use of slag as cement replacement improved the workability of concrete. Wood (1981) reported similar results, noting that concrete containing slag had superior workability and placeability properties than concrete without slag. In another study by Wu and Roy (1982), it was believed that the slag particles helped to disperse the paste better than cement particles. Therefore, concrete containing slag exhibited a higher fluidity than without slag. Meusel and Rose (1983) reported that as much as a 50 mm greater slump loss was found in concrete using 50 % slag replacement compared to samples using 100 % portland cement, as shown in Figure 2.11. On the whole, it has been well established in research that the use of slag in concrete improves the workability of concrete.
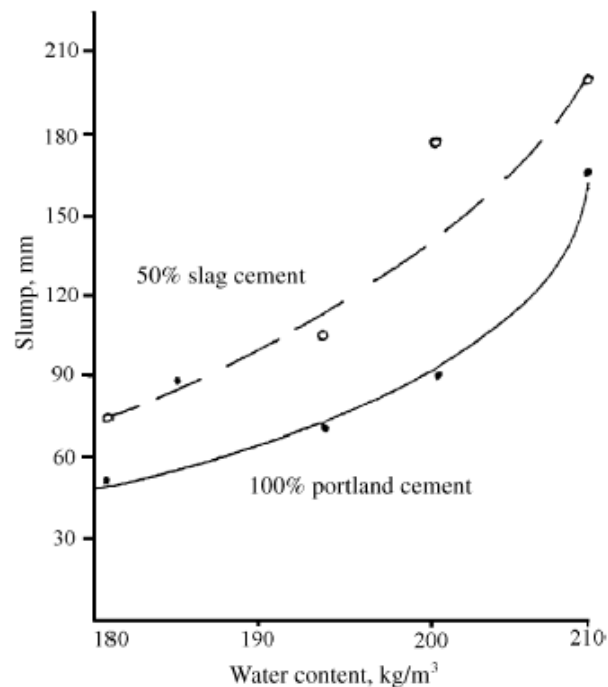
Figure 2.11: The effects of slag on slump (Meusel and Rose, 1983)

Generally, the specified compressive strength at 28 days is not affected by the slag content; however, compressive strength at earlier times between 1 to 3 days may show weaker strength development than concrete without slag (Hogan and Meusel, 1981). The slower strength development is attributed to slag hydration, which favours the production of C_2S rather than C_3S.

2.2.2.6 Freeze-Thaw Damage in Concrete

An entrained air void system plays a major role in preventing frost damage in cement paste. Klieger (1952) looked at the effects of air content on concrete performance with respect to freeze-thaw damage and found that a higher air content is required when smaller aggregates are used in concrete rather than if larger aggregates are used. Based on Klieger's work, CSA A23.1 (2004) recommends a 5 to 8 % air content in concrete to minimize the damage of freeze-thaw cycles. Powers (1954) suggests that the average spacing (spacing factor) between two adjacent entrained air bubbles may be more important than the air content. This is because it dictates how far unfrozen water must travel to relieve the internal stresses.   It is recommended that an entrained air void system require an average spacing factor of less than 0.2mm (Powers, 1949; Verbeck, 1978) in order to be effective against frost damage.

In North America, million of tonnes of de-icing salts are spread on the road to battle slippery road conditions. De-icing salts, which are usually composed of $NaCl$ or $CaCl_2$ (ACI 201, 2002), function by melting the ice as dissolution of $NaCl$ and $CaCl_2$ are exothermic. Also, the melted ice solution new freezing temperature is lower, which makes it more difficult to re-freeze.

Salt is naturally hygroscopic, which means that it has the tendency to attract other water molecules. By attracting more water, higher saturation levels are achieved in capillary pores, thus increasing the likelihood of frost damage. The secondary effect of de-icing salt is that it decreases the freezing point of water, thus allowing the cooled liquid to be more easily adsorbed on the concrete surface. As the surrounding ice or snow melts, it decreases the concentration of the salt solution such that the freezing point of the liquid rises close to the freezing point of water, thus causing the liquid to partially freeze. Therefore, the action of freezing and thawing occurs more frequently with the presence of de-icing salt than without (Neville, 1981), which triggers an acceleratory affect of freeze-thaw damage. Finally, de-icing salt has been known to promote rapid corrosion of reinforcing steel, which would be highly detrimental to the durability of reinforced concrete.

2.2.2.7 *Corrosion of Reinforcing Steel in Concrete*

Corrosion of reinforcing steel (rebar) in concrete is one of the most common forms of concrete deterioration. The damage develops in the form of corrosion product expansion and results in cracking, spalling, and loss of concrete cover (Mehta et al., 1993). Aside from the concrete damage, it leads to structural deficiency as the effective steel cross-section is reduced. It was estimated that the direct cost of rehabilitation and repair of bridges in North America alone was approximately \$23 billion in 1998. In addition, the indirect social impact it has on our economy is enormous, as reported by the Federal Highway Administration (FHWA, 1999).   Thus, corrosion in concrete is of a great concern to the performance and durability of concrete.

The corrosion of steel in concrete is an electrochemical process that can be described as the reverse process of metallurgical extraction (Fontana, 1988). Initially, the oxide ores extracted from the Earth undergo a metallurgical process to make steel.   This process is thermodynamically unstable as energy is added to the system to produce steel from oxides. Nature likes to revert to the lowest energy form, thus the corrosion process occurs by reducing steel back to the original oxides, as shown in Figure 2.12.
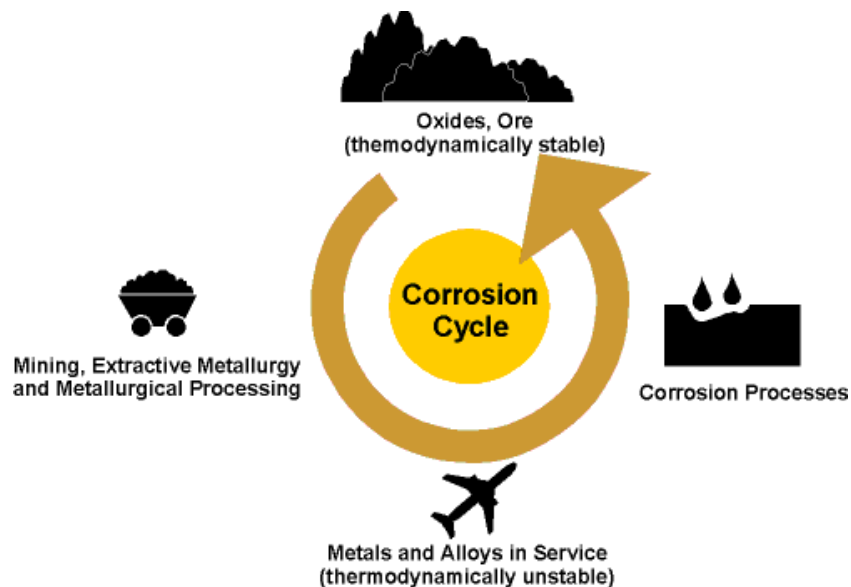
Figure 2.12: Corrosion life cycle (Corrosion-club, 2007)

23

The corrosion dynamics can be simplified using a half-cell potential model described in Equation 2.14 and Equation 2.15. The anode is the site where metal is dissolved and electrons are liberated. The cathode is the site where oxygen is reduced, with the aid of electrons from the anodic reaction, to produce hydroxyl ions and hydrogen gas. The simplification of this model can be illustrated using a bridge deck with two layers of reinforcing steel, each representing an anodic and a cathodic site, as shown in Figure 2.13. The vertical rebar, or stirrup, provides a path for the electrons to travel between the two sites and hydroxyl ions diffuse from the cathode to anode site through the concrete. This model is known as macro-cell corrosion, where a finite distance separates the anodic and cathodic site.

$$Anode : Fe \rightarrow Fe^{2+} + 2e^-$$ Equation 2.14

$$Cathode : 2e^- + \tfrac{1}{2}O_2 + H_2O \rightarrow 2OH^-$$ Equation 2.15

It is often more common to observe the micro-cell corrosion rather than the macro-cell corrosion in reinforced concrete. Micro-cell corrosion occurs when the anodic and cathodic site is on adjacent sites on a rebar, as illustrated in Figure 2.14. Localised corrosion is often more dangerous, as the material loss is not uniform but instead may cause perforation of the reinforcing steel.
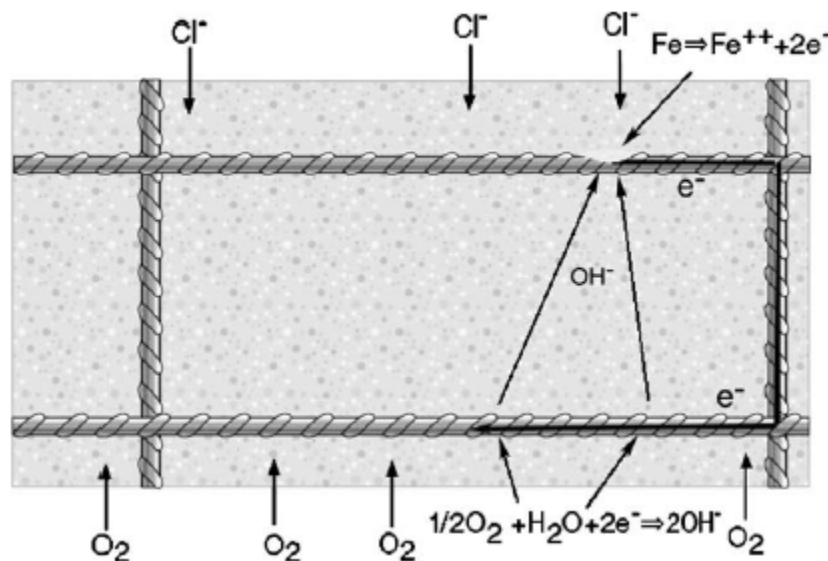
Figure 2.13: Idealized bridge deck representing macro-cell corrosion (Hansson et al., 2006)

24
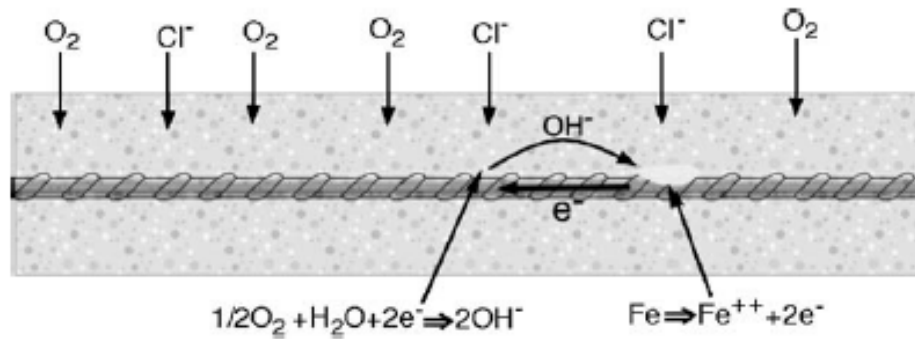
Figure 2.14: Idealized micro-cell corrosion activity (Hansson et al., 2006)

When steel is exposed to a highly alkaline environment, it forms an iron oxide film. The oxide film or passive film is a highly corrosion-resistant layer that is only a few nanometers thick. Concrete is the perfect environment for rebar because it protects the steel by providing a physical barrier against water and moisture penetration. In addition, concrete provides a passive environment for the embedded steel due to its alkaline nature. Typically, the pH of concrete is around 12.5 to 13.7, which places iron in the passive region, as shown in a simplified E/pH or Pourbaix diagram as shown in Figure 2.15. In order for corrosion to occur, there needs to be a breakdown of the passive film, the presence of water and oxygen, and a low ionic conductivity of concrete to allow the hydroxyl ions to travel from the anode to the cathode in macro-cell corrosion.

The role of chlorides in localised corrosion is significant since, in most cases, it presence reduces the pH of concrete and promotes an additional oxidizing reaction, as expressed in Equation 2.16. What makes chloride-induced corrosion even more dangerous is the fact that the anodic reaction process does not consume the chloride, leaving it to react with the iron again, initiating an autocatalytic reaction. Therefore, the corrosion of reinforcing steel in concrete is more severe in the presence of chlorides.

$$Anodic: Fe + 3Cl^- \rightarrow FeCl_3^- + 2e^-$$ Equation 2.16
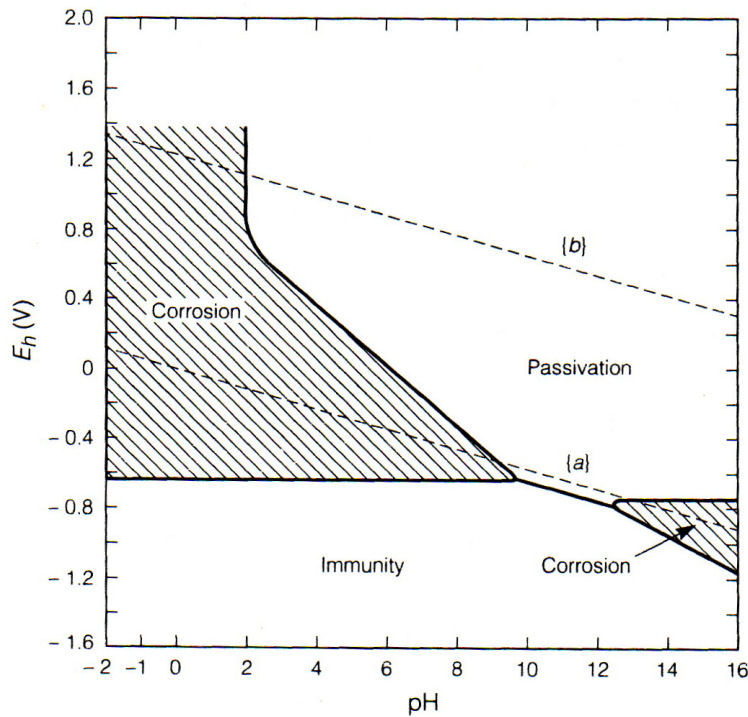
Figure 2.15: A Pourbaix diagram for iron (Pourbaix, 1974)

2.3 THERMAL ANALYSIS

In the past, several methods such as calorimetric or conductometric titration were used to determine the free $Ca(OH)_2$ in cementing materials (Ramachandran, 1979). However, these chemical techniques were not reliable as the solvent used in the extraction process may attack other compounds (Pressler et al., 1961). Since thermogravimetric analysis (TGA) is independent of the chemical reaction and the technique is performed in a controlled environment, it has been suggested as a reliable method for determining free $Ca(OH)_2$ found in cementing material hydration (Glasser et al., 1978). TGA results can be used to determine the effects wash water may have on the hydration of cementing materials.

Thermogravimetric analysis techniques measure the changes in weight as a function of temperature. This is expressed in a thermogram, as illustrated in Figure 2.16. The rate of mass loss as a function of temperature or differential thermogravimetric (DTG) can also be determined

from mass loss curve (TGA), shown together on a thermogram. The information that is obtained from the test can be used to show the decomposition and oxidation of certain compounds (Skoog et al., 1998) based on a known thermogram. For this project, it can be used to quantify the $Ca(OH)_2$ content found in different cement pastes.
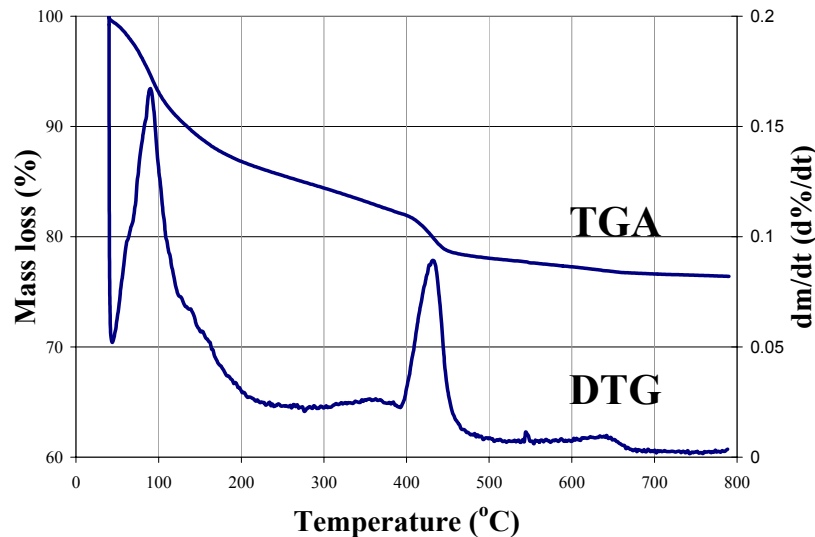
Figure 2.16: Example of a thermogram using thermogravimetric analysis

Typical thermal analysis equipment consists of a furnace, thermal control, and crucibles, which sit on a weight sensor balance. Inside the furnace chamber there are two crucibles, a sample and a reference crucible, sitting on highly sensitive weight balance arms. Before the test can begin, the system must be calibrated by performing baseline calibrations under the same thermal loading conditions as would be used in the actual sample test. Once the baseline calibration curves are established, the system is ready for testing. To prevent oxidation or reduction of the sample, the system is usually purged with an inert gas such as helium.

2.4 WASH WATER CONCRETE

Concrete produced using wash water has been mostly limited to relatively low strength concrete without air entraining (Mammoliti, 2007), such as concrete used as a filler material. This section

will discuss the wash water operations used to produce wash water concrete at a ready-mixed concrete plant, as well as available literature with respect to this topic.

2.4.1 Wash Water Operation

When a ready-mix concrete truck returns to the plant, any significant amount of leftover fresh concrete is deposited at a designated site within the facilities. The deposited concrete may be used as concrete blocks or left to harden and then crushed before disposal at a landfill site. It may also be used as recycled construction materials for example for sub-bases in pavement (Paolini and Khurana, 1998) or as coarse aggregate in concrete (ACI 555R-01, 2001).

After a thorough rinse, all of the water used in the process is deposited in a reservoir, as shown in Figure 2.17 and Figure 2.18 step J. Usually the cleaning process also requires a second rinse to make sure the truck is completely clean. Upon entering the reservoir, the coarse aggregate should be removed from the wash water using a screw auger. Ideally, any water that passes the screening for coarse aggregate should only contain fine aggregate and diluted cement paste. The reservoir is agitated in step K to avoid particulate settlement at the bottom and promote homogeneity of the wash water. Then, the water is pumped out of the reservoir, as shown in step M. Now, the wash water is ready to be used in the production of new concrete, as illustrated in steps N, O, and P.

Figure 2.17: Concrete truck cleaning and rinsing at Dufferin Ready-Mix Concrete

A Aggregate delivery
B Aggregate receiving hopper
C Aggregate storage
D Conveyor belt
E Cementing material storage
F Weigh hopper
G Cement delivery
H Mixer

I Admixtures
J Ready mix truck with returned concrete
K Recycled water
L Reclaimed aggregates
M Pump
N Water storage
O Concrete loaded in ready-mix truck
P Control Room
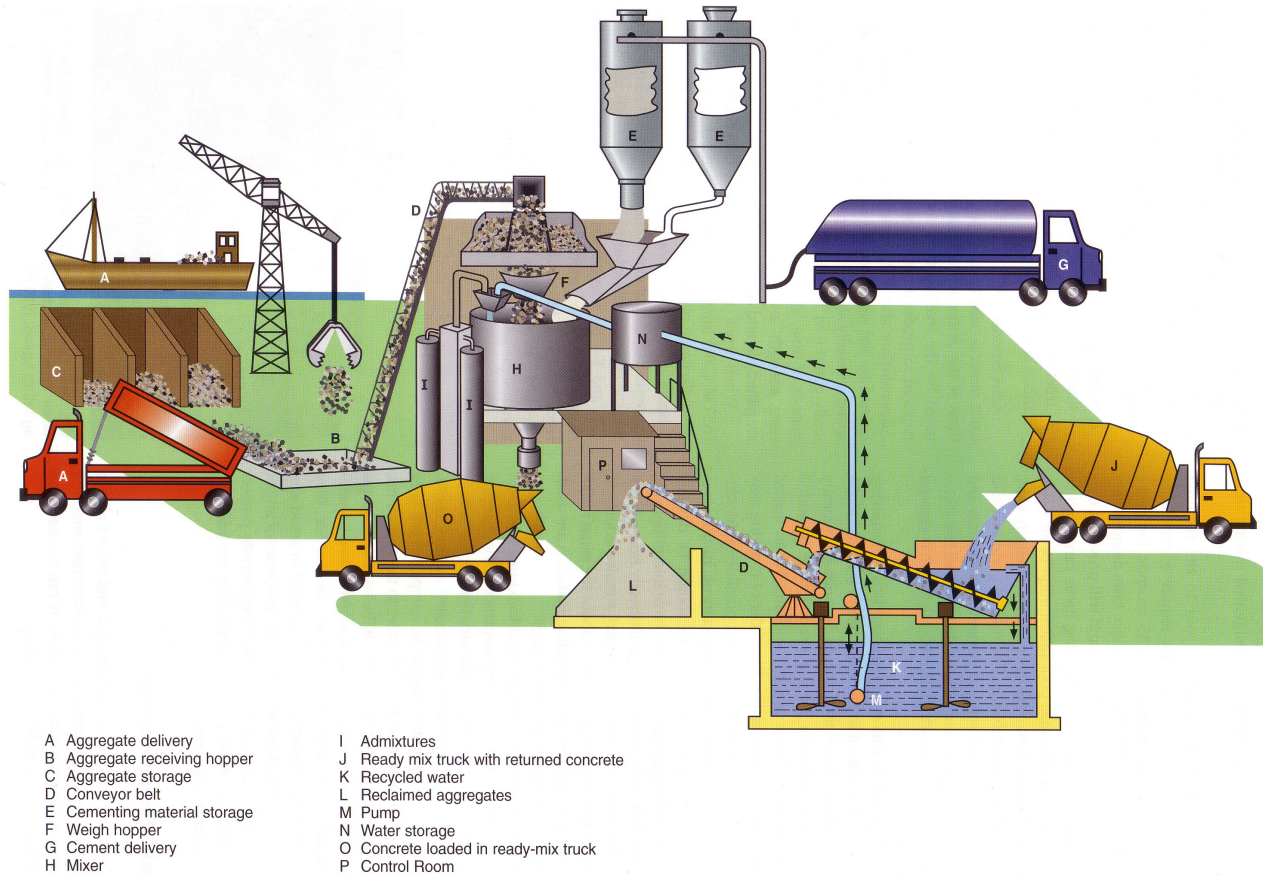
Figure 2.18: A typical wash water operation (Kosmatka et al., 2002)

2.4.2 Wash Water Concrete Research

Literature has shown that wash water concrete has been investigated as early as in the 1970s. Ullmann (1973) was one of the first to document the reuse of wash water as mixing water. He concluded that the wash water had no significant effect on the plastic properties of concrete such as slump, air content, and water demand during mixing. Meininger (1973) also found that wash water containing a small amount of solids had no significant effect on the plastic and hardened properties of concrete.

Borger et al. (1994) reported advantageous properties of a high solid content, such as an increase in strength, contradicting Meininger's results; however, the comparison is not direct, as

29

Meininger (1973) reported strength reductions in concrete whereas Borger et al. (1994) reported strength gains from mortar tests. It is believed that the interaction of cement and sand versus cement, sand, and coarse aggregate produces two distinctly different materials that may not be comparable to one another. Interestingly, higher mortar strengths were reported when using wash water that was collected within 4 hours after a washing discharge and lower mortar strengths when using wash water that was collected 24 hours after a washing discharge. In both cases, it was higher than the control mortar strength. For the strength gain, the authors attribute this to the lower effective water to cement ratio compared to the control mortar, but there is no clear indication of strength reduction for using wash water that is older. Perhaps, the hydrated cement particles in the mortar do not completely bind with the cement-mortar matrix; therefore, a slightly weaker cement-mortar interaction system is produced. Borger et al. (1994) also showed that wash water concrete had better resistance against sulphates and a lower permeability. The set-times, however, were generally reduced up to 20% from the control pastes.

Recently, the emphasis on sustainability in concrete technology has prompted more research regarding the use of wash water. Both Sandrolini and Franzoni (2001) and Selih et al. (2002) showed that the workability of wash water concrete is slightly reduced due to a lower effective water to cement ratio. Sandrolini and Franzoni (2001) concluded that wash water concrete compressive strengths were within 96 % of the control specimens. In addition, the concrete capillary water absorption and mortar porosity were lower than counterpart specimens. Selih et al. (2002) found that the air content in fresh concrete was significantly reduced, from 7.0% to 4.8% when switched from tap water to wash water use, and the authors believe that fine particulates in wash water may be responsible for the decrease in air content. In addition, the author believes that other possibilities, aside from fine particulates, may have an influence on the effectiveness of air entraining admixture such as high alkalinity and residual chemical admixture.

Su et al. (2002) performed a study on wash water and found that there was an increase in alkalinity, solid, chloride and sulphate content near the bottom of the wash water reservoir when compared to the top. The authors found that due to higher alkalinity of the wash water, it was able to activate a pozzolanic reaction of fly ash and slag to develop higher early compressive strength. In addition, the authors concluded that the set time of mortar using wash water was within 30 minutes of the tap water mortar set time, however, the final set times were similar between the mortar prepared with wash water and tap water.

Chini et al. (2001) reported that wash water has no significant effect on the fresh properties and that both the compressive and flexural strengths were within 90 % of the control specimens, as specified by ASTM C94 (2004) for questionable water supply used for mixing concrete. In addition, the authors concluded that wash water concrete performance in a rapid chloride permeability test, RCPT, (ASTM C1202, 2004), was similar to that of the control specimen. Secondly, the authors conducted an impressed current accelerated corrosion technique, using a 6 V power supply, to accelerate the corrosion activity, as shown in Figure 2.19 found that the control concrete performed better than the wash water concrete. Overall, Chini et al. (2001) concluded that the use of wash water have an insignificant effect on corrosion properties. However, impressed current technique of evaluating corrosion may be unreliable, as accelerated corrosion techniques use a considerable potential range to drive the chloride ions into the concrete (Hansson, 2000).

Rickert and Grube (2006a, 2006b) looked at the influence of wash water on plastic and hardened concrete properties. The authors showed that in normal strength concrete (approximately fc' = 40 MPa), the 28 day compressive strength was not affected by the use of wash water, however, in a high- strength concrete (approximately fc' = 90 MPa), the 28 day compressive strength was slightly lower than the 28 day compressive strength of tap water concrete. This suggests that wash water may have an effect on the compressive strength of high-strength concrete. One explanation for this could be that the solids in wash water may prevent a good adhesive bond

31

from forming between the cement paste and aggregates; therefore, the compressive strength of high-strength concrete is slightly affected. Rickert and Grube also suggests that when the wash water is used immediately after being generated, it improves the fresh concrete consistency and has no affect on the stiffening of the concrete; whereas if the wash water is used 72 hours after being generated, it results in a slight stiffening of the concrete.
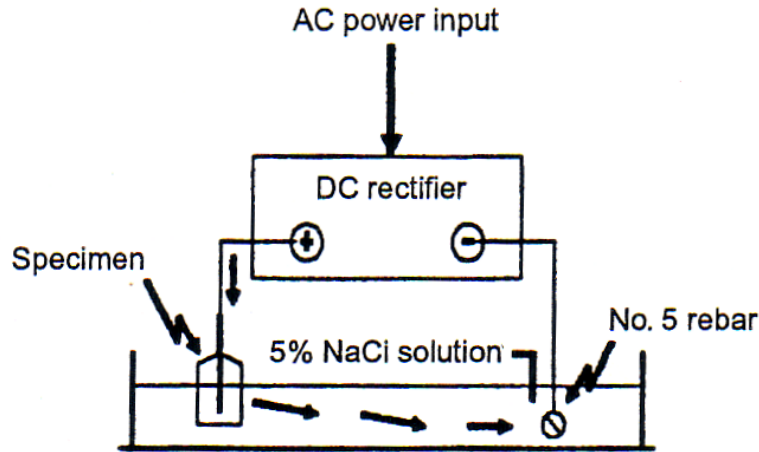
Figure 2.19: Impressed current as an accelerated corrosion technique (Chini et al., 2001)

In summary, most of the research focuses on the plastic properties, as well as the tensile and compressive strengths of wash water concrete. Presently, there is a lack of research in this topic with respect to durability, particularly concerning the corrosion performance of steel-reinforced concrete and the concrete resistance to surface scaling due to freeze-thaw exposure. Furthermore, the effect of wash water on entrained air stability was generally disregarded. The goal of this project is to investigate the influences of wash water on key issues that have not been previously found in any literature.

2.5 RESEARCH SIGNIFICANCE AND OBJECTIVES

Sustainable development should be the focus of concrete technology; otherwise the planet Earth cannot continue to support the increasing waste of its natural resources. By incorporating the use of wash water in the production of new concrete, the ready-mixed concrete industry can

effectively reduce the consumption of fresh water, as well as eliminate the need to store or dispose of wash water.

To date, only limited research has been published on the use of wash water in concrete and most of this focus on concrete strength and workability parameters. There appears to be a gap in the literature with respect to the performance of wash water on long-term durability. The goal of this project is to focus on how wash water affects the properties of concrete and how it may influence the long-term durability. This will be done using a multi-component experimental program outlined as follows:

1. The analyses of wash water, pore solution, and compositions.

2. Plastic and mechanical properties of concrete such as set-time, mortar air content, compressive, and flexural strength tests.

3. The effect of wash water on air entraining agents and the impact it has on surface scaling of concrete surfaces exposed to freeze-thaw cycles.

4. Corrosion of reinforcing steel using macro-cell, micro-cell, and half-cell potential monitoring techniques.

CHAPTER 3
EXPERIMENTAL PROGRAM

3.1 GENERAL

An experimental program was developed to investigate the effects of wash water as mixing water on the durability of concrete. Several concrete properties were examined of both plastic and hardened concrete properties, along with compositional analyses of wash water and pore solution. These are listed below:

1. Wash water analysis for major cations and anions, as well as pH.

2. Compositional analysis of pore solution extracted from hardened cement paste.

3. Stability of entrained air bubbles in wash water over time.

4. Plastic properties with respect to cement paste set time test and air content in mortar.

5. Mechanical properties with respect to compressive strength and flexural strength.

6. Concrete surface resistance to salt scaling when exposed to freeze-thaw cycles.

7. Hardened concrete air void analysis used in salt scaling resistance test.

8. Corrosion tests with respect to macro- and micro-cell corrosion tests, half-cell potential, and concrete resistance tests.

9. Thermogravimetric analysis of cement paste powder.

3.2 CONCRETE MIXTURE PROPORTIONS

The mixture design selections were based on two distinctly different concretes: one representing concrete that can be used in residential basement construction and the second representing concrete that can be used in structural applications. Class N and C2 concrete meets those

requirements, according to CSA A23.1-04 classification (CSA A23.1-04, 2004). Class N concrete is typically intended for use in non-structural applications that will not be exposed to freezing and thawing, whereas Class C2 concrete is typically intended for use in non-structural applications that may be exposed to chloride and freezing and thawing conditions. For this project, Dufferin Concrete provided the two different types of concrete to meet those requirements, which have specified 28 days compressive strengths of 25 MPa and 35 MPa for class N and C2, respectively. For each concrete, two sources of water were used: tap water from the municipal water supply and wash water produced at the Dufferin Concrete Kitchener plant. This yielded four distinctly different concretes labelled as TL, WL, TH, and WH, as shown in Table 3.1. The mixture proportions for concrete provided by Dufferin Concrete are given in Table 3.2. The mixture designs for concrete samples made in the laboratory for use in the salt scaling test were the same as the concrete supplied by Dufferin. In addition, wash water from Dufferin were used to mix the concrete.

Table 3.1: Concrete mixture designations

Specified strength (f_c') @ 28 days	Tap water	Wash water
25 MPa (lower strength)	TL	WL
35 MPa (higher strength)	TH	WH

Table 3.2: Mixture proportions for concrete provided by Dufferin

Materials per m^3 of concrete	Specified 35 MPa, TH & WH	Specified 25 MPa, TL & WL
Type GU Cement content	351 kg	185.5 kg
Slag content	39 kg	79.5 kg
Water content	150 kg + 25.5 kg on site*	153 + 6 kg on site*
Water to binders (w/b) ratios	0.45	0.60
Coarse aggregate	1100 kg	1045 kg
Fine aggregate	735 kg	860 kg
Air entraining admixture	40 mL/100 kg of cement	--
Water reducer	30 mL/100 kg of cement	--

* Water added on site to meet workability needs.

3.3 WASH WATER ANALYSIS

Four samples of wash water (WW) from Dufferin Ready-Mixed Concrete Plant were taken on October 2005, the same day that the wash water concrete was made. The samples were sent to the Earth Science water analysis lab at the University of Waterloo for analysis. The results were compared to the Kitchener Quality Water Report (Regional Municipality of Waterloo, 2005) as tap water (TW).

3.4 PORE SOLUTION EXTRACTION AND ANALYSIS

Cylinders of cement paste, 50 mm diameter by 100 mm height, with a w/b ratio of 0.45 were casts as follow. Four cylinders were cast for each of the four cement paste types: TL, WL, TH, and WH. The paste mixture designs were based on the concrete mixture designs prepared in the lab (Table 3.2), except without aggregates. The mixing procedure consisted of 3 minutes of mixing, followed by a 3 minute rest and then an additional 2 minutes of mixing, in accordance with CSA A23.2 (2004) batching and machine mixing standard.

In cement paste with a w/b ratio in excess of 0.50, excess water separates from the paste and rises to the top of the cylinder before fully hardening. This is known as bleeding. Therefore, TL and WL cylinders were rotated at 5 revolutions per minute, as shown in Figure 3.1 for the first 48 hours after casting to mix evenly as the paste hardened. To prevent water evaporation from the cylinder, a layer of vapour sheet (Para Film) was placed between the wet paste and cylinder cap, regardless of the type of cement paste used. The TH and WH samples were allowed to harden in the vertical position without rotation. After 48 hours, the cylinder were sealed in plastic Ziplock bags, placed in a plastic box, and placed in the humidity room to cured for 6 months until the time of pore solution extraction.
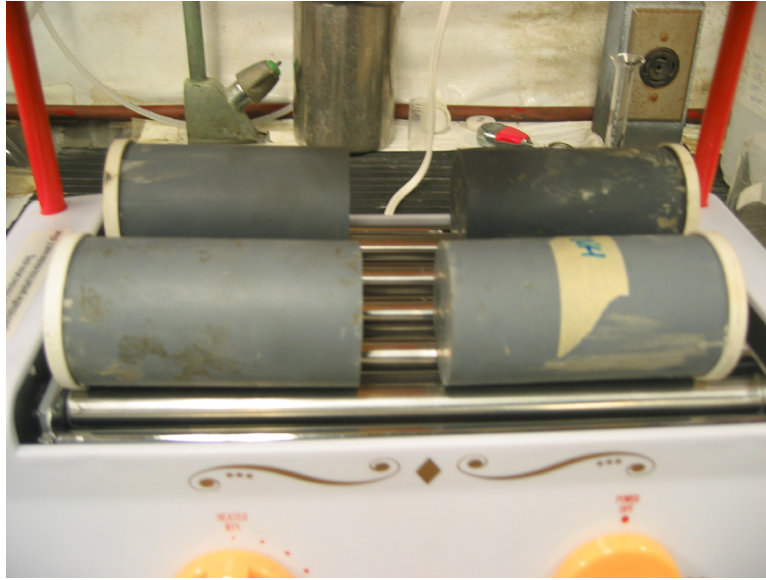
Figure 3.1: Cement paste cylinder rollers

To extract the pore solution from the cement paste, the cylinder was placed in a stainless steel cylinder chamber holder that was the same size as the cylinder sitting on a grooved base plate. A load was then applied to the stainless steel piston, shown in Figure 3.2. The piston was depressed at a rate of 2mm/min increments. The cylinder was loaded up to 300, 600, and 900kN and held for 5 minutes at each step. By holding the specimen under high load, the pore solution permeates out of the cement paste cylinder and collects in the groove of the base plate. The base plate has a line out for a syringe to collect and store the pore solution during the extraction process without exposing the solution to air. Pore solutions were extracted from four different 6-month old cement paste samples. After each extraction, head air was removed from the syringe and the pore solution was then transported to a glass container in an inert environment to minimize any interactions with the air. The pore solution samples were sent to a commercial laboratory (SGS Lakefield Research) for inductively coupled plasma-optical emission spectrometric (ICP-OES) and ion chromatographic (IC) analysis.
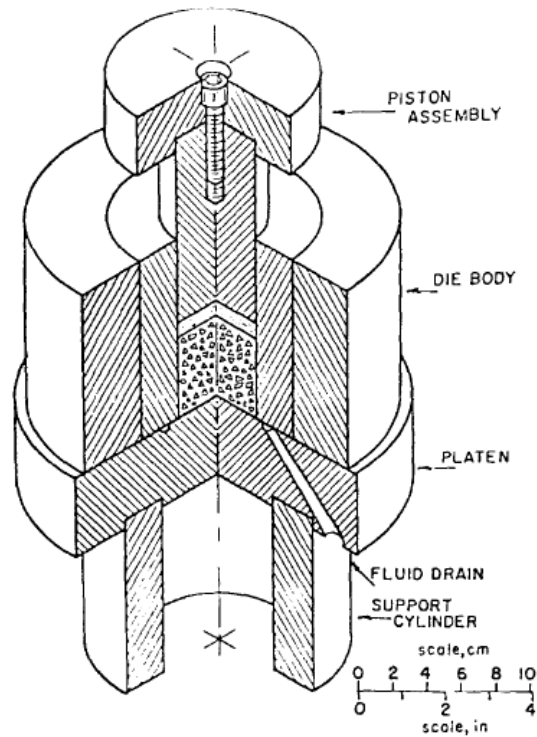
Figure 3.2: Schematic setup of the pore solution extraction
apparatus (Barneyback et al., 1981)

3.5 STABILITY OF ENTRAINED AIR BUBBLES TEST

The goal of this test was to identify the effects, if any, of wash water on the stability of entrained air bubbles over time. Beakers, containing 100mL of tap water, wash water, or 50/50 mixture of the two types of water, were set up. One millilitre of Euclid AIR-XL air entraining admixture (AEA) was added to each beaker. The solutions were simultaneously mixed for 3 minutes using magnetic stirrers. An initial visual observation was made to assess the quantity of entrained air bubbles formed on the surface of the solutions, as shown in Figure 3.3. Observations were made at 15 and 30 minute intervals to assess the stability of the bubbles over duration of 5 hours and the test was performed twice for repeatability.

Figure 3.3: Initial conditions for the entrained bubbles after mixing

3.6 PLASTIC CONCRETE TEST SETUP

3.6.1 Cement Paste Set Time

A Vicat needle test was used to determine the set time of the TL, WL, TH, and WH cement pastes, in accordance with ASTM C191 (1992). The pastes were prepared using the same mixture designs and mixing procedures as the cement pastes used in pore solution extraction described in Section 3.2.2.

The Vicat needle apparatus consists of a non-absorbent cup material and a guided needle attached to a standard weighted steel rod, as shown in Figure 3.4. The cup was filled to the top with paste, levelled, and allowed to set. The initial set time is the time required for the paste to resist penetration of the needle to 25 mm. Final set time is the time required for when the needle is unable to penetrate into the paste. Measurements were taken at 15 minute intervals beginning at 2 hours after mixing. Any measurements before 2 hours are unnecessary, as the paste is unable to resist any penetrating force. As a result, the needle penetrates straight through to the bottom, causing damage to the slender needle due to buckling.
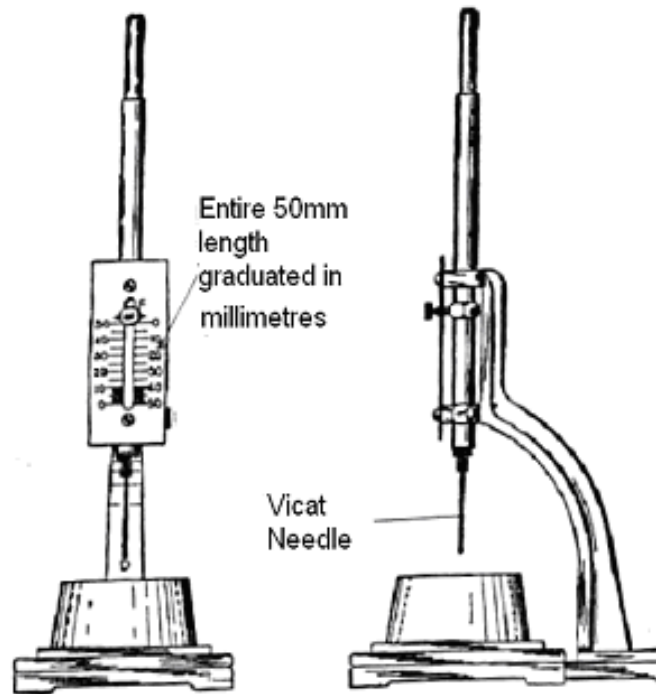
Figure 3.4: Vicat Needle apparatus (ASTM C191, 1992)

3.6.2 Air Content in Mortar

Chace indicator tests (AASHTO T199, 2000) were used to determine the air content in mortar from the TL, WL, TH, and WH concrete mixtures. The mortar mixture designs are based on the mixture designs for concrete prepared in the lab, except without coarse aggregate. The same mixing procedures were used as described in Section 3.2.2.

The Chace indicator apparatus contains a brass base cup and a glass tube with a stem indicator, as seen in Figure 3.5. The brass cup is filled with mortar, levelled, and then the glass tube is securely placed over it. Isopropyl alcohol is then used to fill the glass tube up to the initial stem level. After closing the stem end, the Chace indicator is lightly agitated for 30 seconds to allow the mortar and alcohol to mix. It is then brought back to an upright position and the small plug is released. The measurement is taken by reading the level of alcohol in the stem to the nearest half graduation.

Figure 3.5: Chace indicator apparatus

3.7 STRENGTH TESTS

Two types of tests were performed on concrete cylinders and prisms to determine the compressive and tensile strength. The concrete used for strength tests are the concrete provided by Dufferin Concrete, shown in Table 3.2.

3.7.1 Compression Test

Standard cylindrical plastic moulds with dimensions of 100 mm diameter by 200 mm were used to make concrete cylinders. Each concrete cylinder was poured in 3 layers and each layer was rodded 25 times using a 10 mm diameter rod, in accordance with ASTM C192 (2002). The cylinders were wet cured with burlap and plastic for the first two days, removed from the mould, and then air cured for the duration of time, as specified in the standard practice for making and curing concrete in the field (ASTM C31, 2003). The cylinders were capped with a high strength sulphur capping compound to level the ends of the cylinder. They were then allowed to harden for 4 to 6 hours before testing. All samples were visually inspected for any defective caps, as the quality of the cap is operator dependent.

41

Compressive tests were performed on concrete cylinders to determine the compressive strength, according to ASTM C39 (2003). The cylinders were tested at 3, 7, 28, and 56 days. Each sample was placed in the centre of the Forney Testing Machine Model QC50DR, seen in Figure 3.6, and loaded until failure.

Figure 3.6: Concrete cylinder compression test

3.7.2 Flexural Test

Standard 150 x 150 x 525 mm concrete prisms were cast in wooden moulds. The concrete was poured in 2 layers and compacted using a vibrator for each layer. The beams were wet cured with burlap and plastic for the first two days, then removed from the mould, and air cured for the duration of time as specified in the standard practice for making and curing concrete in the field (ASTM C31, 2003).

Flexural tests, based on the ASTM C78 Standard Test Method for Flexural Strength of Concrete, were used to determine the tensile strength of concrete (ASTM C78, 2002). Concrete beams were subjected to a four-point bending load, as shown in Figure 3.7. The support length was 450 mm and two point-loads are placed at the centre of the beam, 150 mm apart.
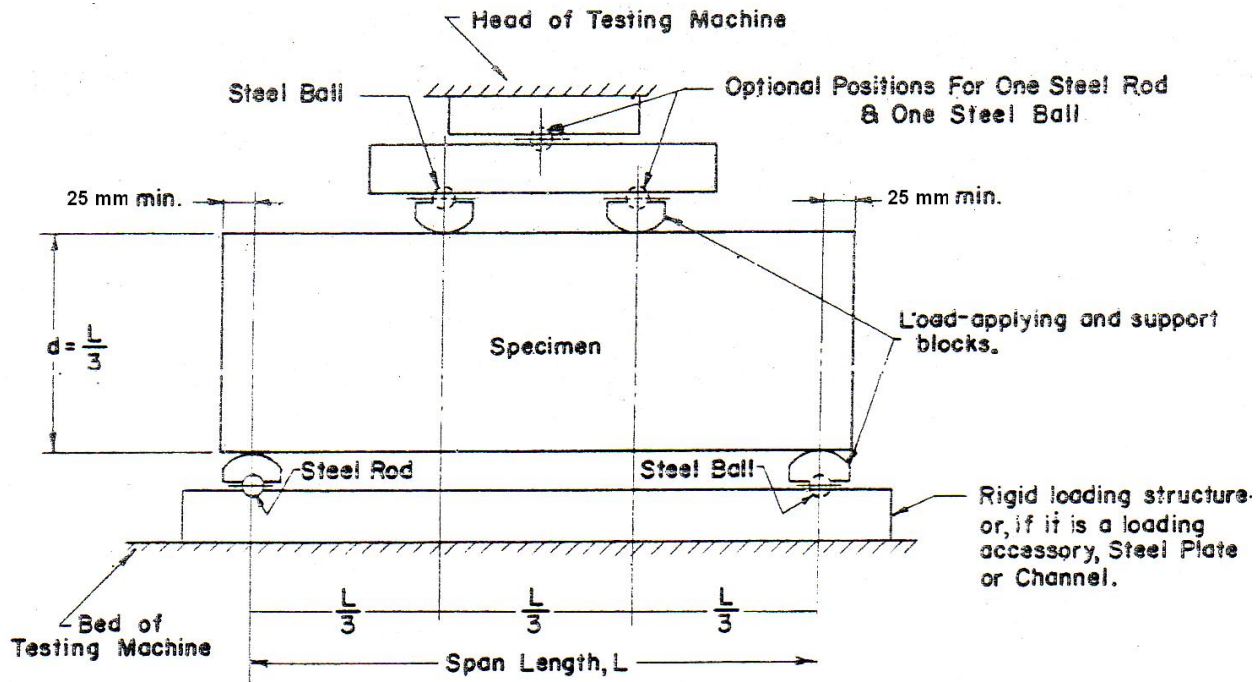
Figure 3.7: Flexural test on standard concrete prism (ASTM C78, 2004)

The prisms were tested on a MTS 810 Testing System frame at a loading rate of 7 kN/minute. Each beam was tested until rupture and all of the fracture planes were required to be in between the two point load as shown in Figure 3.8. The peak load recorded by the MTS system was used to determine the modulus of rupture (stress) using Equation 3.1 from ASTM C78 (2004)

$$\sigma_r = \frac{PL}{bd^2}$$ Equation 3.1

where P is the peak load, L is the length of the support span, b is the average width of the beam, and d is the average depth of the beam at the fracture surface. The prisms were tested at 7, 28, and 56 days. Three specimens were tested for each type of concrete.

43

Figure 3.8: Flexural test on standard prism mode of failure

3.8 SALT SCALING RESISTANCE TEST SETUP

The resistance of the concrete to salt scaling was evaluated using concrete slabs tested in accordance with ASTM C672 (2003) and evaluated using the MTO LS-412 (2006) standard. Four concrete slabs were cast for each laboratory concrete mixture design shown in Table 3.2. The concrete was mixed according to standard practice for making and curing concrete test specimens in the lab (ASTM C192, 2002). Four specimens were made per mixture design, for a total of 16 specimens. However, only three specimens were available for the experiment as one concrete slab per mixture design was used as a dummy cell to monitor the internal temperature of the concrete during the freeze-thaw cycling.

The specimens were cast in two lifts to provide the desired specimen design. The dimensions of the slab were chosen to meet the minimum required exposed area of 0.045 m^2 and 75 mm depth specified by ASTM C672 (2003). The concrete slabs were first cast with the following dimensions: 266 x 266 x 76 mm, as shown in Figure 3.9. Then, the slabs were broom finished approximately 1 hour after casting, or when all the bleeding on the concrete surface has stopped. The broom finish was selected for the concrete surface, as it gives a more realistic representation

of concrete surfaces in service, such as sidewalks and road pavements. Shortly after brooming, a second cast was done to create an extra 25 mm high mortar dike. A plastic liner was used to enclose a 216mm x 216mm square area of the broom-finished concrete surface, as seen in Figure 3.10. The dike and plastic liner were used as a ponding well to hold the de-icing solution.
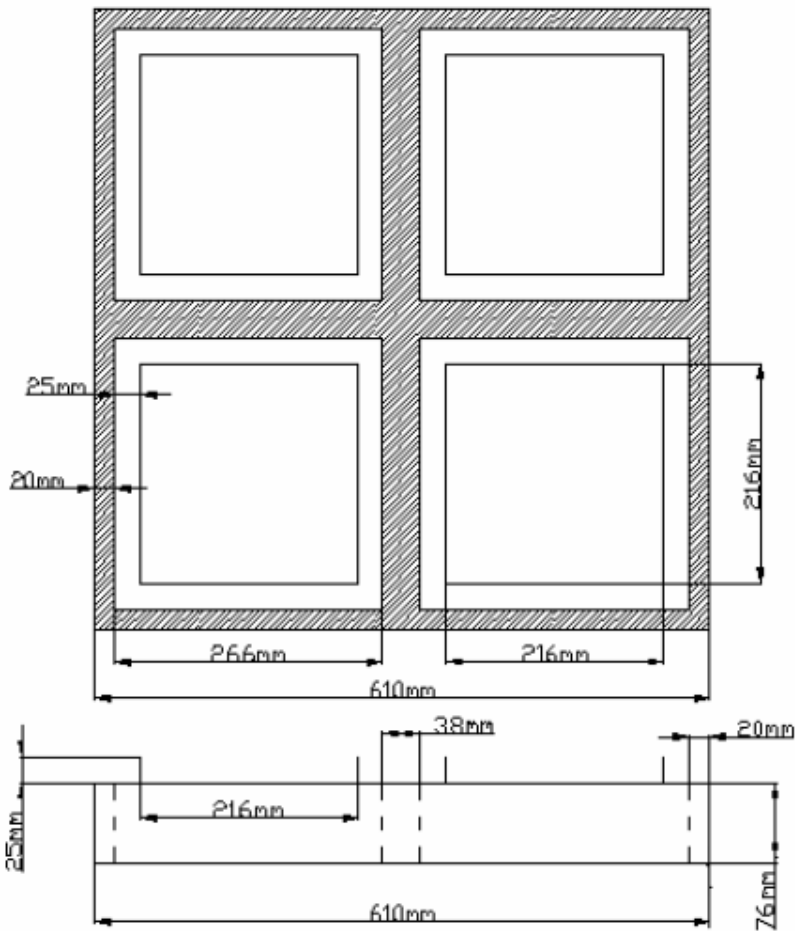
Figure 3.9: The dimensions of the concrete slab moulds

The concrete slabs were cured with wet burlap and a plastic sheet for the first two days before being removed from the moulds. They were wet cured for an additional 12 days in the humidity room followed by two weeks of air dry curing following the requirements of ASTM C672. After the slabs were air cured, a two part Sika epoxy was used to seal the inside perimeter of the ponding well to prevent leakage.
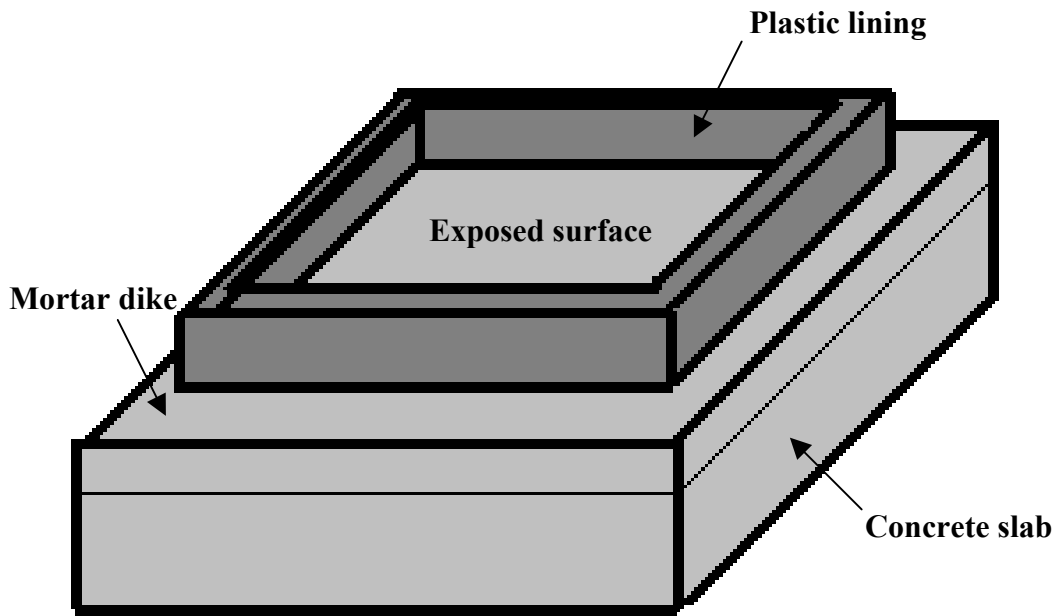
Figure 3.10: Concrete slab used in salt scaling test

The specimens were placed in the environmentally controlled chamber and the ponding well was filled with a solution of 4% anhydrous calcium chloride in tap water. A minimum cover depth of 6 mm salt solution was maintained at all times during the experiment. In the environmental chamber, the specimens experienced temperature cycling of $-18 \pm 3°C$ for 17 hours followed by $23 \pm 3°C$ for 7 hours. The relative humidity was kept at 45% to 55% for the duration of the test. The idea was to expose the concrete surface to freezing and thawing conditions in the presence of de-icing salts, simulating a mild winter pattern in a northern climate.

After every 5 cycles, the test was stopped for a visual evaluation (ASTM C672, 2003). Since the nature of a visual inspection is very subjective (Pigeon and Pleau, 1995), an alternative mass loss assessment method was also used to quantify the severity of the damage (MTO LS-412, 2006). Mass loss due to scaling of the concrete surfaces was collected and weighed every 5 cycles. In addition, detailed pictures of the concrete surfaces were taken to quantify the amount of scaled area. The scaled area was determined using AutoCAD, as shown in Figure 3.11. The accumulative mass loss was recorded at the specified intervals, up to a total of 50 cycles, to

determine the performance of the concrete surfaces. At the end of the test, air void system in each concrete was characterized.
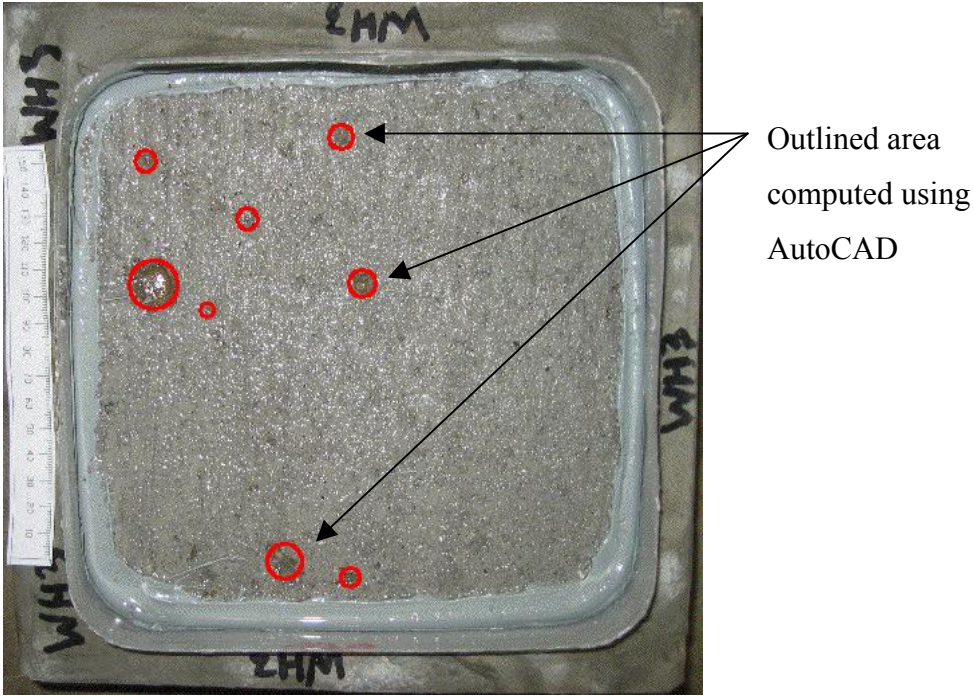
Figure 3.11: Evaluation of a surface scaled area using AutoCAD

3.9 HARDENED CONCRETE AIR VOID TEST

Hardened concrete air void analysis tests were performed using the ASTM C457 (1998) Procedure A: Linear Traverse and Procedure B: Modified Point Count method to determine the total air content.

As indicated previously, entrained air in concrete is essential for freeze-thaw durability. A 100 x 100 x 15 mm concrete sample was wet cut from the centre of each of the TH and WH concrete slab from the salt scaling test as shown in Figure 3.12 and used for a hardened air void analysis. Only the TH and WH concrete slabs were analysed, because they were air-entrained, whereas the TL and WL concrete slabs were not.
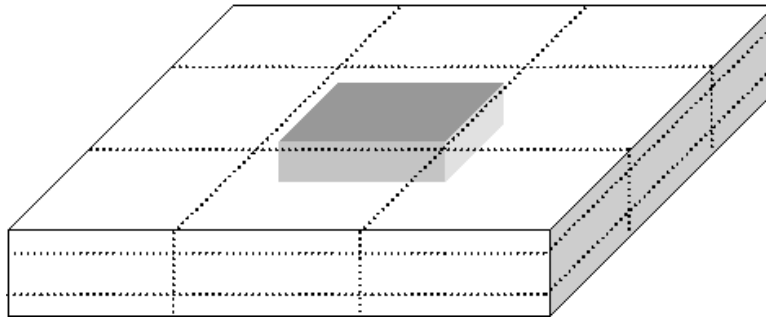
Figure 3.12: Cut specimen used for air void analysis

3.9.1 Sample Preparation

A pre-grinding stage was required as during the cutting of the sample, there are deep saw marks of depression or bump observed. A grinding block was used to remove all noticeable saw marks. At this point, the sample was inspected to ensure that the 100 x 100 mm surface was flat. This stage is critical to the quality of sample preparation, and also has a large impact on the time it takes to prepare the sample in subsequent steps.

The specimen was mounted on a custom-made PVC block using heavy-duty double-sided 3M adhesive tape. This allowed the block, along with the specimen, to be fastened to a single specimen holder. Several PVC blocks were made in order to prepare multiple samples without needing to remove the double-sided tape in between grinding. The block could be fastened and removed quickly from the single specimen holder shown in Figure 3.13.

The grinding stage was performed using the Leco Spectrum 2000 automatic grinding system in the following steps:

1. The specimen was thoroughly rinsed to remove all debris and dried in air.

2. A wax-based crayon was used to draw a grid pattern on the surface, which indicated if the surface has been evenly ground.

3. A thin layer of diluted lacquer, containing 1 part lacquer to 5 parts acetone solution was applied to the drawn surface of the specimen and allowed to dry in air. The lacquer helps to prevent pull-out of particles during the grinding processes.

4. The specimen holder containing the PVC block and concrete sample was mounted on the automatic grinding machine.

5. Silicone carbide adhesive-backed grinding paper with a grit size number of 60 was selected for the first step in the following grinding program:

    a. Load 5 to 10 lbs (22 to 44 N) of force in the centre.

    b. The table speed was set to 100 rpm clockwise and the head speed to 60 rpm in the counter-clockwise direction.

    c. Water was used as a lubricant for the duration of the grinding step, which takes approximately 5 minutes.

6. After completing each grit size, the concrete specimen surface was examined for crayon marks. If all the markings had been removed, another check was done to see if the surface is flat by using a straight edge placed along the surface. If any light could be seen shining between the straight edge and the surface, then the surface was not level. When the crayon and straight edge check conditions had both been satisfied, steps 1 to 5 were repeated using grit size number 120, 320, and 600, in turn. If either condition was not satisfied, step 5 was repeated.

7. After completing each grit number, the concrete sample was examined under the stereomicroscope. The grinding procedure was carried out until the concrete appeared to be free of scratches. For accurate analysis the paste should appear smooth, without any ripping or tearing, and the air void edges should be sharp. From experience, this occurs only after grinding with grit number 320 or higher.

8. After completing the grinding steps, the concrete sample was dipped into a shallow bath of acetone to remove any lacquer that might have been left. The prepared sample,

shown in Figure 3.14, was then ready to be coloured and impregnated with barium sulphate ($BaSO_4$) powder for use in the Rapid Air System.
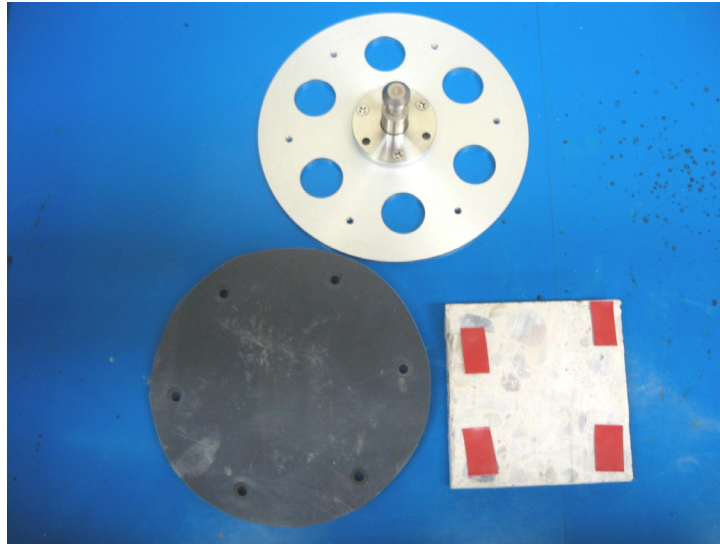
Figure 3.13: Mounting concrete specimen holder
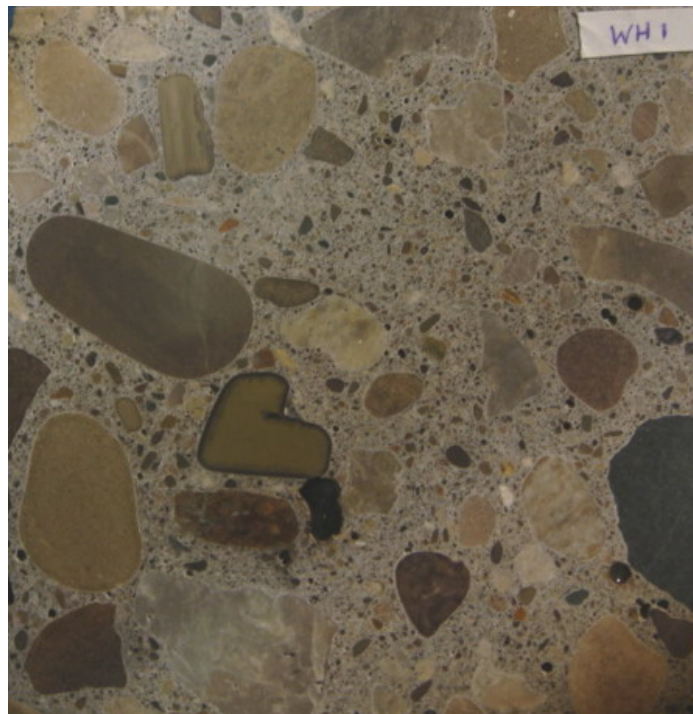
Figure 3.14: Prepared concrete sample after grinding

To use the Rapid Air System, the entrained air voids need to be markedly different from the paste and aggregates. Following steps were used for impregnation:

1. A wide flat tip permanent black marker was used to colour the entire sample surface moving in one direction, one line at a time. Then the ink was allowed to dry thoroughly before applying a second layer of black marker.

2. Barium sulphate powder was sprinkled on the surface and using a large rubber stopper to firmly press the powder into surface.

3. Excess powder was removed from the surface using a rubber stopper edge by dragging it across the surface on an angle. Then clean the remaining powder off the surface of the specimen with the palm of the hand in circular motion until the surface appeared free of powder and shiny.

4. With a fine tip permanent marker, colour all the aggregates with voids to prevent aggregate voids from being mistaken as an entrained air void.

5. The coloured sample, like the one shown in Figure 3.15, was ready to analyse.
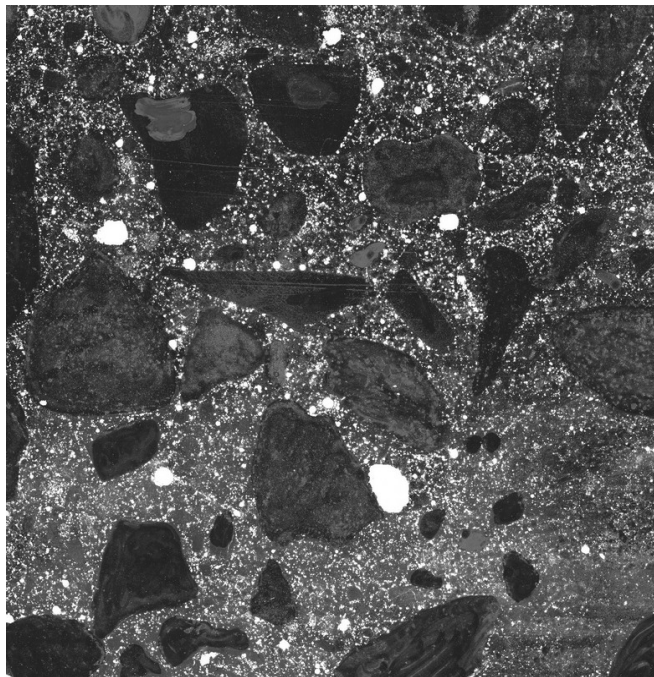
Figure 3.15: Coloured sample ready for air void analysis

3.9.2 Rapid Air System

Hardened air void analyses were performed using the Rapid Air system, manufactured by Concrete Experts International (CXI). The instrument, seen in Figure 3.16, is able to measure the air void system in accordance with ASTM C457 (1998) using two different procedures.
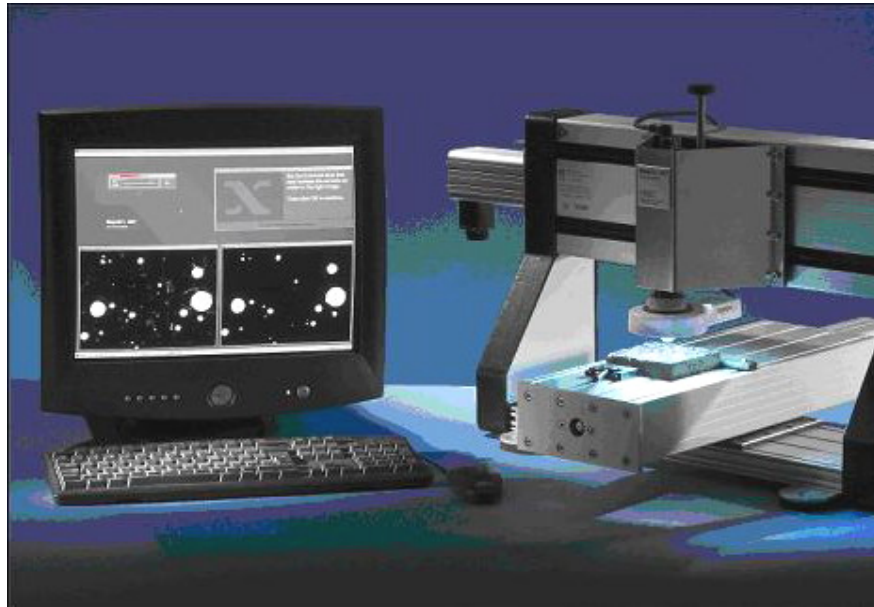
Figure 3.16: Rapid Air system

3.9.2.1 Procedure A: Linear Traverse

This procedure is used to determine the percentage of air voids (A), average chord length ($\bar{l}$), paste-air ratio $\left(\dfrac{p}{A}\right)$, and spacing factor ($\bar{L}$) using Equation 3.2 to Equation 3.6. The spacing factors given by Equation 3.5 and Equation 3.6 were based on two air void model presented by Powers (1954) depending on the paste to air void ratio.

$$A = \frac{T_a}{T_t} x 100$$

Equation 3.2

$$\bar{l} = \frac{T_a}{N}$$

Equation 3.3

$$\frac{p}{A} = \frac{T_p}{T_a}$$

Equation 3.4

$$\overline{L} = \frac{T_p}{4N} \quad if \; \frac{p}{A} \le 4.342$$

Equation 3.5

$$\overline{L} = \frac{3}{\alpha}\left[1.4\left(1+\frac{p}{A}\right)^{1/3} - 1\right] \quad if \; \frac{p}{A} > 4.342$$

Equation 3.6

where T_a = total traverse length over air voids, T_t = total traverse length, N = number of air voids, T_p = total traverse length over paste, p and A are the total paste and air contents. The analysis occurs along a series of evenly spaced lines, as shown in Figure 3.17. The minimum traverse length for a 100 x 100 mm concrete sample with 19 mm maximum size coarse aggregate is 2286 mm (ASTM C457, 1998).
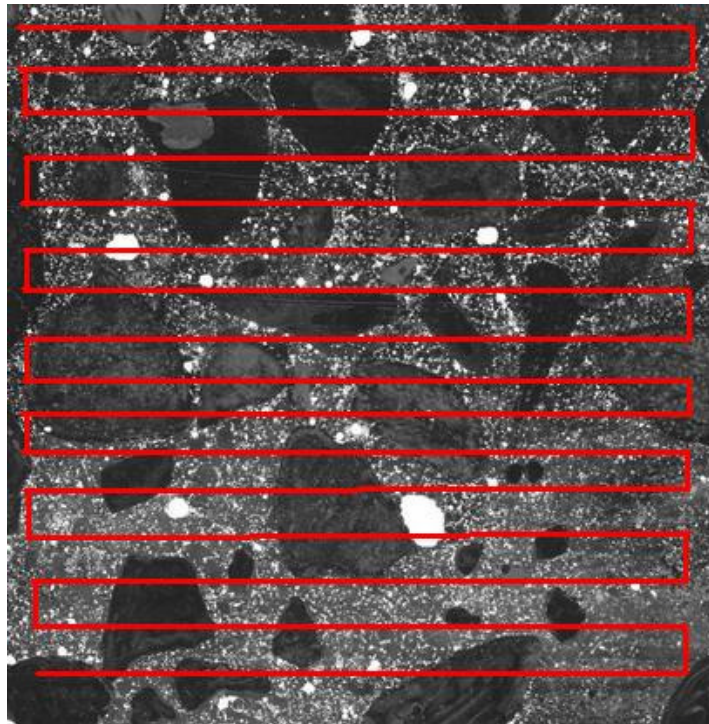
Figure 3.17: Procedure A - Linear traverse method

The following settings were used to analyse the concrete specimens, because they produced the most consistent results and met the requirements of ASTM C457 (1998):

1. Threshold value = 130, light = 7, contrast = 90

2. Traverse length = 3000 mm and analysed area = 90 x 90 mm

3.9.2.2 Procedure B: Modified Point Count

This procedure is used to determine the air, paste, and aggregate contents, using Equation 3.7 to Equation 3.9. The method operates by determining whether a point should be classified as air, paste, or aggregate. Analysis occurs along a series of points in a grid system, as shown in Figure 3.18. To help distinguish the difference between aggregate and paste, a modified point count must be carried out before colouring the sample surface. The advantage of using a modified point count is in determining the paste and aggregate content of concrete, in absence of a mixture design, as in most forensic petrographic examinations (ASTM C856, 2004). However, the disadvantage of using this method is operator bias, because the results are highly operator dependent.

$$Air \ content \ \% = \frac{No. \ of \ air \ counts}{Total \ point \ count} \times 100 \qquad \qquad \text{Equation 3.7}$$

$$Paste \ content \ \% = \frac{No. \ of \ paste \ counts}{Total \ point \ count} \times 100 \qquad \qquad \text{Equation 3.8}$$

$$Aggregate \ content \ \% = \frac{No. \ of \ aggregate \ counts}{Total \ point \ count} \times 100 \qquad \qquad \text{Equation 3.9}$$
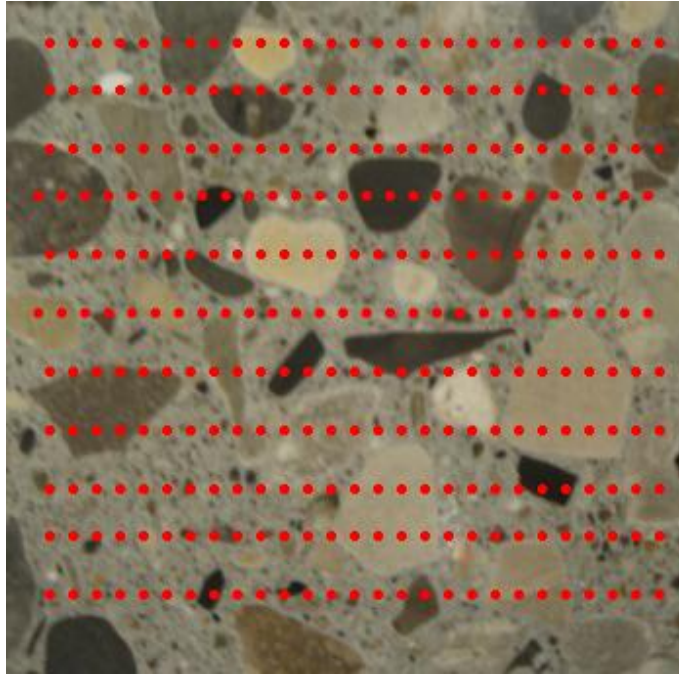
Figure 3.18: Procedure B - Modified point count

3.10 CORROSION TESTS

Corrosion monitoring tests were performed on standard G109 corrosion specimens (ASTM G109, 1999). Five G109 specimens were made from each of the four types of concrete mixtures. Dufferin Ready-Mix Concrete provided the concrete. The G109 samples were cast from the same concrete used in the strength tests.

3.10.1 G109 Specimens

A standard G109 sample consists of a concrete block with three embedded reinforcing bars and a ponding well, as shown in Figure 3.19. Special moulds were prepared to modify the standard G109 specimens to include a cast-in-place concrete ponding well, as seen in Figure 3.20. The prisms were cast upside down to produce a 75 x 75 x 150 mm cast-in-place ponding well. The ponding well blocks were made from high-density Styrofoam in order to facilitate the demoulding phase after cast. Three 10 mm diameter black steel rebars were cast into each prism. One rebar was centred in the top layer and two rebars were placed in the bottom layer at equal distance from the sides. The multiple rebars were used to enhance macro-cell corrosion, as a

larger cathodic area would result in a greater reduction reaction for the dissolution of metal at a smaller anodic site, leading to a higher corrosion rate (Jones, 1996). A 25 mm concrete cover depth was used on all prisms. Each rebar had one end drilled for the attachment of a copper wire using solder. The rebars were then coated with three layers of epoxy at both ends, leaving 200 mm of exposed length each within the prisms.

The G109 prisms were cast and wet cured with burlap and plastic sheet for the first two days and then air cured for 12 days, in accordance with the ASTM G109 standard (1999). Then the specimens were coated with 2 layers of epoxy on all vertical concrete surfaces. The specimens were exposed to 3 % chloride solution 4 weeks after they were cast for macro-cell and micro-cell corrosion studies.
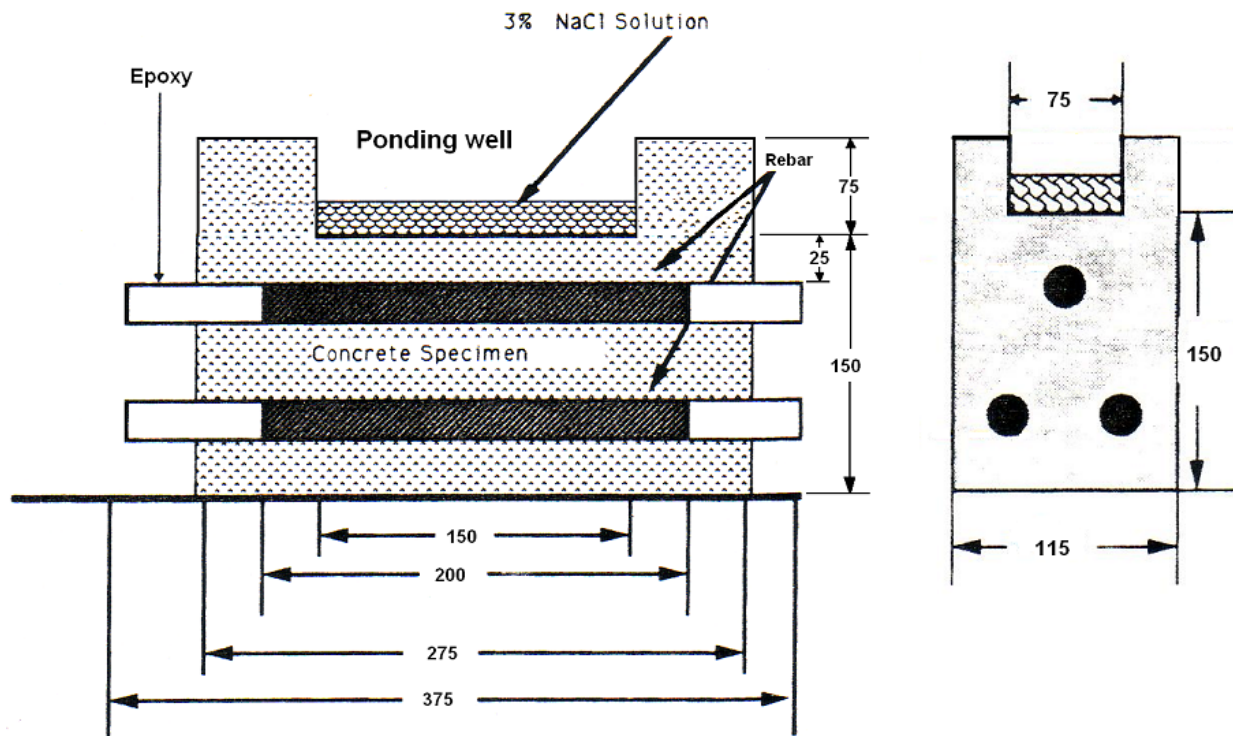
Figure 3.19: Profile view of a standard G109 specimen (ASTM G109, 1999)
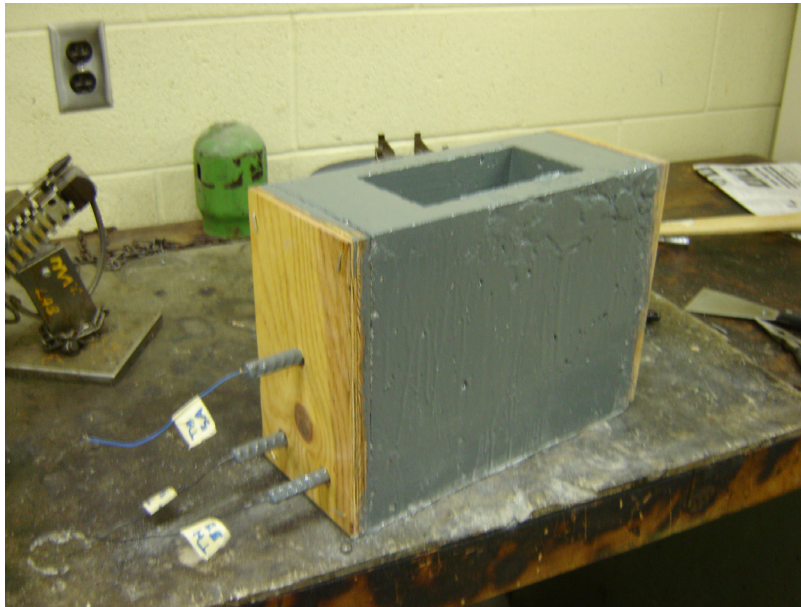
Figure 3.20: Modified G109 specimen with a cast-in-place ponding well

3.10.2 Exposure Conditions for Reinforcement Corrosion Studies

The ponding wells were filled with a minimum of 400 mL of 3 % chloride solution for the two weeks of every four, starting 28 days after casting. Plastic sheets were used to cover the ponding well to minimize evaporation. The wetting and drying cycles increase the driving force of chloride diffusion into concrete, therefore promoting faster corrosion initiation.

3.10.3 Macro-Cell Corrosion Measurements

In the macro-cell corrosion setup, the two lower rebars were connected to each other, and the top and bottom layers were connected through a 100 Ω resistor. The macro-cell corrosion current was calculated using Ohm's Law, given by Equation 3.10, from the measured potential, V, across the resistor. The corrosion density (i_{corr}) was calculated by dividing the current by the assumed corroded area. One third of the exposed area of the top rebar was used as a nominal corroding area.

All twenty G109 specimens were connected to a Keithly Model 2750 multimeter switch system. The potentials were regularly monitored during exposure testing using ExcelLinx software, which was programmed to measure the potential at the end of each wet and dry cycle. The electrical connections were inspected regularly over the duration of the study.

$$I = \frac{V}{R} = \frac{V}{100 \ \Omega}$$

Equation 3.10

3.10.4 Micro-Cell Corrosion Measurements

Micro-cell corrosion measurements of the top bars were performed at the beginning and end of each wet cycle using the linear polarisation resistance (LPR). In addition, the saturated calomel electrode (SCE) was monitored to evaluate the probability of corrosion and galvanostatic pulse and electrochemical impedance spectroscopy (EIS) techniques were used to assess the concrete electrical resistance.

The micro-cell corrosion measurement setup consisted of a saturated calomel reference electrode, a stainless steel counter electrode placed in the ponding well, and the top rebar as a working electrode. They were connected to a poteniostat/galvanostat model Parstat 2263-2, manufactured by Princeton Applied Research (PAR), as shown in Figure 3.21. Corrosion potential, current, and concrete resistance were measured using PowerSuite software.

The linear polarization resistance corrosion measuring technique was used to measure the corrosion current, which can be converted to corrosion rate using Faraday's Law. Stern and Geary (1957) observed the linear relationship between applied potential and corrosion current when ± 10 mV from the open circuit potential was applied, as illustrated in Figure 3.22.
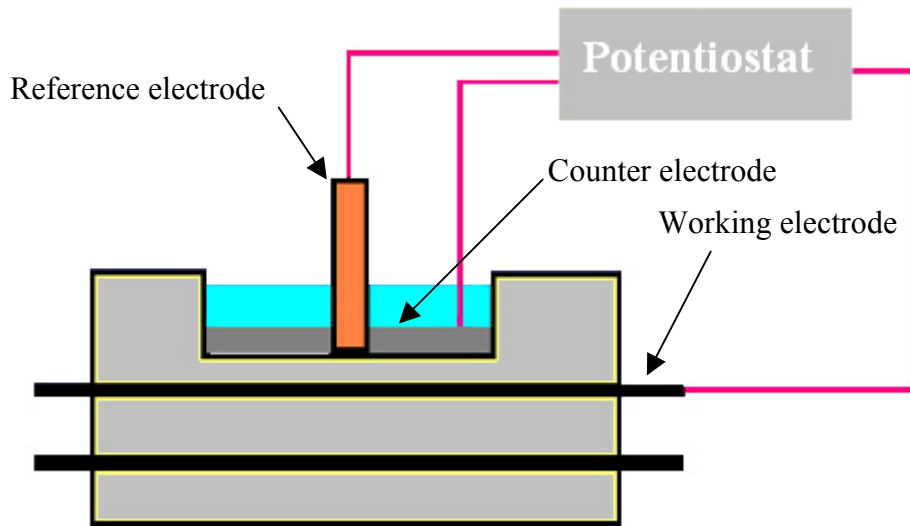
Figure 3.21: G109 micro-cell corrosion measurement setup
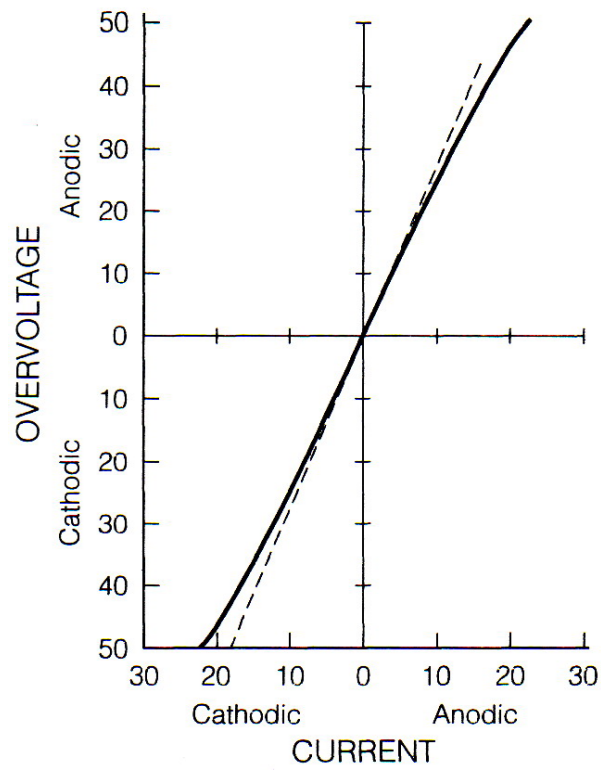
Figure 3.22: Linear behaviour of a polarization resistance curve (Jones, 1996)

In the case of steel in concrete, ± 20 mV is used to compensate for the resistance of the concrete. Thus, the corrosion current was determined by applying ± 20 mV from the open circuit potential (E_{corr}) and then measuring the resulting steady state current, as shown in Figure 3.23. The polarization resistance (R_p) was calculated using Equation 3.11. The term B is the proportionality constant, which is calculated using Equation 3.12, where β_a and β_c are Tafel slope constants for the anodic and cathodic curves. Andrade and Gonzalez (1978) concluded B constant to be 0.026 V and 0.052 V for active and passive corrosion conditions of black steel in concrete, respectively. After obtaining R_p, the corrosion current (I_{corr}) was calculated using Equation 3.13. Finally, the corrosion density (A/m²) was calculated by dividing the corrosion current by the corroded area, which was assumed to be one third of the exposed area of the rebar.
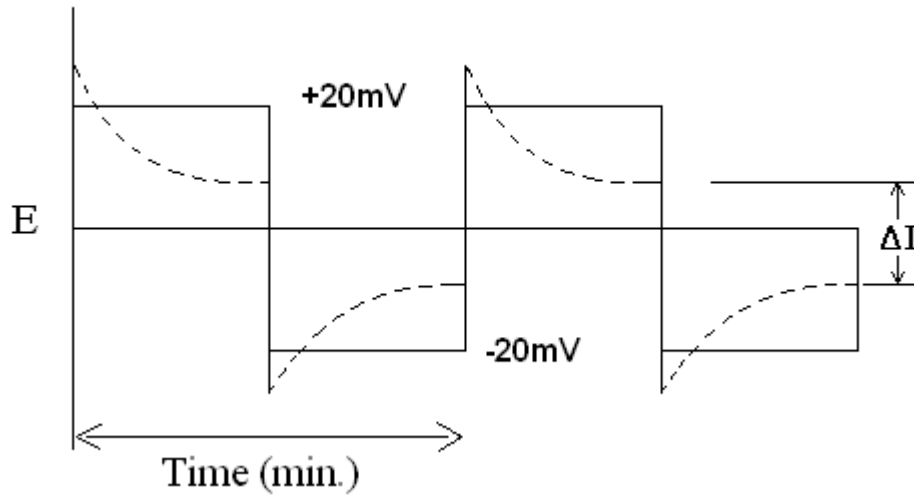
Figure 3.23: Applied potential and resulting current plot

$$R_p = \frac{\Delta E}{\Delta I_{app}}$$

Equation 3.11

$$B = \frac{\beta_a \beta_c}{2.3(\beta_a + \beta_c)}$$

Equation 3.12

$$I_{corr} = \frac{B}{R_p} = \frac{0.026}{R_p}$$
<div style="text-align:right">Equation 3.13</div>

3.10.4.1 Half –Cell Potential

The half-cell potential (E_{corr}) measuring technique measures the potential energy difference between the working electrode and a known reference electrode, which, in this case, was a saturated calomel electrode. The ASTM C876 (1999) uses the following half-cell potential interpretation guideline:

1. < -350 mV vs. Cu/CuSO$_4$ electrode (-280 mV vs. SCE) correspond to a greater than 90 % probability of corrosion occurring

2. > -200 mV vs. Cu/CuSO$_4$ electrode (-130 mV vs. SCE) correspond to a greater than 90 % probability of no corrosion occurring

3. Between -200 mV and -350 mV vs. Cu/CuSO$_4$ electrode correspond to the uncertainty of corrosion occurring

3.10.4.2 Electrical Concrete Resistance

The electrical resistance of concrete was monitored using two types of techniques: galvanostatic pulse and EIS techniques. Both of the techniques use the Parstat equipment and the same setup as the LPR technique.

The galvanostatic pulse technique was used to measure the resistance of the 25 mm concrete cover depth over the top rebar. The technique operates by applying a constant current of 25 μA for three seconds and measuring the responding potential, as shown in Figure 3.24. The instantaneously rise in potential (ΔE) is attributed to the Ohmic electrolyte resistance between the working and reference due to the applied current applied used to polarize the system (Jones,

1996). Therefore, using Ohm's law, the concrete resistance (R_Ω) can be calculated using Equation 3.14.
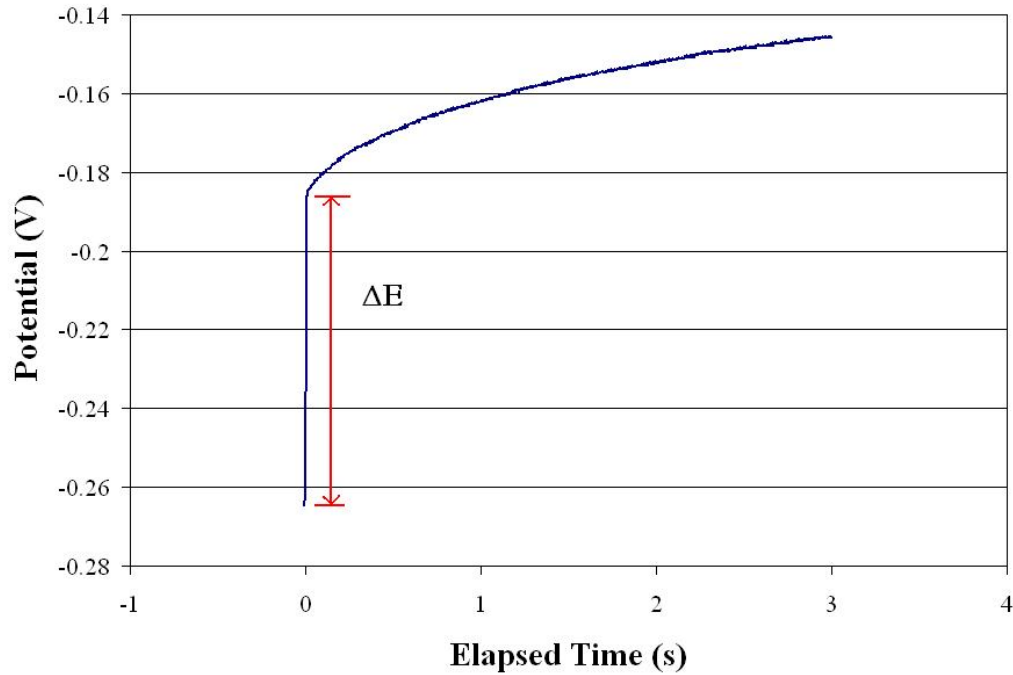
Figure 3.24: Plot of potential vs. time of concrete resistance using galvanostatic technique

$$R_\Omega = \frac{\Delta E}{25\,\mu A}$$

Equation 3.14

Electrochemical impedance spectroscopy is another technique that can be used to evaluate concrete resistance. The technique involves the application of an AC voltage across the surface of the working electrode and in the presence of a Helmholz double layer on the surface of the steel. The response can be modeled as a Randle circuit cell, as shown in Figure 3.25. At low frequency, the double layer capacitor acts similar to an open circuit and at high frequency the capacitor is electrically connected, by-passing the resistor (Fontana, 1986). A typical plot of imaginary versus real impedances can be seen in Figure 3.26 in a Nyquist plot. By applying a

high AC frequency voltage in the range of 2 MHz to 0.1 Hz, the technique was use to evaluate the concrete resistance (R_e), as shown in Figure 3.27.
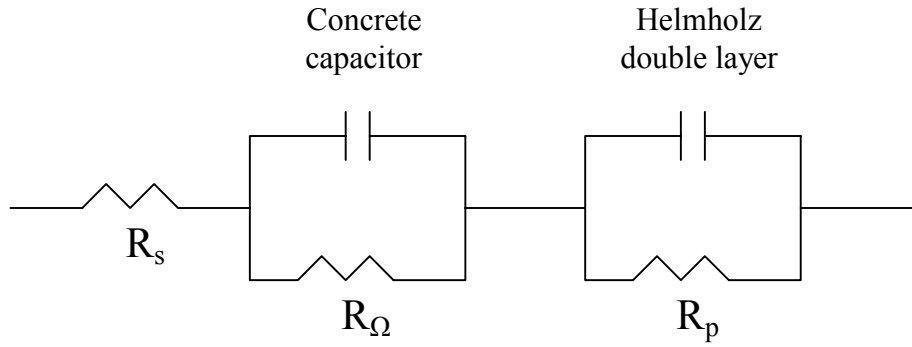
Figure 3.25: A simplified EIS circuit model of an equivalent concrete system
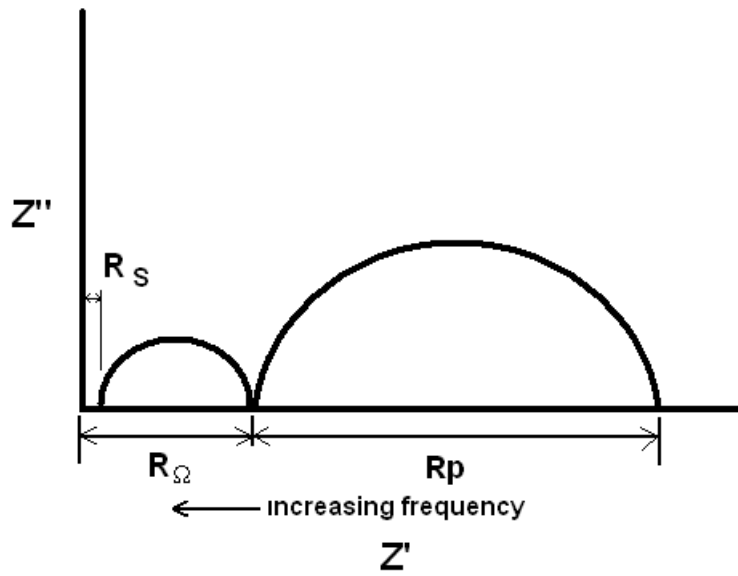
Figure 3.26: Schematic diagram of a Nyquist plot
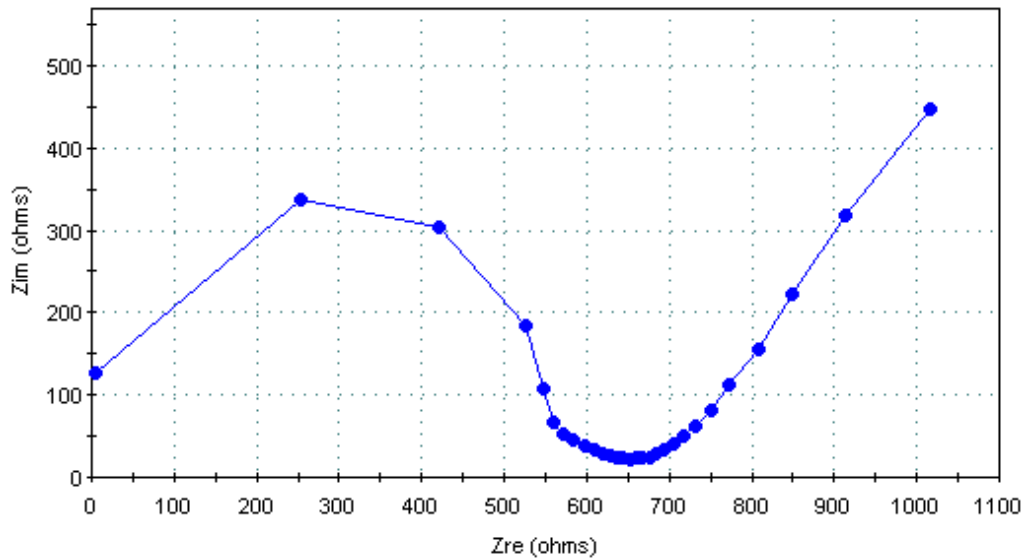
Figure 3.27: Nyquist plot of concrete impedance using EIS technique

3.11 THERMOGRAVIMETRIC ANALYSIS TEST METHOD

A thermogravimetric analysis (TGA) was used to determine any difference in cement pastes prepared with wash water and those prepared with tap water. This was performed by comparing the mass loss as a function of temperature (thermogram) due to the evaporation of water and decomposition. The differential thermogravimetric curve (DTG), accentuates the temperature range at which the mass loss occurs as peaks.

Hardened cement paste cylinders, which were prepared for pore solution extraction from section 3.2.2, were also used for thermogravimetric analysis (TGA). The cylinders, which were 6 months old at the time of TGA analysis, were dried and then crushed to a fine powder. Cement paste powders were analysed using the TA Instrument with ceramic crucibles, as seen in Figure 3.28. The test was performed using the following settings:

1. Heating rate, 10 ºC/minute.

2. Temperature range, 40 to 800 ºC.

3. Helium gas for inert environment.

4. Baseline calibration parameters:

    a. Limits 51.79 and 794.64 ºC

    b. Slope 9.6341

    c. Offset −17.776

    The baseline calibration parameters are the parameters that were collected in a dry run in the same heating condition as the test run.

Each cement paste powder sample was tested at least two times using the same configuration each time.

Figure 3.28: Thermogravimetric analysis equipment

CHAPTER 4

EXPERIMENTAL RESULTS AND DISCUSSION

4.1 GENERAL

This chapter presents the results of all the tests described in the experimental program. A detail discussion for each of the tests is also presented following the results.

4.2 MIXING WATER ANALYSIS

In order to analyze any differences between the behaviour of concrete made with wash water and that of concrete mixed with tap water, the mixing waters were analyzed. Inductively coupled plasma-optical emission spectrometry (ICP-OES) and ion chromatography (IC) were used to determine the cations and the anions in wash water (WW), respectively. Alkalinity tests were also performed to determine the OH^- and HCO_3^- concentrations. The wash water analyses were obtained from the University of Waterloo Earth Science lab on January 2006. Tap water (TW) analyses were obtained from the Kitchener Municipal Water Report 2005 (Regional Municipal of Waterloo, 2005). The wash water composition presented in Table 4.1 is a summary of the analysis and it represents the average value of four tests. The complete water analysis can be found in Appendix A. The composition of the tap water presented in Table 4.1 is taken from the "Kitchener Water Quality Report" (Regional Municipality of Waterloo, 2005) and the values represent the monthly average found at the Manheim Pumping Station, the closest water station to Dufferin Concrete. Also included in the table are the maximum allowable limits according to CSA A23.1-04 (2004).

From the analyses, it can clearly be seen that wash water contains substantially higher concentrations of solids, Cl^-, and SO_4^{2-} than tap water. But they are still below the optional limit

according to ASTM C94 (2004) and CSA A23.1-04 (2004). Optional requirements suggests that the concrete producer only needs to comply with the limit if the purchaser specifically requests it (NRMCA Information, 2005); otherwise, there is no restriction on solid content, as long as the concrete producer can show that wash water concrete meets compressive strength (Section 4.6.1) and set time (Section 4.5.1) requirements. Also, elevated concentrations of alkali metal, in the form of Ca^{2+}, Na^+, and K^+, were detected in wash water, whereas only traces of alkali metals were detected in tap water. Currently, the limit on alkali metal concentrations is 500 mg/L and the limit on the total equivalent alkali as Na_2O is 600 mg/L. Both of which are optional limits. The elevated pH of 12.4 was attributed to the high concentration of alkali metals detected in wash water.

Table 4.1: Analyses of wash water compared with municipal water report

	Solids mg/L	Cl⁻ mg/L	SO_4^{2-} mg/L	Ca^{2+} mg/L	Na^+ mg/L	K^+ mg/L	$Na_2O + 0.658K_2O$ Sodium equivalent mg/L	pH
TW	675	38	54	71	18	<5	28	7.5
WW	5730	178	1275	787	173	810	875	12.4
Limit*	50000	500	3000	--	--	--	600	--

*CSA A23.1-04, 2004

As expected, there were significantly more solids detected in the wash water than in the tap water. The reported solid content was 5730 mg/L (~0.5 % by weight), which is consistent with a wash water analysis by Su et al. (2002) of 4200 mg/L. To confirm the measured value, samples of wash water were evaporated in a petri dish.   The solid content, which includes fine particulates such as sand, was again found to be 0.5% by weight. Dried samples of the residue were observed under an optical microscope and the micrograph is shown in Figure 4.1. Sandrolini and Franzoni (2001) confirmed that the evaporated wash water residue was primarily $CaCO_3$, and traces of SiO_2 were also detected using X-ray diffraction. Currently, the optional limit for total solids specified by both CSA A23.1-04 (2004) and ASTM C94 (2004) for water used in making concrete provision is 50000 mg/L (5 % by weight), and thus the wash water analysis for solids was found to be well below the optional limit.

The chloride content found in wash water was approximately five times higher than in tap water. It may have come from the cement, slag, aggregates, and/or chemical admixtures used in the washed-out concrete. Traces of chloride can be found in the production of cement and slag (Taylor, 1990). Chloride can also be found in aggregates, which contributes to the total chloride content found in concrete. Chlorides may also be present in some chemical admixtures.
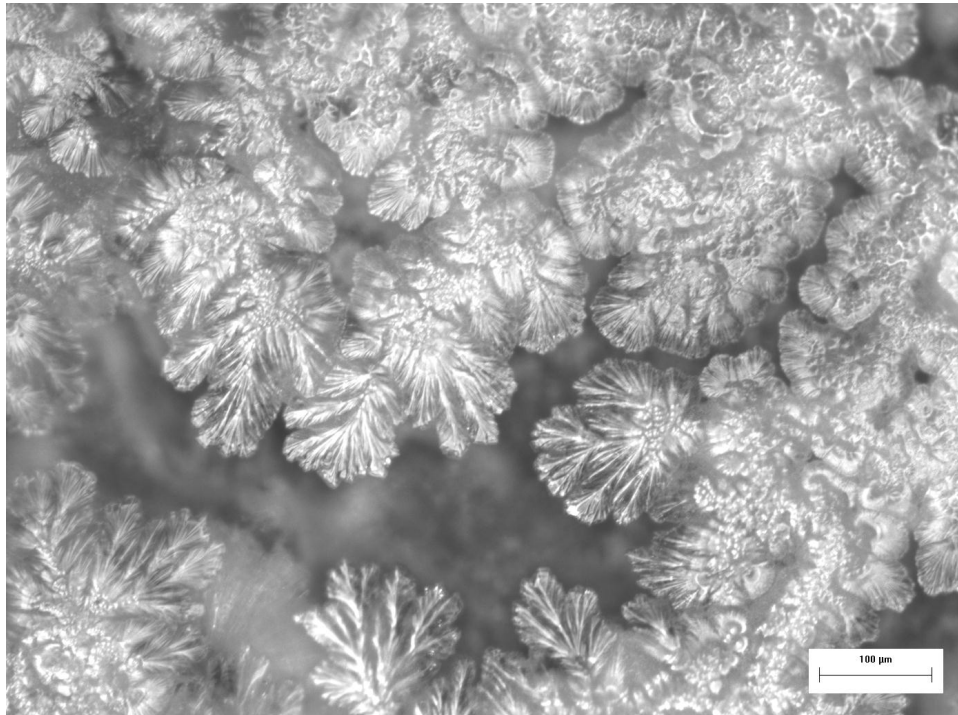
Figure 4.1: Optical micrograph of hydrated cement found in wash water

Chlorides have been known to influence the corrosion of reinforcing steel in concrete; thus, an optional limit of 500 mg/L is placed on mixing water (CSA A23.1-04, 2004; ASTM C94, 2004). The chloride contents found in the wash water analyses were well below the specified limit of 500 mg/L for water used as mixing water in the production of concrete.

Gypsum, in the form of $3CaSO_4 \cdot 2H_2O$, is usually blended into cement to prevent flash set. It may be responsible for the higher sulphate content observed in wash water. Dufferin Concrete also confirms the presence of sulphate in cement and slag (St. Mary Cement Mill Test report,

2006). Although the sulphate content of the wash water is higher than in the tap water, it is still well below the optional permissible sulphate content limit of 3000 mg/L.

As expected, the three alkali metals, Ca^{2+}, Na^+, and K^+ detected in the wash water were significantly higher than in tap water. According to Miller and Tang (1996), Na^+, K^+, and Ca^{2+} are present in cement as sulphates (K_2SO_4, $3K_2SO_4 \cdot Na_2SO_4$, $2CaSO_4 \cdot K_2SO_4$). When cement hydrates, the sulphates bind the aluminate phase to produce lower solubility products such as ettringite or C-S-H, leaving the alkali metals behind (Taylor, 1990). Therefore, a high concentration of alkali metals in wash water was expected from the analysis. More importantly, the total alkali content can influence the formation of alkali-aggregate reactions, which are detrimental to the performance of concrete (ACI 221.1R, 1998). Assuming that all the Na^+ and K^+ cations found in wash water were associated with Na_2O and K_2O, the maximum equivalent Na_2O concentration was determined to be 875 mg/L. This indicates that the total alkali concentration exceeded the optional limit of 600 mg/L. The alkali limit is intended to address the concern for AAR (CSA A23.2-27A, 2004). The 600 mg/L of Na_2O equivalent concentration limit represents a maximum mass of 105 g of Na_2O equivalent that is permissible per cubic metre of concrete for every 175 litres of wash water used in the Dufferin Concrete mixture design for concrete meeting C2 classification, as specified in Table 3.2. A maximum limit of 1.8 kg/m^3 Na_2O equivalent is required when reactive aggregates are used (CSA A.23.2-27A, 2004). With respect to the maximum permissible Na_2O limit, a contribution of 105 g is less than 6 % of the 1.8 kg/m^3 limit, which appears to be insignificant. Nonetheless, wash water should be checked for possible AAR.

Currently, there is no specified limit on pH for water used in the production of concrete, as long as the strength (Section 4.6.1) and set-time requirements (Section 4.5.1) are satisfied.

4.3 PORE SOLUTION ANALYSIS

The pore solutions were extracted from the four types of cement paste: TL, WL, TH, and WH. The solutions were sent to a commercial laboratory for full ICP and IC analysis as shown in Appendix B and summarized in Table 4.2.

Table 4.2: Pore solution analyses of the cations and anions

			TL	WL	TH	WH
Cations	Ca^{2+}	mg/L	85	80	51	48
	K^+	mg/L	4870	5540	8840	9580
	Na^+	mg/L	2610	2860	6820	7160
Anions	Cl^-	mg/L	<5	<5	<5	<5
	SO_4^{2-}	mg/L	100	140	1200	1300

Since the pH of the pore solutions was not measured, the pH measurements were calculated using a charge balance method. Assuming that the OH^- ion was the only one attached to Ca^{2+}, Na^{2+}, and K^+, an approximate OH^- concentration was determined. The SO_4^{2-} and Cl^- ions were subtracted from the total OH^- total to give a net OH^- concentration, which was used to calculate the pH of the pore solutions, as shown in Table 4.3.

Table 4.3: pH calculation based on ICP and IC charge balance

			TL	WL	TH	WH
ICP	Ca^{2+}	mmol/L	2.12	1.99	1.27	1.19
	K^+	mmol/L	125	142	226	245
	Na^+	mmol/L	114	124	297	311
Net OH^- balance	OH^-	mmol/L	240	267	500	532
	pOH	--	0.62	0.57	0.30	0.27
	pH	--	13.38	13.43	13.70	13.73

The pore solution analysis showed higher K^+ and Na^+ concentrations in both WL and WH than in TL and TH, respectively. However, the reverse trend was observed in Ca^{2+} concentration. Larbi et al. (1990) showed that the decrease in Ca^{2+} concentration must be due to the reaction SiO_2 (s) + Ca^{2+} (aq) + $2OH^-$ (aq), which consumes Ca^{2+} ions to form C-S-H. This reaction occurs more readily with a higher OH^- concentration; thereby resulting in a decreased

concentration of Ca^{2+} ion. The differences in OH- concentration of the pore solutions were found to be minimal (less than 32 mmol/L), therefore, the differences in pH were assessed as insignificant.

IC analysis shows that there was less than 5 mg/L of Cl^- in the pore solution, which is negligible. The SO_4^{2-} ion concentrations observed in both WL and WH were very similar to the control cement paste samples TL and TH, respectively. However, significantly higher SO_4^{2-} ion concentrations were noticed in TH and WH compared to TL and WL. Both TH and WH cement pastes contained a w/b = 0.45 and 10 % slag replacement content, whereas both TL and WL contained a w/b = 0.60 and 30 % slag replacement content. The differences in mixture proportioning are believed to have influenced the concentration of SO_4^{2-}. As discussed in Section 2.2.1.7, the initial hydration of slag is slow, however, with the aid of hydroxyl ions from alkali and calcium hydroxide, the rate of hydration increases. It is believed that with higher slag replacement content, the hydration of slag uses hydroxyl ions from alkali and sulphate ion as an activator. Lea (1970) concluded that the sulphate ions are being used in the hydration of slag, which would explain a significantly lower concentration of SO_4^{2-} found in TL and WL pore solutions. Finally, the source of sulphate is from the cement, and there was a higher cement content in TH and WH than in TL and WL cement pastes, which also contributes to the higher SO_4^{2-} concentration in TH and WH than in TL and WL cement paste pore solution.

The use of wash water as mixing water appears to have a negligible effect on the pH of the pore solutions. The difference in pH between wash water and tap water is less than 0.05 for both types of cement paste. Also, the SO_4^{2-} and Cl^- found in wash water does not appear to have a significant impact on the OH^- concentration. Based on the result of the analyses, it does not appear that wash water has a significant effect on the ion concentrations found in pore solutions.

4.4 STABILITY OF AIR ENTRAINING ADMIXTURE BUBBLES IN WASH WATER

The stability of air entraining admixture bubbles was determined by observing the bubbles formed on top of three beakers containing tap water, wash water, and a 50/50 mixture of the two types of water.

The 50/50 mix displayed the most bubbles after initial stirring, with the wash water sample displaying the least. After 15 minutes, the bubble levels in the tap water and 50/50 mix did not seem to change, however, the bubbles in wash water seemed to be diminishing. It was also interesting to note the sizes of the bubbles; both the tap water and the 50/50 mix had many small bubbles that were evenly distributed, whereas the wash water sample produced large bubbles that were randomly distributed, as shown in Figure 4.2.

After 30 minutes, more bubbles disappeared from the wash water sample and small quantity of bubbles disappeared in the 50/50 mix sample as well, while the bubble level in tap water seemed to be unchanged. Between 30 and 45 minutes, the bubbles in the 50/50 mix decreased almost completely, while the bubbles in wash water were gradually disappearing. The bubble level in the tap water sample seemed to be stable and still remained nearly constant throughout the first 45 minutes, as shown in a time-lapse photo presented in Figure 4.3.

The stability of the bubbles in tap water remained after 5 hours whereas the bubbles in the wash water and 50/50 mix were nearly gone after 2 hours. There is strong evidence from this test indicating that the wash water causes the entrained air bubbles to de-stabilize.

One distinct difference between the two types of water is the calcium content, with approximately 10 times higher content in the wash water compared to tap water. A water hardness comparison chart (USGS, 2006), shown in Table 4.4, shows that wash water would be classified as extremely hard, water while the tap water in Kitchener would be classified as moderately hard.

Figure 4.2: Time-lapse photos of the bubbles at 15 minutes
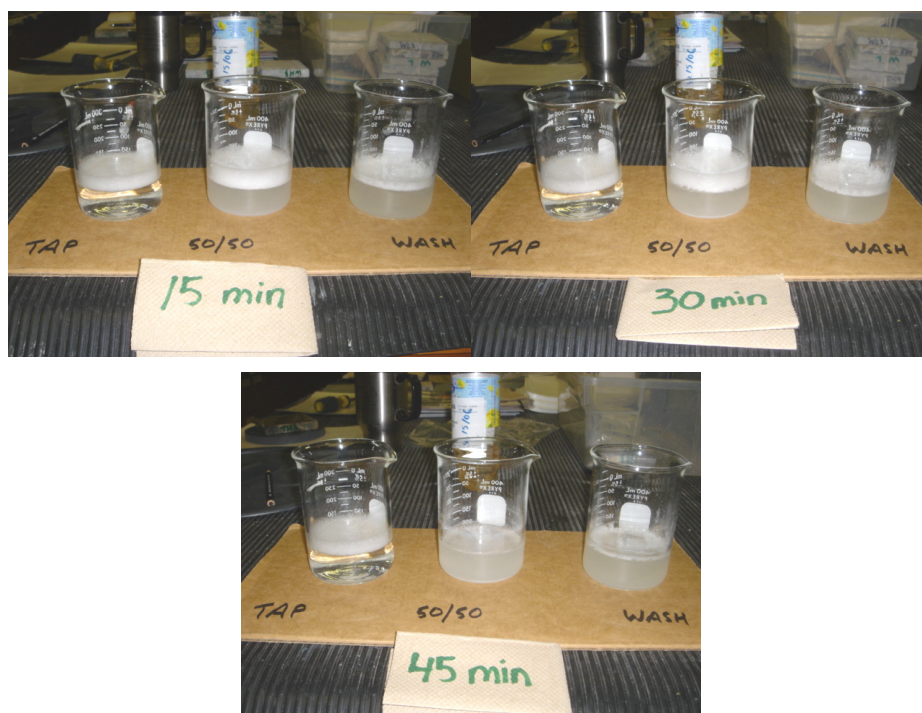
Figure 4.3: Time-lapse photos of the bubble levels at 15, 30, and 45 minutes

Table 4.4: Water hardness comparison (USGS, 2006)

Scale (mg/L)	Ratings	Tap Water (mg/L)	Wash Water (mg/L)
0-60	Soft		
61-120	Moderately Hard	80-100	
121-180	Hard		
>180	Very Hard		778

Since most air entraining agents are carboxylic acid or sulfonic acid groups (ACI 212.3R, 2004), their effectiveness in producing bubbles and the stability of the bubbles may be neutralized by the anions in wash water. Based on the results of the test and the analysis of wash water, there is reason to believe that wash water does have an effect on the formation and stability of air entraining bubbles. This may explain why a significantly shorter bubble lifespan and fewer bubbles were observed in the wash water.

4.5 PLASTIC CONCRETE TESTS

Two tests were used to evaluate the plastic properties of concrete. The Vicat Needle penetration test was used to determine the set time of cement pastes. The Chace indicator test was used to determine the air content in mortars containing an air entraining admixture.

4.5.1 Cement Paste Set Time

The set time was determined from an average of two sets of samples for each type of cement pastes. The penetration depth of TL/WL and TH/WH cement pastes are plotted versus time as shown in Figure 4.4 and Figure 4.5. In each of the set time plots, the solid circles represent the tap water paste and the open circles represent wash water paste. In both plots, the open circle curve is shifted to the left of TL and TH curves, indicating that the wash water pastes reached initial and final set earlier. The length of time to reach the initial and final set is shown in Table 4.5 for each paste type.
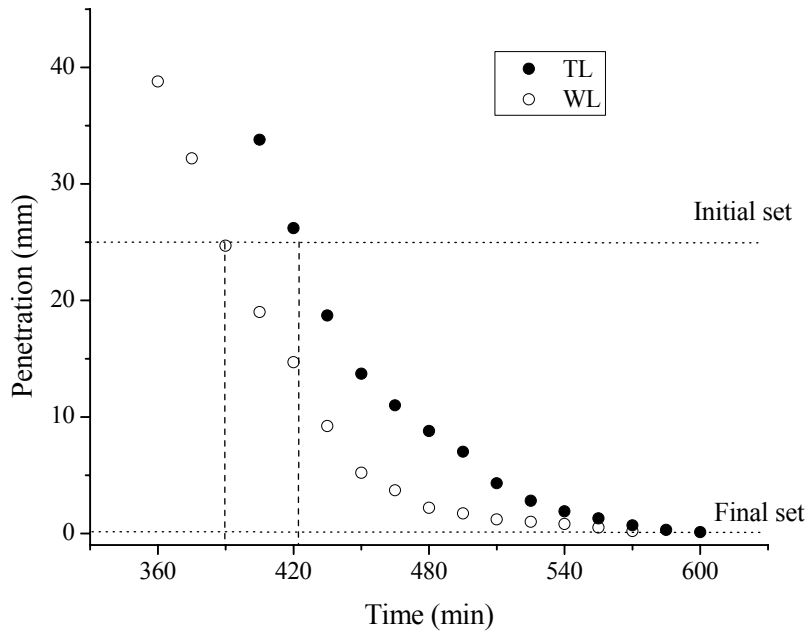
Figure 4.4: Determining the set time of TL and WL cement pastes using a Vicat Needle
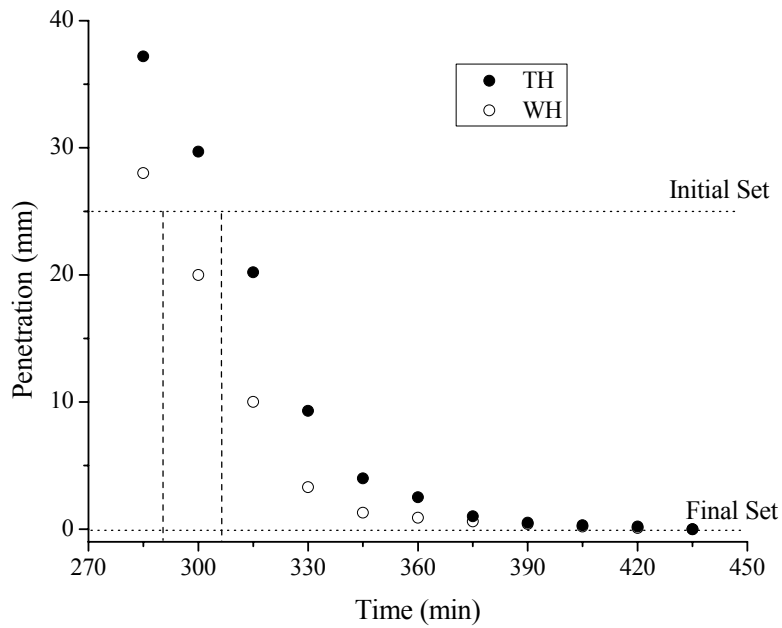
Figure 4.5: Determining the set time of TH and WH cements paste using a Vicat Needle

Table 4.5: Length of time it takes to reach initial and final set

Length of Time (min)	TL	WL	TH	WH	Limit
Initial Set	425	390	307	290	+90/-60
Final Set	600	570	435	435	+90/-60

The wash water cement pastes were observed to set faster than the control samples. Initially, as water mixes with cement, hydrolysis occurs. The process liberates Ca^{2+} and OH^- ions into the solution rapidly; however, the rate of hydrolysis slows down quickly with increasing OH^- concentration because the high alkalinity in the solution causes a micro-film layer to cover the surface of cement particles, thereby controlling the chemical reaction through diffusion (Lea, 1971). The dormant period is caused by the solution's need to reach a critical Ca^{2+} and OH^- concentration before calcium hydroxide and C-S-H can start to crystallized (Mindess and Young, 1981). Initial set typically occurs toward the end of the dormant period and final set occurs at some point during the acceleration period. Since the alkalinity of wash water is already high due to the saturation of calcium hydroxide, the length of time it takes to reach the critical Ca^{2+} and OH^- concentrations during the dormant period is reduced. Therefore, using wash water as mixing water will result in shorter initial and final set-times.

The difference in set-time between the TL and WL specimens was observed to be longer than between the TH and WH cement paste specimens. This may be due to the higher slag replacement content in the TL and WL mixes. The hydration of slag is different than cement, as it requires calcium hydroxide or hydroxyl ions from other groups to activate its cementitious property, whereas portland cement is hydraulic and can react spontaneously with water. Using wash water as mixing water appears to initiate both the hydration of slag and cement simultaneously. Meanwhile the use of tap water requires the cement to liberate a sufficient amount of hydroxyl ions before the hydration of slag can occur. Since TL and WL had a 30 % slag replacement content compared to 10 % in TH and WH, the difference in set time was more noticeable with the higher slag replacement mixture compared to the 10 % slag replacement mix.

4.5.2 Air Content in TH and WH Mortars

Air content was measured using a Chace indicator. The total air content, which includes entrained and entrapped air, found in TH and WH mortars are shown in Table 4.6. Three samples were taken for each mortar type. The air content difference between TH and WH was less than 0.5%, indicating that the air content found in wash water mortars were comparable to its counterpart.

Table 4.6: Air content of TH and WH mortars

Sample No.	TH	WH
1	6.7 %	5.2 %
2	5.2 %	6.7 %
3	8.1 %	6.7 %
Average	6.7 %	6.3 %

4.6 STRENGTH TESTS

Compression tests were performed on concrete cylinders at 3, 7, 28, and 56 days. A flexural test was performed on concrete beams to determine the modulus of rupture at 7, 28, and 56 days.

4.6.1 Compression Test

The compression strength of the cylinders is plotted against the age of the concrete in Figure 4.6 and Figure 4.7 and a complete summary of the compressive strengths is presented in Appendix C. The dotted line is the specified minimum compressive strength for each type of concrete at 28 days. The results indicate that WL compressive strengths are generally higher than TL, but both specimen types surpass the 25 MPa specified strength. CSA A23.1-04 (2004) and ASTM C94 (2004) specifies that concrete prepared with wash water needs to be within 90% of the tap water concrete strength at 28 days.

77

In Figure 4.7, the reverse trend is observed for the TH and WH specimens. WH compressive strengths are generally lower than TH, particularly at 3 and 7 days. At 28 and 56 days, however, the strengths are comparable to TH. Both the TH and WH concretes exceed the specified compressive strength. Moreover, the compressive strengths of the WH samples were within the allowable deviation (CSA A23.1-04, 2004; ASTM C94, 2004).

4.6.2 Flexural Test

The modulii of rupture of TL/WL and TH/WH are plotted versus the age of concrete in Figure 4.8 and Figure 4.9, respectively. Complete summary of results from the 4-point bending test can be found in Appendix C. Similar to the TL/WL compressive strength results, the WL samples exhibit higher modulii of rupture than the TL samples. At 7 days, the modulii of WL samples are substantially higher than TL samples and the same trend is observed at 28 days. At 56 days, WL strengths are comparable to TL strengths. The TH/WH results exhibit a peculiar trend such that the WH modulus of rupture was comparable to TH at 7 days; however, at 28 and 56 days the modulii of rupture were significantly lower than TH. At 28 days, WH modulus of rupture was observed to be lower than at 7 days, which is not normal as concrete is expected to grain strength with age. At 56 days, the modulii of rupture appear to be less than the control sample but comparable to the modulii at 7 days.

The unusual flexural strength behaviour at 28 days prompted a closer examination of the fracture location and surface. However, the fracture morphology was consistent with that of the other samples. At 56 days, one of the WH samples had a modulus of rupture that was lower than expected (approximately 80% of the TH concrete modulus) while the other sample was at least 90% of the control concrete sample. At this point, there is no rationale that would explain the difference in 28-day flexural strengths. Currently, there is no flexural strength requirement for wash water concrete, therefore, the lower 28-day flexural strengths (at least 80% of the control concrete sample) observed in WH samples are adequate.
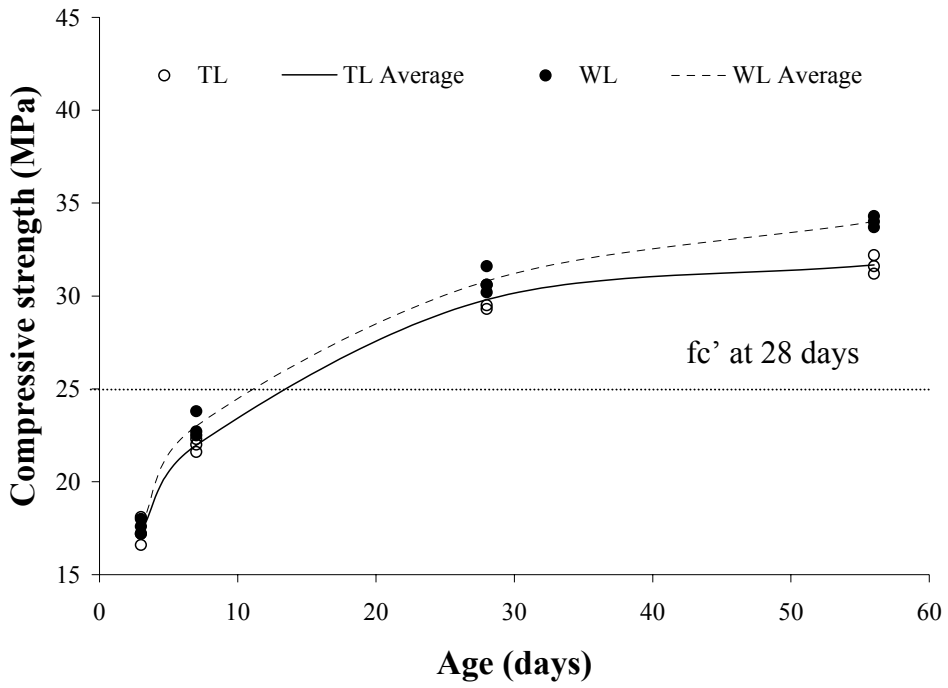
Figure 4.6: Compressive strength gain for TL and WL concrete
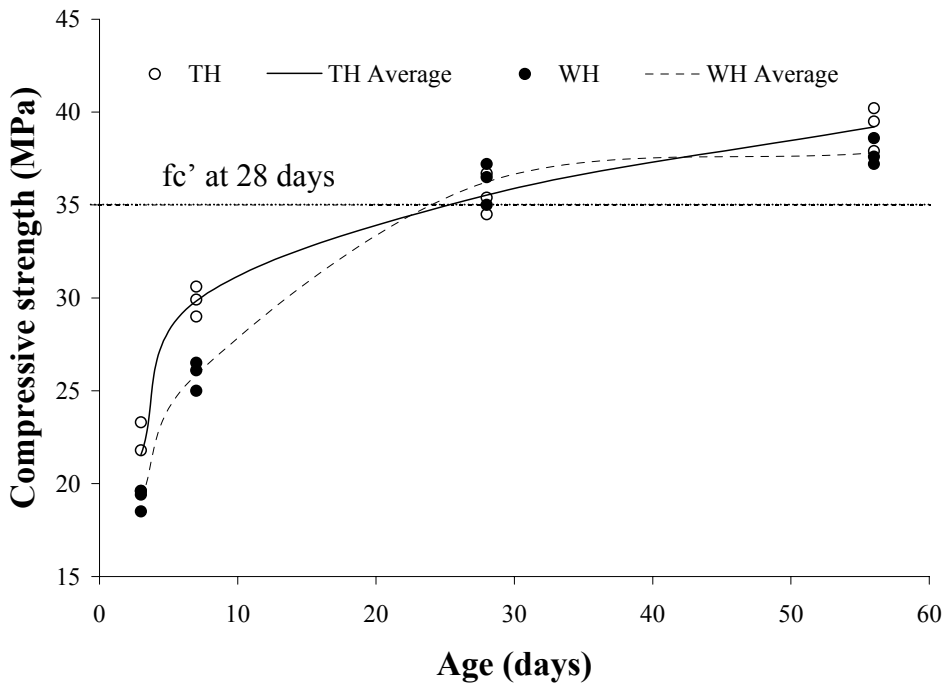
Figure 4.7: Compressive strength gain for TH and WH concrete

79
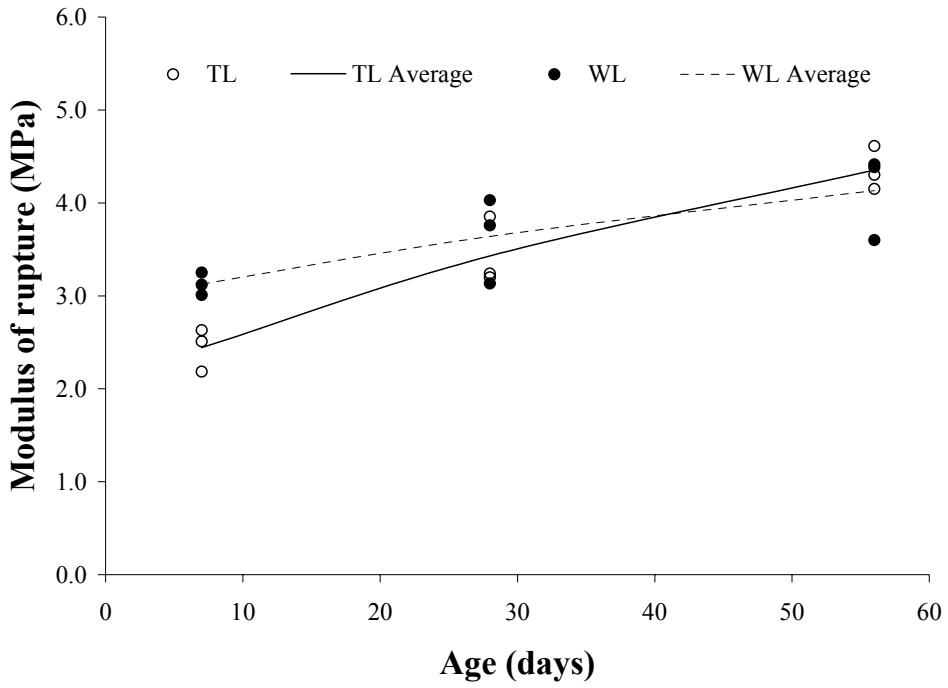
Figure 4.8: Flexural strength gain for TL/WL concrete
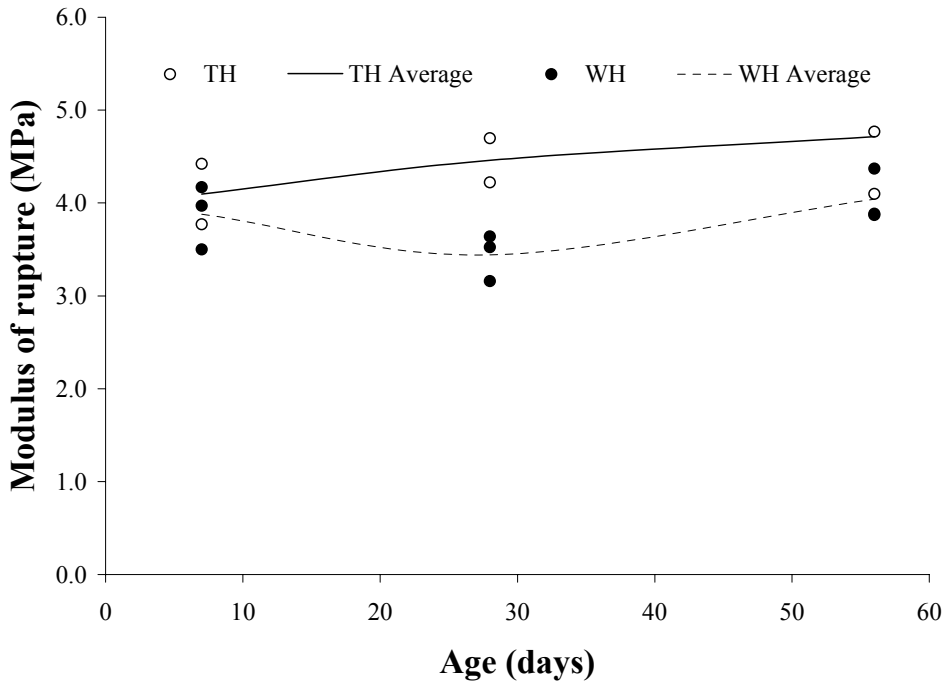
Figure 4.9: Flexural strength gain for TH/WH concrete

80

4.7 SALT SCALING RESISTANCE TEST

Concrete mass loss collected from the concrete salt scaling resistance tests is plotted as a function of the number of freeze-thaw cycles for TL/WL and TH/WH in Figure 4.10 and Figure 4.11, respectively. The key difference between TL/WL and TH/WH concrete specimens is that the former are not air entrained concretes and the latter are air entrained. The horizontal dash line at 40 g (0.8 kg/m^2) represents the MTO LS412 (2006) maximum acceptance limit criterion for mass loss after 50 cycles. After 5 cycles, all the TL and WL samples exceeded the mass loss limit; severe mass loss was observed at every stage and the test was stopped prematurely before reaching 50 cycles. Interestingly, the results show that the cumulative mass loss from all of the TL samples was less than that collected for all of the WL samples.

The TH and WH concrete specimens were batched with air entraining admixture according to the specified mixture proportions shown in Table 3.2. In the first 10 cycles, all of the specimens had less than 2 g of mass loss. After the next 10 cycles, WH2 mass loss appeared higher than all the others, but was still less than 5 g. Clearly, the WH2 and WH3 performances in salt scaling resistance test were not comparable to the TH series and WH1 specimen; however, all the specimens were able to complete the 50 freeze-thaw cycles and remain below the MTO LS412 (2006) limit of 40 g for specimens of this dimension.

A visual evaluation of the concrete surfaces was conducted using the evaluation criteria outlined in Table 4.7. In addition, two quantitative measurements were established as part of this study to provide a more consistent rating and can be seen in Table 4.8. For example, a concrete sample with a 1 rating needs to satisfy the surface condition, scaled area, and mass loss criteria. Otherwise, if one of the criteria is not satisfied, the specimen quality will be reduced to a level 2 rating. Only the TH and WH samples were evaluated using the modified rating system since the TL and WL samples exceeded the MTO limit after 5 cycles. The results are shown in Figure 4.12 and Figure 4.13, respectively.
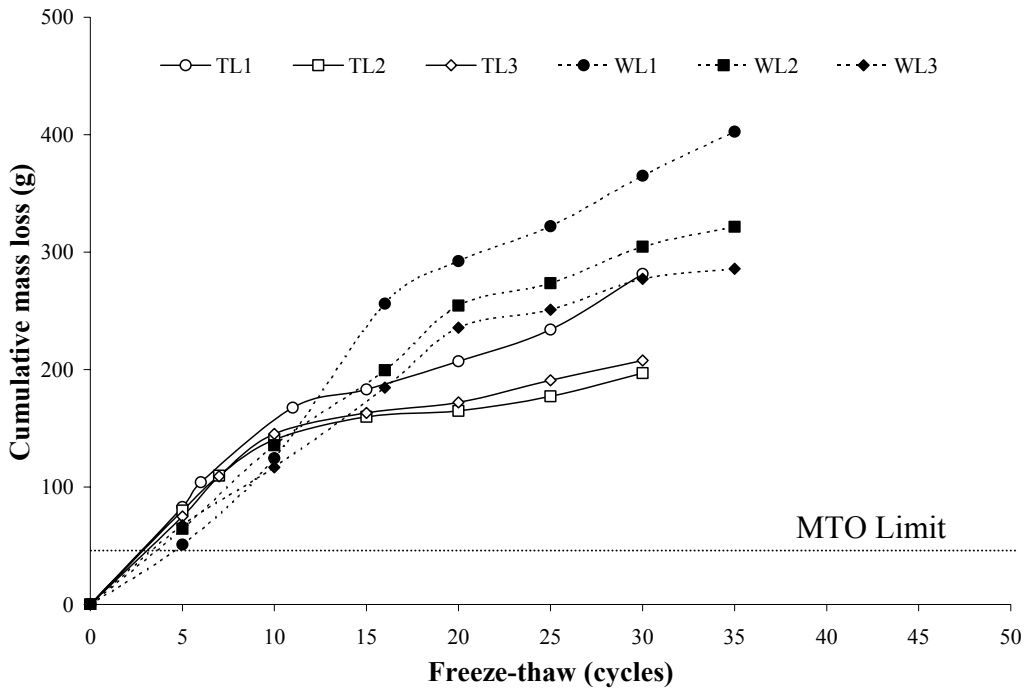
Figure 4.10: Cumulative mass loss vs. freeze-thaw cycles for TL and WL concrete
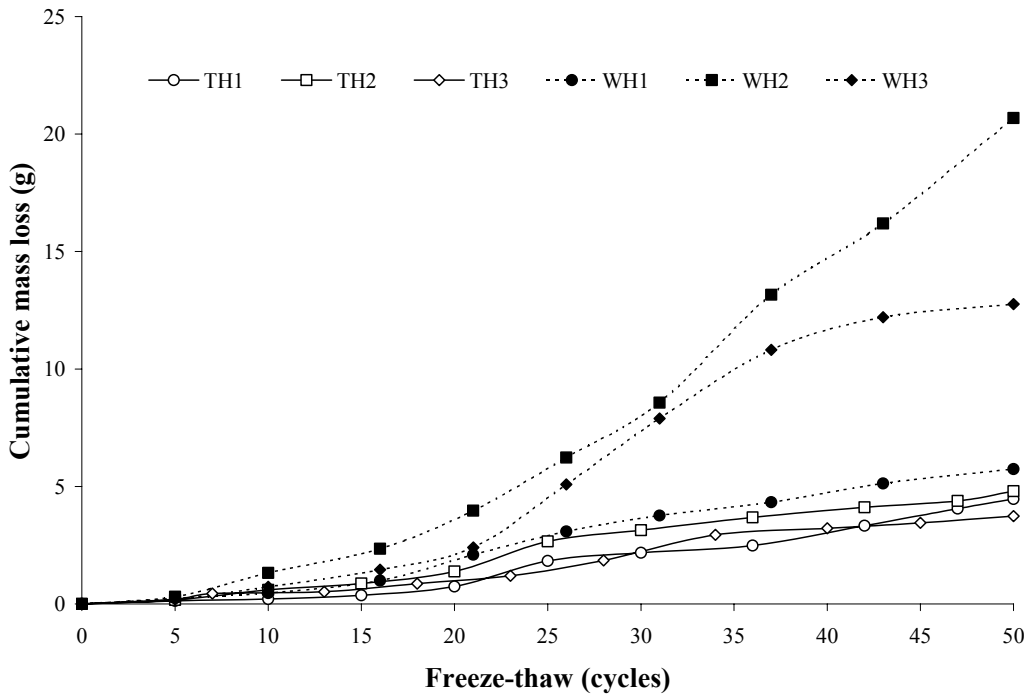
Figure 4.11: Cumulative mass loss vs. freeze-thaw cycles for TH and WH concrete

Table 4.7: Visual evaluation criteria based on ASTM C672 (2003)

Rating	Condition of Surface
0	No scaling
1	Very slight scaling (3 mm depth, max, no coarse aggregate visible)
2	Slight to moderate scaling
3	Moderate scaling (some coarse aggregate visible)
4	Moderate to severe scaling
5	Severe scaling (coarse aggregate visible over entire surface)

Table 4.8: Additional criteria used for concrete surface evaluation rating

Rating	Scaled Area	Mass Loss
0	0	< 1 g
1	< 5 cm^2	< 5 g
2	< 10 cm^2	< 10 g
3	< 20 cm^2	< 20 g
4	< 50 cm^2	< 40 g
5	> 50 cm^2	> 40 g

In the first 30 cycles, all three TH samples performed very well and the surface condition rating was at 1. After the next 20 cycles, two out of three specimens reached a level 3 rating and one remained at level 2. After 50 cycles, all the concrete surfaces sustained less than 20 g of mass loss and 20 cm^2 of scaled area were observed. Photographs of the concrete surfaces can be found in Appendix D.

The WH samples were evaluated using the same rating system, and the results are shown in Figure 4.13. After 30 cycles, two out of three specimens reached a level 3 rating and one remained at level 2. After 50 cycles, there was one sample at each of the level 3, 4, and 5 ratings. All the WH concrete surfaces were observed to have sustained higher mass loss and scaled area than the TH concrete. WH surface photographs can be found in Appendix D.

The performance of concrete surface salt scaling test depends on many factors, such as the concrete broom finish, ponding-well integrity, and operator evaluation; however the most important influencing factor on the performance is the air void system of the concrete.

Broom finishing of concrete surface was used to give a better representation of the concrete surface for pavements and sidewalks. The timing of broom finishing was found to be very important; ASTM C672 (2003) recommends brooming after the concrete surface has stopped bleeding. If the surface is broomed prematurely, a weaker surface layer will form (Pigeon et al. 1996), whereas if the surface is broomed too late, a proper broom finishing depth may not be achievable. It was found that WH samples stopped bleeding earlier than TH samples; therefore, brooming had to be done earlier with WH samples.

ASTM C672 (2003) requires that a minimum of 6 mm depth of $CaCl_2$ solution should be ponded on the concrete surface at all times during the test. As such, samples were monitored daily and refilled to ensure that the salt scaling damage would consistently represent 50 freezing and thawing cycles for all samples.

The visual rating of concrete surface performance in the salt scaling test according to ASTM C672 (2003) is very operator dependent. Pigeon and Pleau (1995) showed that when concrete surfaces had no damage or was severely damaged (concrete rating 0 or 5), the visual mean rating was consistent between two groups of operators. However, when the concrete surfaces had intermediate damage (concrete rating between 2 and 4) the visual mean rating varied noticeably between two groups of operators. Therefore, additional evaluation criteria, such as a computer-assisted scaled area calculation and an intermediate mass loss measurement for each rating were used to improve the evaluation precision. Using the modified rating system, the visual rating graph was consistent with the mass loss curves, which proved to be useful for determining the surface condition of samples.
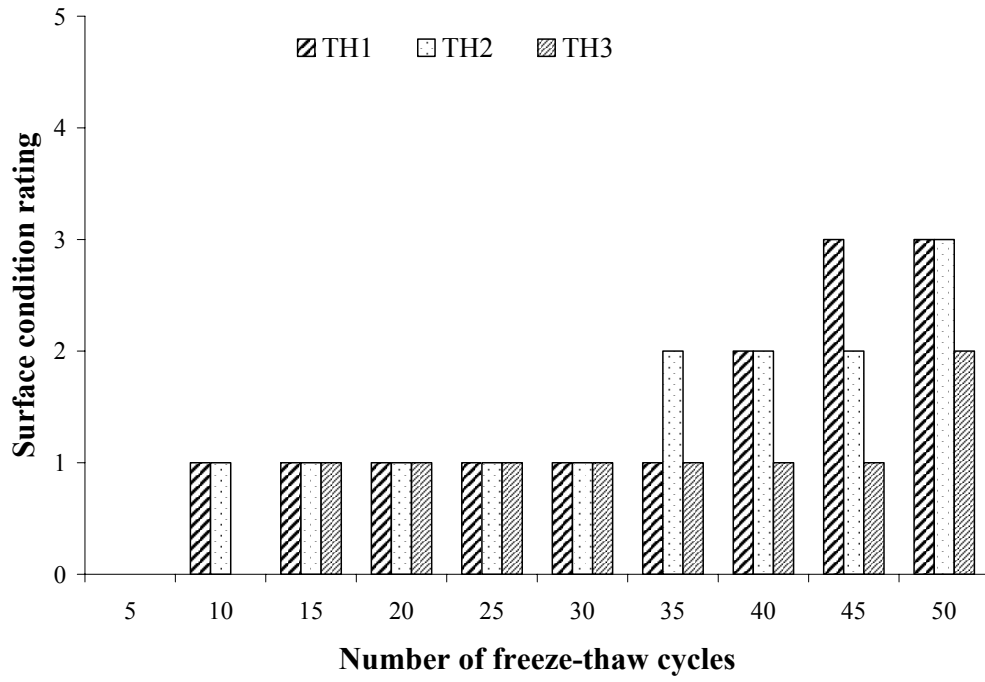
Figure 4.12: TH concrete surface condition rating
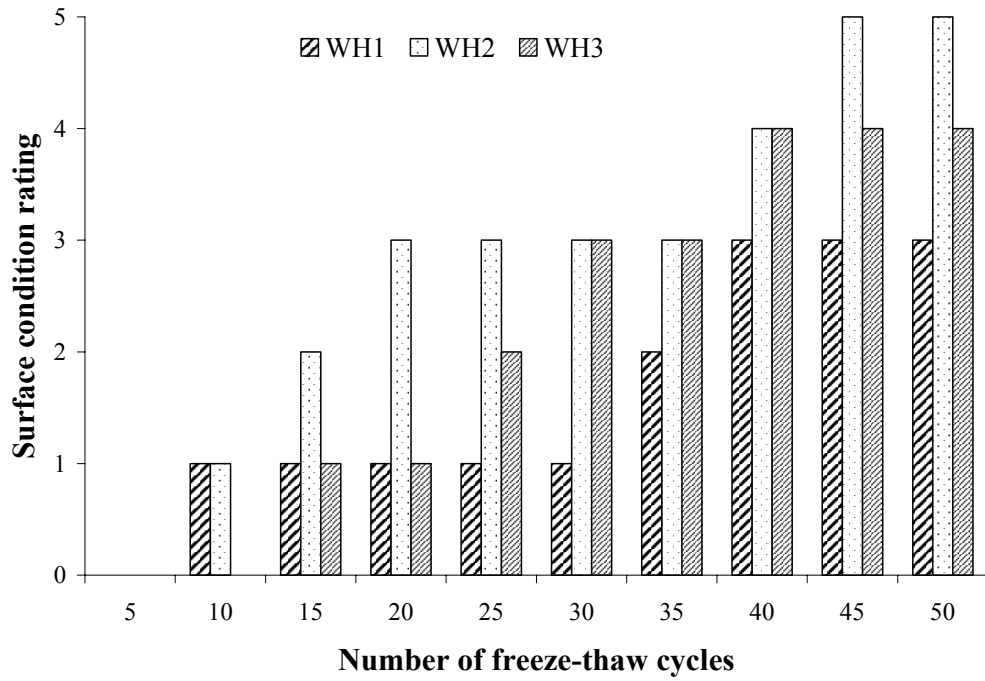
Figure 4.13: WH concrete surface condition rating

Clearly, the most important parameter in resistance of the concrete surface to salt scaling is the air void system produced by the air entraining admixture (AEA). Both the TL and WL concrete samples without AEA failed the MTO LS412 (2006) mass loss limit, while both TH and WH samples with AEA passed the MTO mass loss criterion.

There is reason to believe that the performance of the concrete surface resistance is related to the differences in air content between the TH and WH concrete. Compressive tests were conducted on concrete cylinders that were prepared using the same concrete as the specimens used in the salt scaling resistance test. The average compressive strengths for TH and WH were 36.5 and 41.8 MPa, respectively. Since all other factors were apparently equal, a logical explanation would be that the TH concrete has more air since an increase in air content has been shown to decrease compressive strength (Pinto and Hover, 2001). Based on the salt scaling and compressive test results, there is strong evidence to believe that the two identical concrete mixture designs using tap and wash water produced two distinctly different air contents in the hardened concrete. Therefore, hardened air void analyses were performed on the TH and WH samples to confirm this speculation.

4.8 HARDENED CONCRETE AIR VOID TEST

Hardened concrete air void tests were performed on 100 x 100 mm concrete cross-sections obtained from the concrete slabs used in the salt scaling test. Each sample was analysed for total air content, spacing factor, and chord length, and the results are shown in Table 4.9. The air content data presented in the table excludes air voids with a chord length less than 30 μm and greater than 1000 μm.

The spacing factor is equally important as the air content for salt scaling resistance performance. The maximum spacing factor limit is 230 μm (CSA A23.1-04, 2004; ASTM C457, 1998) and both the TH and WH (less than 150 μm) concrete samples are well below the limit. The spacing factors were also found to correspond well with the mass loss results from the salt scaling

resistance test, such that the concrete specimen with the smallest spacing factor corresponded with the least amount of mass loss and the concrete specimen with the largest spacing factor corresponded with the greatest amount of mass loss.

Table 4.9: Hardened air void analysis on concrete slabs used in the salt scaling test

	TH1	TH2	TH3	WH1	WH2	WH3
Air Content (%)	7.5	7.6	10.0	7.1	5.6	6.0
Spacing Factor (μm)	111	118	92	114	143	134
Average Chord Length (μm)	111	120	122	109	120	115

The salt scaling resistance is related to the air content as illustrated in Table 4.10. Both the WH2 and the WH3 specimens, each having 5.6 % and 6.0 % air content, respectively, meet the recommended 5 to 8 % total air content for frost-resistance in concrete under severe exposure conditions (CSA A23.1, 2004) and the MTO mass loss evaluating criterion; however, they sustained more mass loss than the other samples that had higher air contents.

Table 4.10: Relative salt scaling performance and air content relationship

Relative salt scaling performance	Cumulative mass loss (g)	Concrete sample ID	Air content (%)
Best	3.7	TH3	10.0
	4.5	TH1	7.5
	4.8	TH2	7.6
	5.7	WH1	7.1
	12.8	WH3	6.0
Worst	20.7	WH2	5.6

4.9 CORROSION TESTS

Macro-cell and micro-cell corrosion measurements were made on G109 samples to evaluate the influence of wash water on the ability of the concrete to protect the steel. The electrical

resistance of the concrete cover was also measured using a galvanostatic pulse technique and electrochemical impedance spectroscopy.

4.9.1 Macro-Cell Corrosion Measurements

Macro-cell corrosion measurements were performed on G109 samples to monitor the macro-cell current flowing between the top and bottom steel bars in TL, WL, TH, and WH specimens. The average corrosion rates were not plotted because if one sample starts to corrode first the corrosion rates of that single specimen can be orders of magnitude higher than the rest and it will control the corrosion trend of the entire series, which is not correct. The sinusoidal pattern of current density reflects the wetting and drying cycles, such that the maxima represent the wet cycle measurement and the minima represent the dry cycle measurement. The assumed corroded area used to calculate the corrosion density for all steel bars was one third of the exposed length of the top reinforcing bar.

The macro-cell corrosion rates of TL G109 samples are plotted versus the number of weeks of chloride solution exposure in the wetting and drying cycles, as shown in Figure 4.14. All five samples had an initial current density of the order of 10^{-5} A/m^2. After 10 weeks of exposure, TL4 recorded a higher current density (~10^{-3} A/m^2) than the rest (~10^{-5} A/m^2). It should be noted that the concrete in sample TL4 was poorly compacted compared to the other specimens. This may explain why higher current density was observed after only 10 weeks of exposure since poor compaction could lead to increased permeability. After 25 weeks of exposure, TL2 experienced a similar current density to TL4, while the other three samples remained the same. After 40 weeks, the current density for all of the samples increased to ~10^{-3} A/m^2 and remained constant at this level up to 70 weeks.

A plot of the macro-cell current density vs. number of weeks exposed to chloride solution is shown in Figure 4.15 for the WL samples. In the first 30 weeks, all of the samples had current densities that were less than 10^{-5} A/m^2. After 30 weeks, all of the specimens had current

densities that were on the order of 10^{-3} A/m^2, with the exception of WL1 and that trend continues through until 65 weeks. Overall, the current densities observed in the WL specimens are comparable to the TL specimens, except that it took 30 weeks for the WL samples to reach 10^{-3} A/m^2 compared to 40 weeks with the TL samples.

The current density of steel bar in TH samples was initially in the range of 10^{-6} to 10^{-5} A/m^2, with the exception of TH4, as shown in Figure 4.16. The TH4 sample had the same compaction problem as TL4, therefore active corrosion was initiated almost immediately on exposure to chloride. After 25 weeks, the steel in TH5 began to actively corrode while the steel in the other three TH samples remained close to their initial current densities. After 70 weeks, current densities observed on the steel bars in TH3 and TH5 concrete were in the range of 10^{-3} A/m^2, while the current densities of the steel bar in TH1, TH2, and TH4 were in the order of 10^{-4} A/m^2 or less, indicating that the steel bars were in passive corrosion condition.

In the WH series, all of the samples had initial current densities in the range of 10^{-6} A/m^2, as shown in Figure 4.17. After the first wetting cycle, the current densities quickly rose three orders of magnitude higher. From that point forward, the current densities for all WH specimens decreased with time. After 65 weeks, all the current densities appeared to be similar to their initial rate, which was approximately 10^{-6} A/m^2, suggesting that all of the steel bars in WH concrete are in passive corrosion condition.

Based on the macro-cell corrosion rates, it does not appear that the use of wash water has a negative impact on the macro-cell corrosion performance of steel bar in G109 concrete specimens.
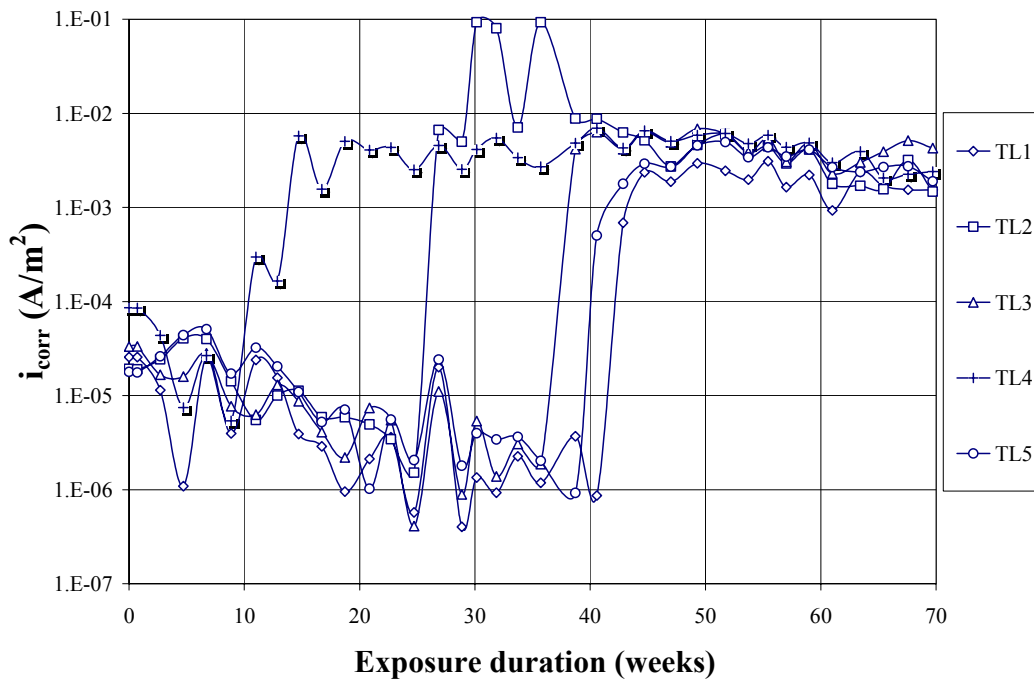
Figure 4.14: TL macro-cell corrosion current density measurements
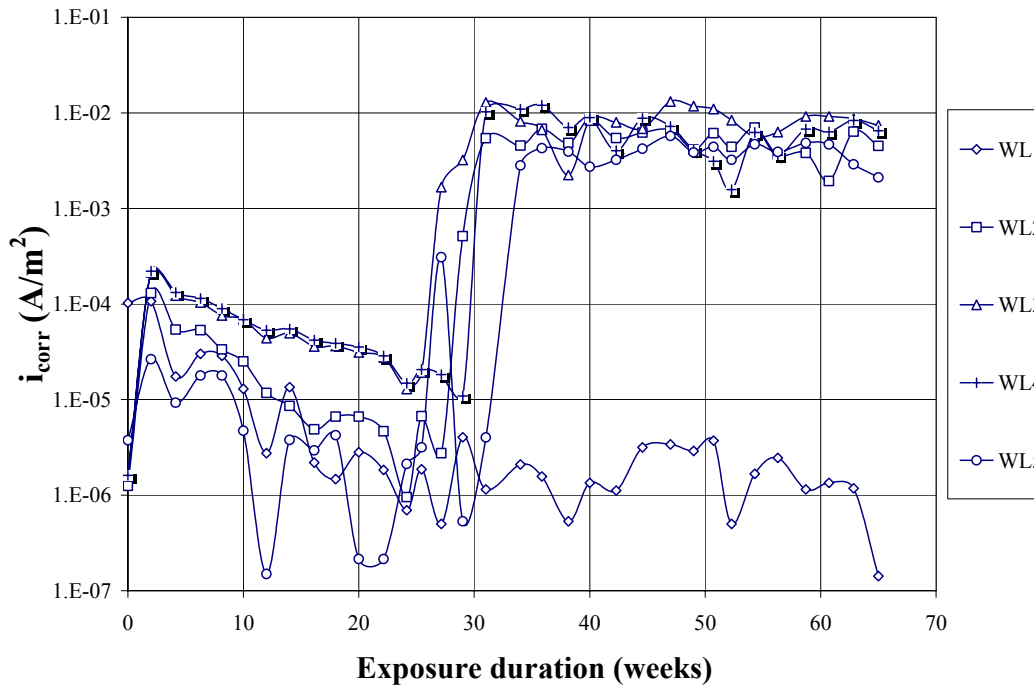
Figure 4.15: WL macro-cell corrosion current density measurements
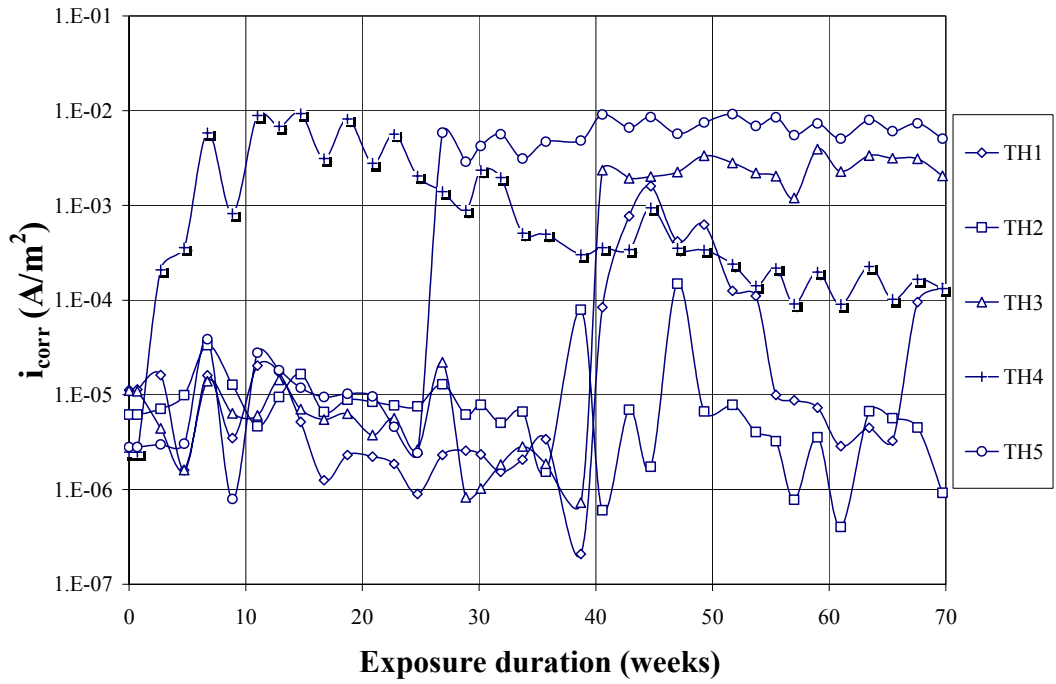
Figure 4.16: TH macro-cell corrosion current density measurements
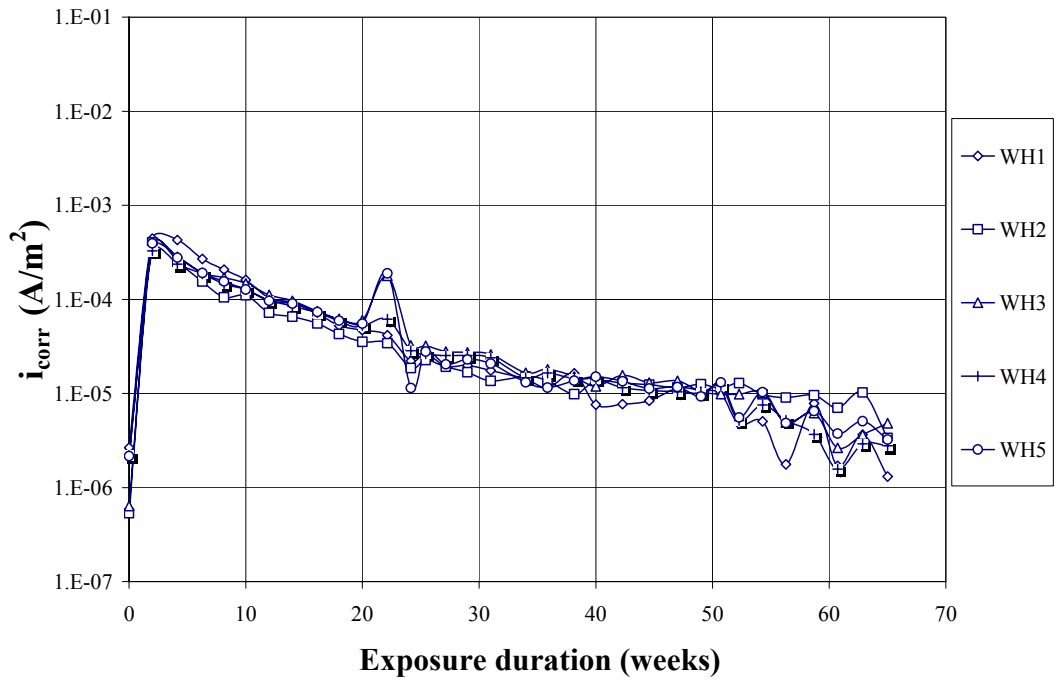
Figure 4.17: WH macro-cell corrosion current density measurements

4.9.2 Micro-Cell Corrosion Measurements using LPR

The micro-cell corrosion rates of the top steel bar in the TL, WL, TH, and WH G109 specimens are plotted in Figure 4.18 to Figure 4.21. The assumed corroded area used to calculate the corrosion density was one third of the exposed length of the top embedded steel bar. Hansson et al. (2006) showed that micro- and macro-cell corrosion represent two distinctly different corrosion systems, therefore, micro-cell corrosion rates are expected to differ from that of macro-cell corrosion rates. Andrade et al. (1990) measured active micro-cell corrosion rate to be in the order of 10^{-2} to 10^{-1} A/m^2 and passive micro-cell corrosion rate to be in the order of 10^{-4} to 10^{-3} A/m^2.

The initial micro-cell current density observed for the steel in the TL series was approximately 10^{-4} A/m^2, as shown in Figure 4.18. The corrosion trend was similar to the macro-cell corrosion behaviour, except the current densities were an order of magnitude higher as they represent two distinctly different corrosion systems. The macro-cell corrosion system assumes that the anodic and cathodic regions are separated through a finite distance, such as the top and bottom steel bars in a G109 sample, while in a micro-cell corrosion system, both the anodic and cathodic sites are adjacent to one another on the same steel bar. Between 30 and 40 weeks, there appeared to be a sharp increase in current density measured on the steel bars, for both TL and WL concretes, suggesting that the steel bars were switching from passive to active corrosion condition within that time period. After 70 weeks of exposure, the measured current densities of five samples were approximately 10^{-2} A/m^2. Therefore, the measured corrosion rates of the steel bars in TL concrete must be an active corrosion condition.

At the end of 65 weeks of exposure, the steel bars in the WL concrete series displayed corrosion current densities that were also approximately 10^{-2} A/m^2, as shown in Figure 4.19. Therefore, the steel bars in WL concrete were also expected to be actively corroding, with the exception of the steel bar in WL5 concrete, which remained in a state of passivity.

The TH micro-cell corrosion trend was also similar to the TH macro-cell corrosion trend, except it was approximately an order of magnitude higher, as shown in Figure 4.20. After 70 weeks, three out of five specimens recorded corrosion rates in the range of 10^{-2} A/m^2 while the other two had corrosion rates that were ten times smaller. Overall, the corrosion rates are stable at the present condition. The corrosion rates of the steel in the WH concrete appear to be constant after 65 weeks and the measured current densities were around 10^{-3} A/m^2. However, at 40 weeks there appears to be a sharp temporary decrease in corrosion density for all the steel bars in the WH concrete. The observed decrease in corrosion density did not produce a continued trend. Since it only appeared on the WH samples, the measured corrosion currents at 40 weeks appear to be a case of anomaly.

Based on the micro-cell corrosion current density results, it appears that the corrosion rates of the steel bars in TL and WL concrete are comparable to one another. On the other hand, three out of the five steel bars embedded in TH1, TH2, and TH3 showed signs of active corrosion, while the other two remained in a passive corrosion condition. Meanwhile, all of the steel bars in the WH concrete specimens were in a state of passive corrosion.
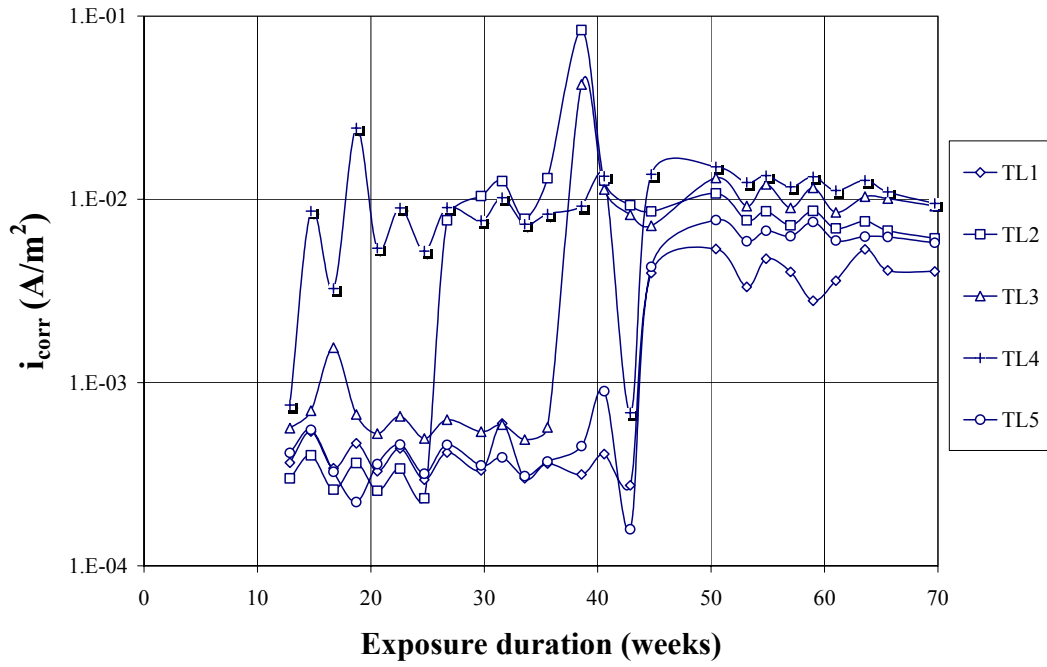
Figure 4.18: TL Micro-cell LPR corrosion current density measurements
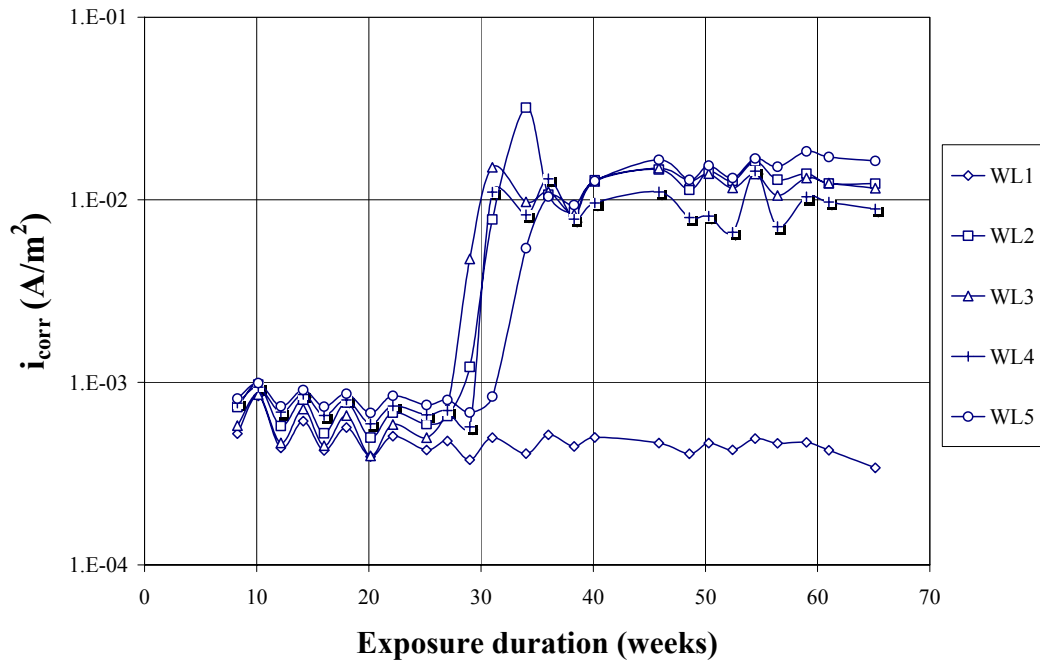
Figure 4.19: WL Micro-cell LPR corrosion current density measurements

94
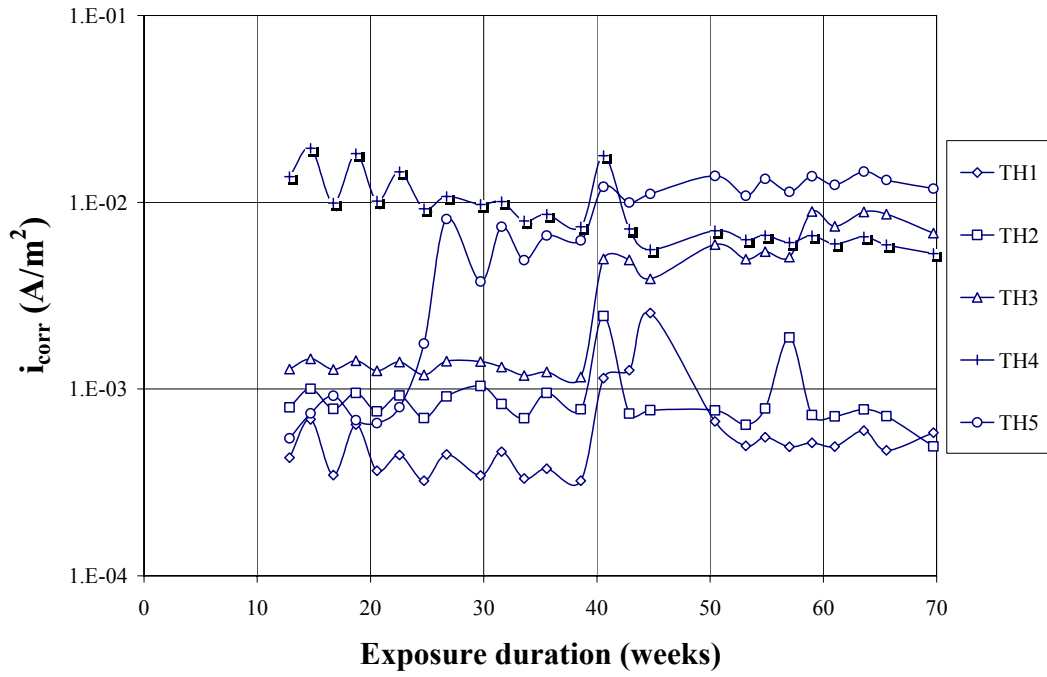
Figure 4.20: TH Micro-cell LPR corrosion current density measurements
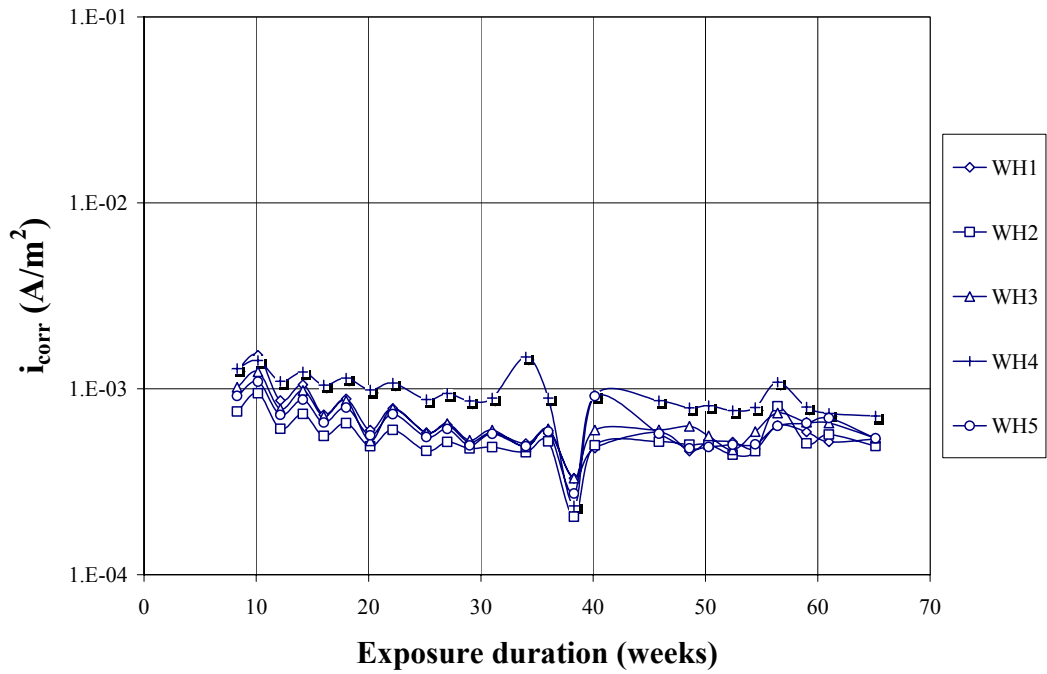
Figure 4.21: WH Micro-cell LPR corrosion current density measurements

4.9.3 Half –Cell Potentials

The half-cell potentials (E_{corr}) were measured for the top steel bar in the G109 concrete specimen while it was electrically disconnected from the bottom steel bars. The half-cell potential measurements versus saturated calomel electrode (SCE) are plotted for the TL, WL, TH, and WH G109 specimens in Figure 4.22 to Figure 4.25. In each of the plots, two dotted horizontal lines, at -130 and -280 mV (-200 and -350 mV versus $Cu/CuSO_4$ reference electrode), represent two boundary lines that divide the half-cell potential into three regions according to the ASTM C876 (1999) for standard half-cell potential interpretation. The first region corresponds to a half-cell potential that is more positive than -130 mV, corresponding to a 90% or greater probability of no corrosion occurring. The second region corresponds to a half-cell potential between -130 and -280 mV, in which the corrosion activity is uncertain. The third region corresponds to a half-cell potential more negative than -280 mV, corresponding to a 90% or greater probability of corrosion occurring.

More negative half-cell potential measurements correspond to a higher probability for micro- and macro-cell corrosion. After 70 weeks, the half-cell potentials of the TL specimens were found to be between –250 and –350 mV vs. SCE, which correspond to both the uncertain region and the 90% probability of corrosion occurring region as shown in Figure 4.22. These values were comparable to the half-cell potentials of the steel bars in the WL specimens, with the exception of WL5 after 65 weeks, as shown in Figure 4.23. The half-cell potential of the steel in WL5 concrete was expected to be more positive than the other steel bars in WL concretes, which were actively corroding.

After 70 weeks, the half-cell potentials of the TH series were found to lie between 0 and –300 mV, with no clear convergence at any particular potential, as shown in Figure 4.24. In contrast, the WH half-cell potentials were very close together, and after 65 weeks the potentials were between 0 and –50 mV, which lies in the 90% probability of no corrosion occurring, as shown in

Figure 4.25. The half-cell potentials were found to be in good agreement with the micro-cell corrosion current densities such that the steel bar with the highest corrosion current density corresponds to the most positive half-cell potential and vice-versa.

4.9.4 Determining the Severity of Corrosion

The concrete cover was removed for two G109 specimens per series to determine the severity of the corrosion and to examine the corrosion product on the top steel bar. The selected samples were the ones that best represented the average corrosion rate in that series: TL2 and TL3 for the TL series, WL2 and WL3 for the WL series, TH2 and TH3 for the TH series, and WH4 and WH5 for the WH series. The rebar was removed from the concrete and examined before and after pickling (ASTM G1, 2003), as shown in Figure 4.26 and Figure 4.27. Two observations were noticed:

1. There was more adhered mortar on the rebars in the higher strength concrete, which is as expected because the mortar is stronger in higher strength concrete. Interestingly, the bulk of the mortar is adhered to the bottom side of the rebar and very little is adhered on the top side. Since the prisms were cast upside down, the weaker mortar on the top side may be due to a bleeding effect; therefore, less adhered mortar was observed on the top side.

2. When fracturing the G109 concrete cover, it was found that the TH and WH concrete have grey regions that appear similar to unhydrated cement in the concrete, while there were no grey patches appearing in the TL and WL concrete.

The corroded area was determined from observations before pickling of the rebar, because it is more representative of the corrosion surface. This is because the pickling process was found to remove both the adhered mortars and mill scale, as shown in Figure 4.28, making it difficult to determine the corroded area. These estimates of the corroded areas were used to re-calculate more accurate micro-cell corrosion density values for these samples.
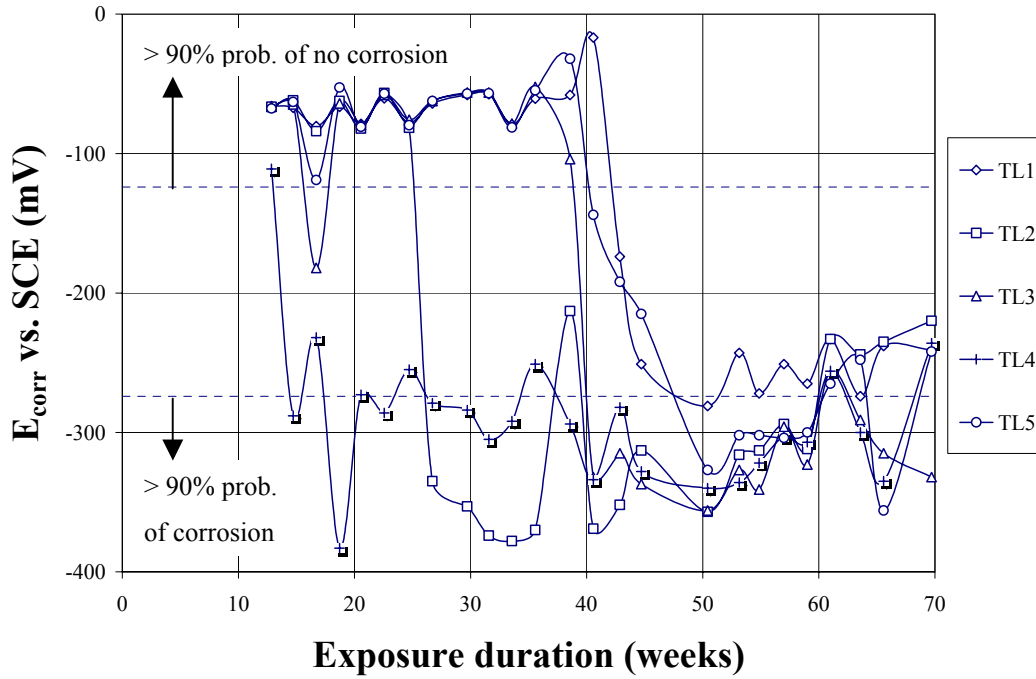
Figure 4.22: TL Half-cell potential measurements
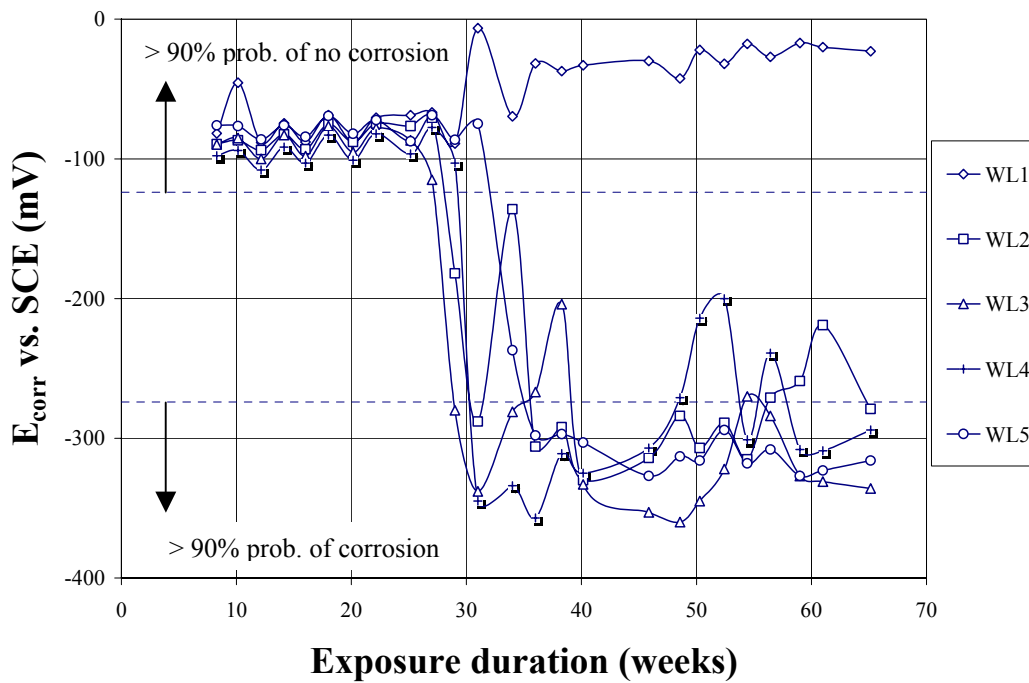
Figure 4.23: WL Half-cell potential measurements
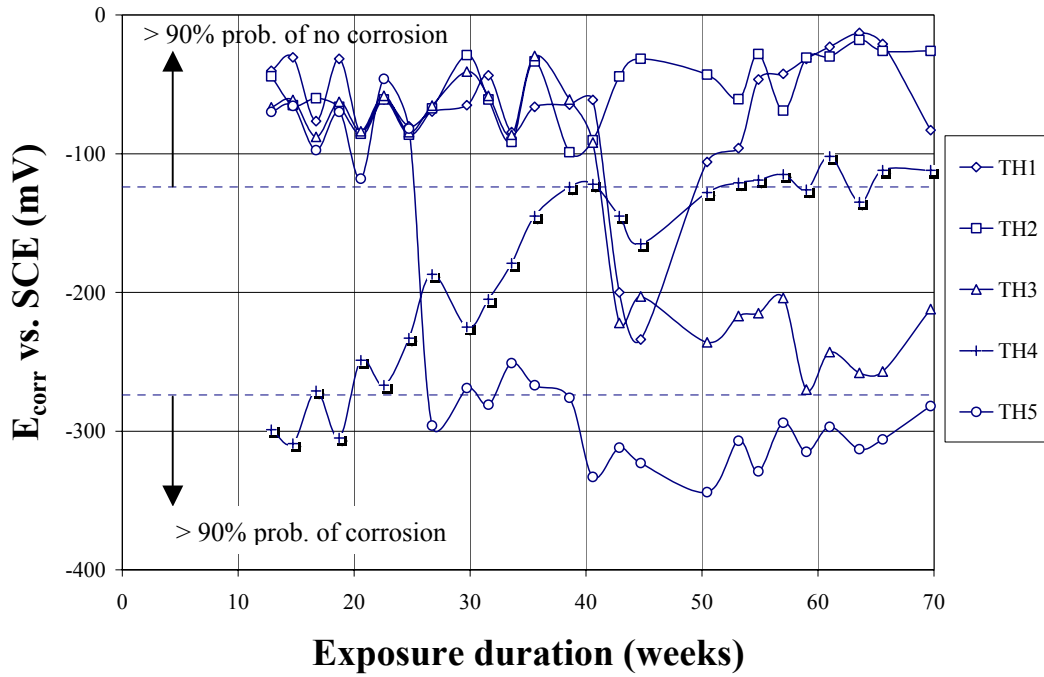
Figure 4.24: TH Half-cell potential measurements
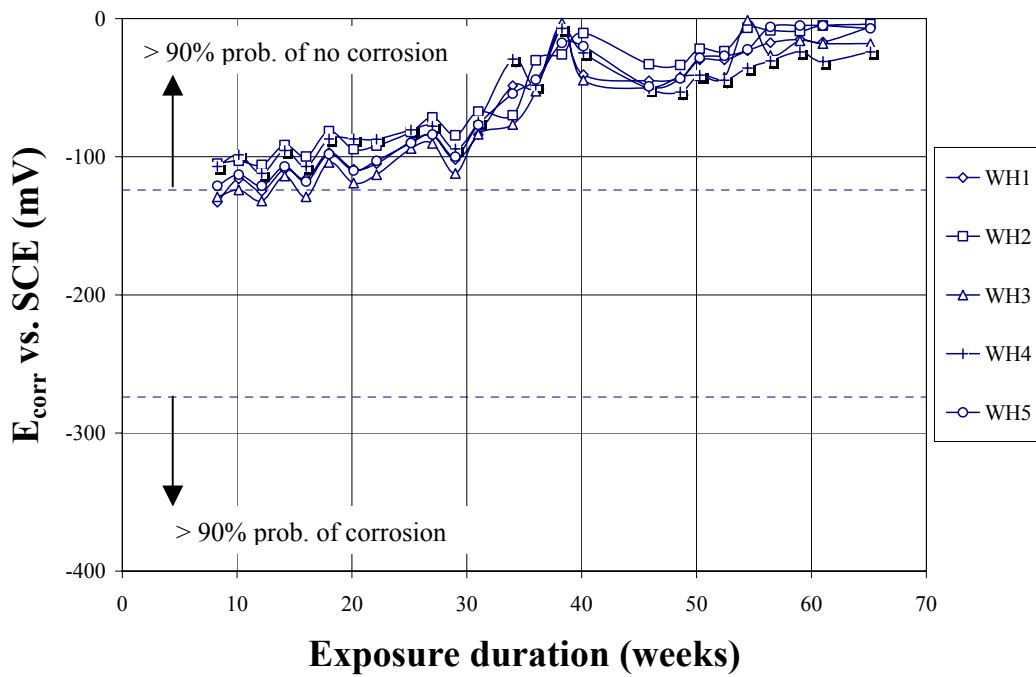
Figure 4.25: WH Half-cell potential measurements

The length of the corroded area found on the steel bar of TL2 and TL3 concrete specimens was approximately 30 mm. It is assumed that the remaining steel bars in the same series would have approximately the same corroded area. The steel bar in WL2 and WL3 concrete specimens also have a corroded area length of approximately 30 mm, and it is assumed that the rest of the steel bar in the WL concrete would have the same corroded length. The steel bar in TH2 and TH3 concrete specimen were selected as they represent two different corrosion rates. It was found that the steel bar in TH2 and TH3 concrete specimens had a corroded length of 10 mm and 20 mm, respectively. Therefore, the steel bar in TH1 concrete specimen was assumed to have the same corroded area as TH2, while the steel bar in TH4 and TH5 concrete specimens were assumed to have the same corroded area as TH3. The steel bar in WH4 and WH5 concrete specimens have a corroded area of approximately 10 mm and it is assume that the remaining WH samples would have the same corroded area. The recalculated micro-cell corrosion rates were obtained by taking the last micro-cell corrosion currents and dividing them by the estimated corroded lengths. A comparison of the old and adjusted corrosion rates for the steel bars in TL, WL, TH, and WH concrete specimens are shown in Figure 4.29 to Figure 4.32. The summary of the adjusted corrosion rates can also be found in Appendix E.

It was clear that the corroded area was much smaller than the initial assumed area. By adjusting the corroded area, a higher but more realistic micro-cell corrosion rate was determined. Both the TL and WL specimen corrosion rates were about 3 to 5 times higher than the original corrosion rate average over 33% of the top bar. Moreover, the corrosion rates of the top bars in TL and WL concrete specimens are comparable to each other. Both the TH and WH specimen corrosion rates increased considerably. Interestingly, using the estimated area, the corrosion rates of TH and WH were more consistent and comparable than before as their corrosion rates are in the same order of magnitude, 10^{-2} A/m^2. Based on the micro-cell corrosion results, it does not appear that wash water has a detrimental effect on the corrosion of the reinforcing steel in the G109 concrete specimens.

Figure 4.26: A corroded rebar removed from the TL3 concrete specimen before pickling

Figure 4.27: A corroded rebar removed from the TL3 concrete specimen after pickling
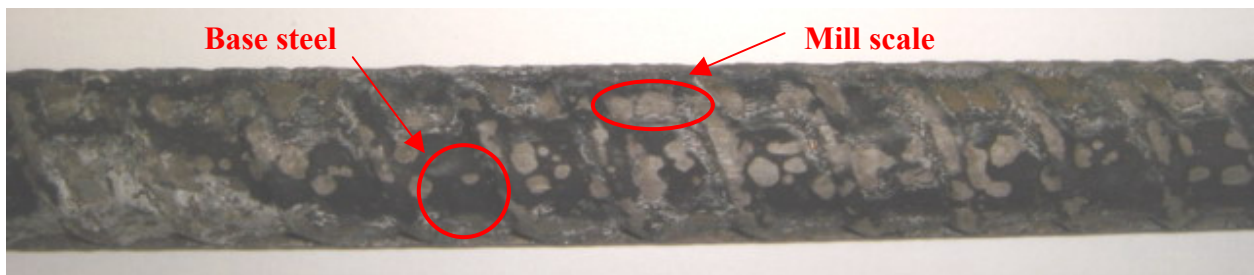
Figure 4.28: Picked rebar with two distinctly different regions

4.9.5 Concrete Resistance

Two techniques were used to determine the resistance of the concrete cover-depth: galvanostatic pulse technique and electrochemical impedance spectroscopy (EIS).
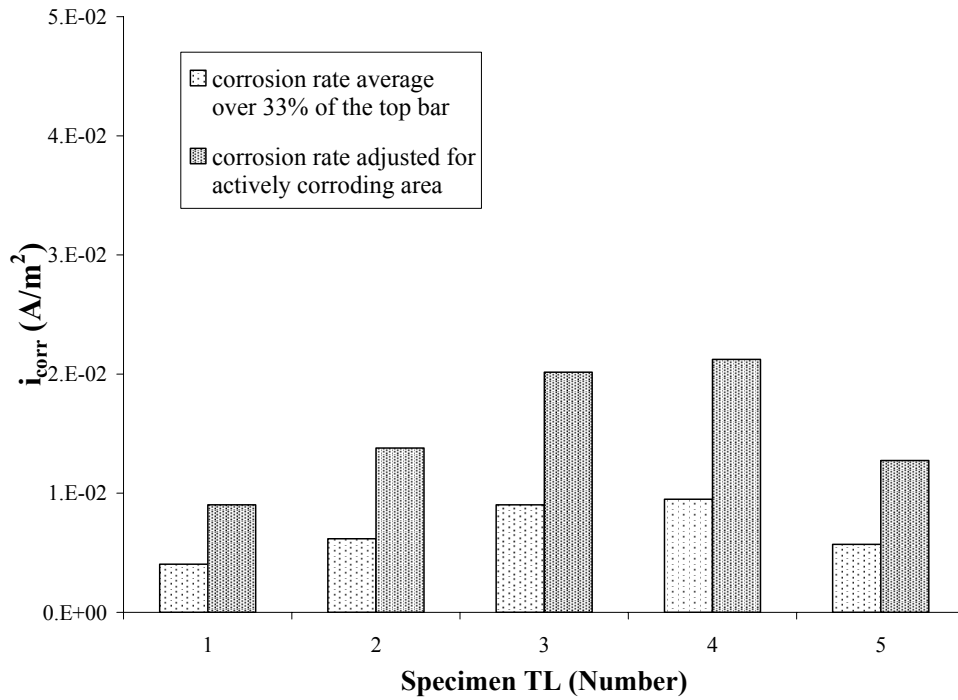
Figure 4.29: Micro-cell corrosion rates of the top bar in TL concrete specimens at 70 weeks
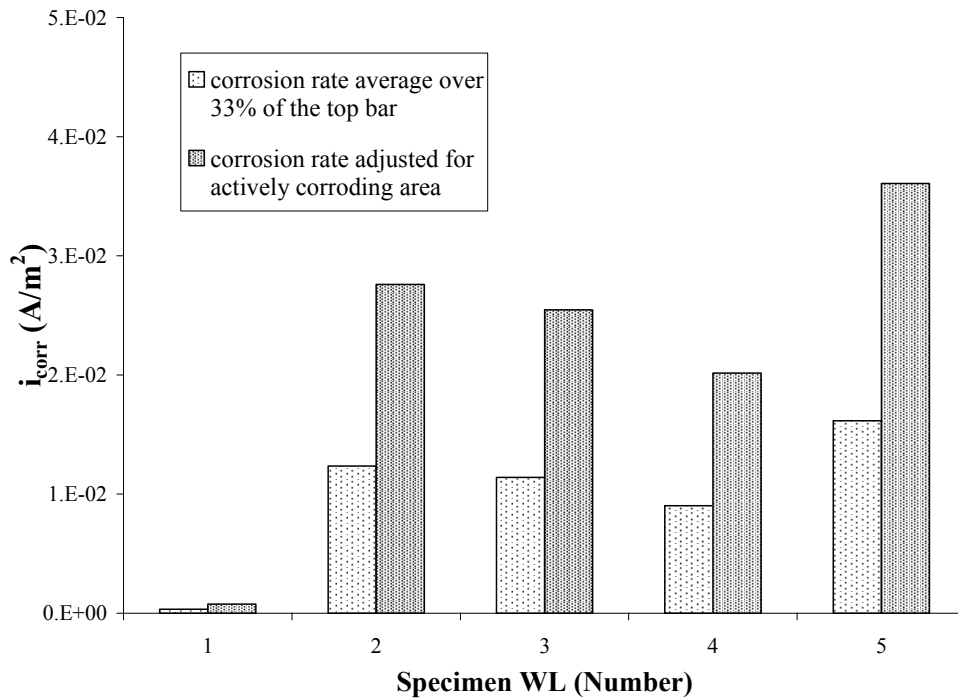
Figure 4.30: Micro-cell corrosion rates of the top bar in WL concrete specimens 65 weeks
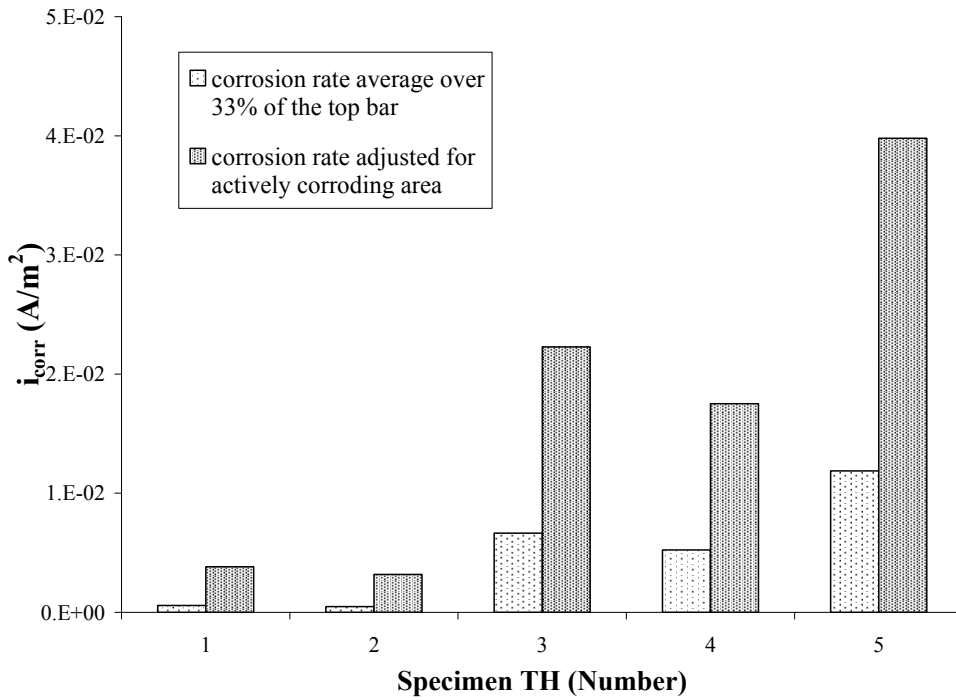
Figure 4.31: Micro-cell corrosion rates of the top bar in TH concrete specimens 70 weeks
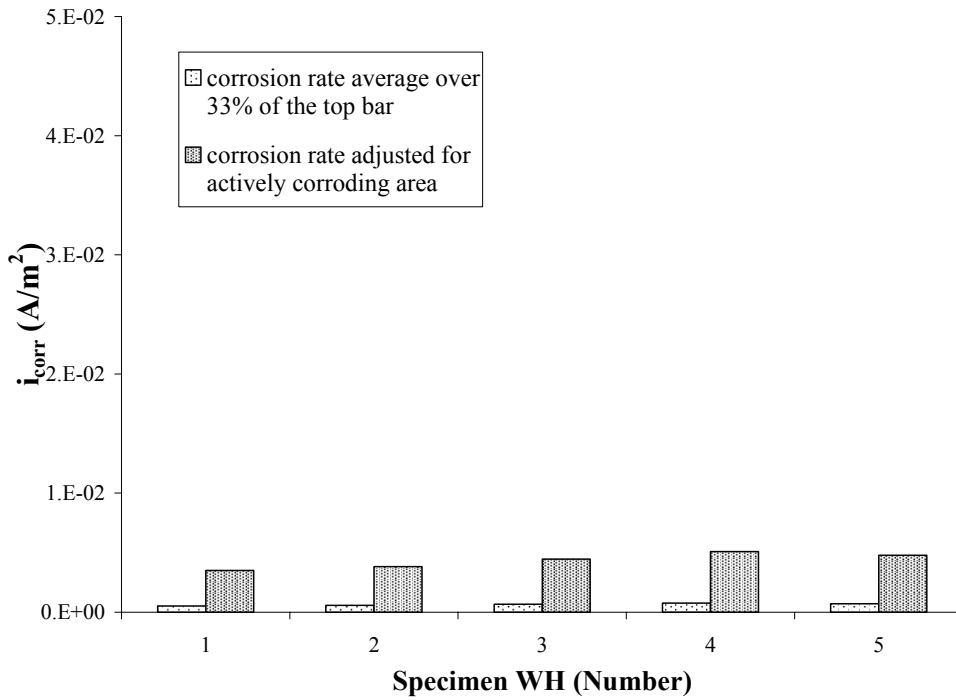
Figure 4.32: Micro-cell corrosion rates of the top bar in WH concrete specimens 65 weeks

Using galvanostatic pulse technique, the resistances of the TL concrete samples were found to be higher than the WL samples, as shown in Table 4.11. On average, the resistance of the TL concrete was 200 Ohms higher than the WL; while the reverse was observed for the TH and WH concrete, as the resistance of the TH concrete was approximately 300 Ohms lower than the WH concrete. The values in Table 4.11 represent the resistance of the concrete after 65 weeks for WL and WH concrete and 70 weeks for TL and TH concrete.

Using the EIS technique, the measured concrete resistance was slightly higher than those recorded using the galvanostatic pulse technique, as shown in Table 4.12. Similar to the galvanostatic technique results, TL resistances were found to be 200 Ohms higher than WL values, on average, while TH resistances were 300 Ohms lower than WH. The order of magnitude of the concrete resistance was the same for both techniques.

The trends observed for concrete resistances were found to be consistent with the half-cell potential and micro-cell corrosion rate trends as well, such that the concrete with the highest resistance (WH) had the least negative half-cell potentials and lowest corrosion rates, while the concrete with the lowest resistance (WL) had the most negative half-cell potentials and the highest corrosion rates. Electrochemical impedance spectroscopy used to measure the concrete resistance values correlated well with the concrete resistance values measured using the galvanostatic pulse technique. However, within each concrete series, the concrete specimen with the highest concrete resistance did not always exhibit the lowest corrosion rate or the lowest negative half-cell potential. Perhaps the scatter in the concrete resistance values for each series was so small (at less than 200 Ohms apart for both techniques), that the concrete specimen with the highest resistance value within the series did not have the lowest corrosion rate. Therefore, the concrete resistance measured using both techniques can be useful in determining the relative performance between different series, but not as useful when comparing concrete performances within the same series.

Table 4.11: Concrete resistance using galvanostatic pulse technique

	Concrete Resistance (Ω)			
No.	TL	WL	TH	WH
1	1000	855	885	1240
2	1000	640	770	1110
3	830	700	770	1075
4	910	780	855	1275
5	940	590	750	1170
Avg	935	715	805	1175

Table 4.12: Concrete resistance using electrochemical impedance spectroscopy

	Concrete Resistance (Ω)			
No.	TL	WL	TH	WH
1	1030	890	895	1280
2	1020	650	790	1120
3	860	720	800	1100
4	945	805	905	1315
5	970	610	770	1200
Avg	965	735	830	1205

4.10 THERMOGRAVIMETRIC ANALYSIS

Thermogravimetric analyses were performed on the four types of cement paste. The mass loss, given as a percent mass vs. temperature (TGA), is plotted for each paste along with the derivative curve (DTG), as shown in Figure 4.33 to Figure 4.36. A minimum of two tests were performed on each type of cement paste.

The thermal plots obtained from the TL and WL cement pastes showed very similar mass loss TGA and DTG curves. The greatest mass loss was observed between 40 and 100°C, which can be attributed to the evaporation of water in ettringite (Skalny and Odler, 1967; Antao et al., 2002) and to a lesser degree the evaporation of water bound in the hydration products such as aluminate hydrates (Kosmatka, 2002). The second major mass loss seen in both cement pastes

occurred between 400 and 500°C and is thought to be associated with dehydroxylation of calcium hydroxide (Perruchot et al., 2006). Between 220°C and 400°C, there is a gradual mass loss, which is associated with the release of gel water (Ye et al., 2007). Then, at approximately 750°C, there appears to be a small amount of mass loss and it is believed to be associated with decarbonation of calcium carbonate (Alarcon-Ruiz et al., 2005).

The DTG curves for the TH and WH cement pastes were found to have major peaks that were similar to those found for the TL and WL cement pastes. While the DTG curves for tap and wash water resemble each other, both WL and WH DTG curves clearly contain extra minor peaks, such as the ones observed at 300°C, 400°C, and 460°C on the WL paste and the one at 550°C on the WH paste, which were not visible on the TL and TH pastes, respectively. Moreover, these peaks are thought to be artefacts because they are not reproducible.

Ramachandran (1982) found that the addition of lignosulfonate as a chemical retarder in hydrated cement lowers the calcium hydroxide peak produced. This evidence suggests that there may be traces of chemical retarder in wash water, since, slightly lower calcium hydroxide peaks were observed on wash water pastes in comparison to the tap water pastes.

Quantitative measurements of the hydration product volumes were obtained by calculating the area under the mass loss curves for the WL and WH (16.17% and 15.64%) pastes were similar to the TL and TH (16.16% and 15.31%) pastes. Based on the thermal analysis results, it appears that wash water has no significant impact on the hydration products; therefore, it is acceptable to use wash water in the production of concrete.
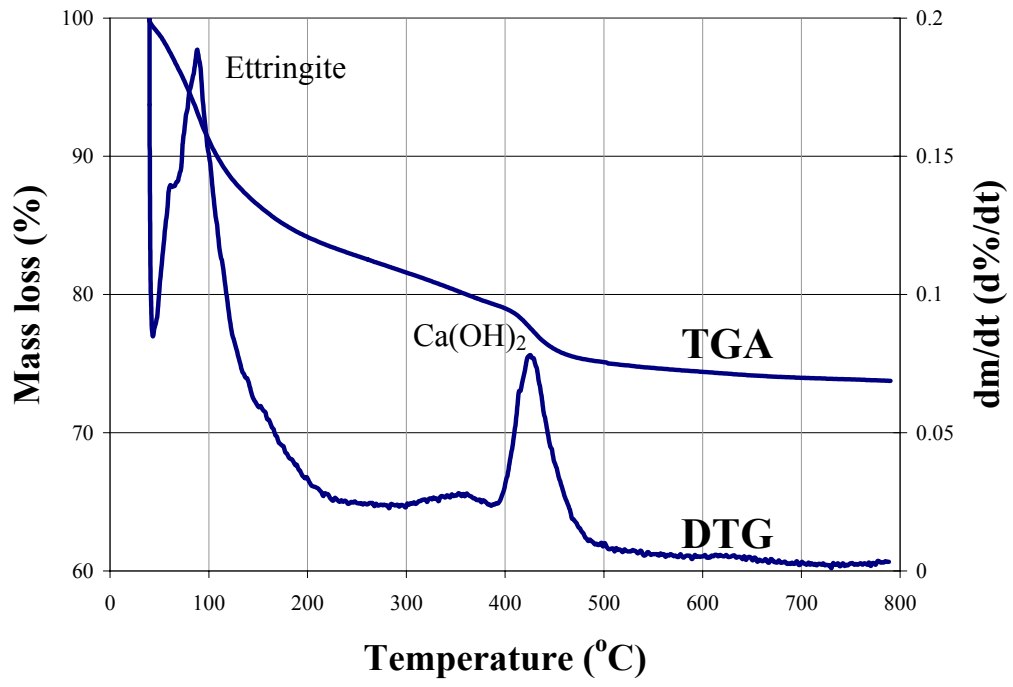
Figure 4.33: TL cement paste Thermogravimetric analysis
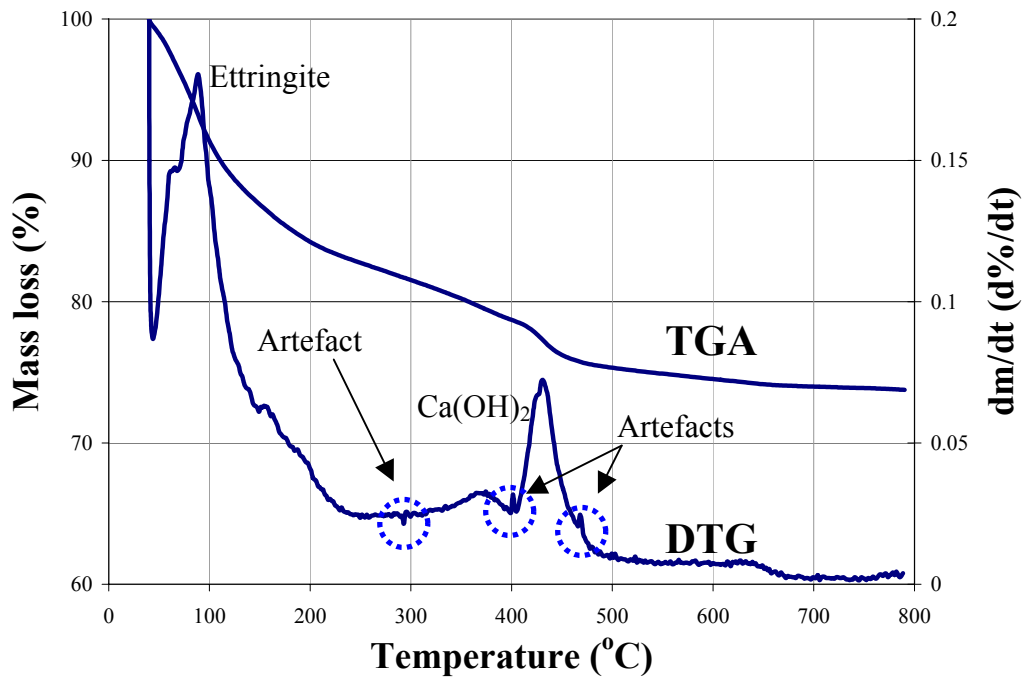
Figure 4.34: WL cement paste thermogravimetric analysis
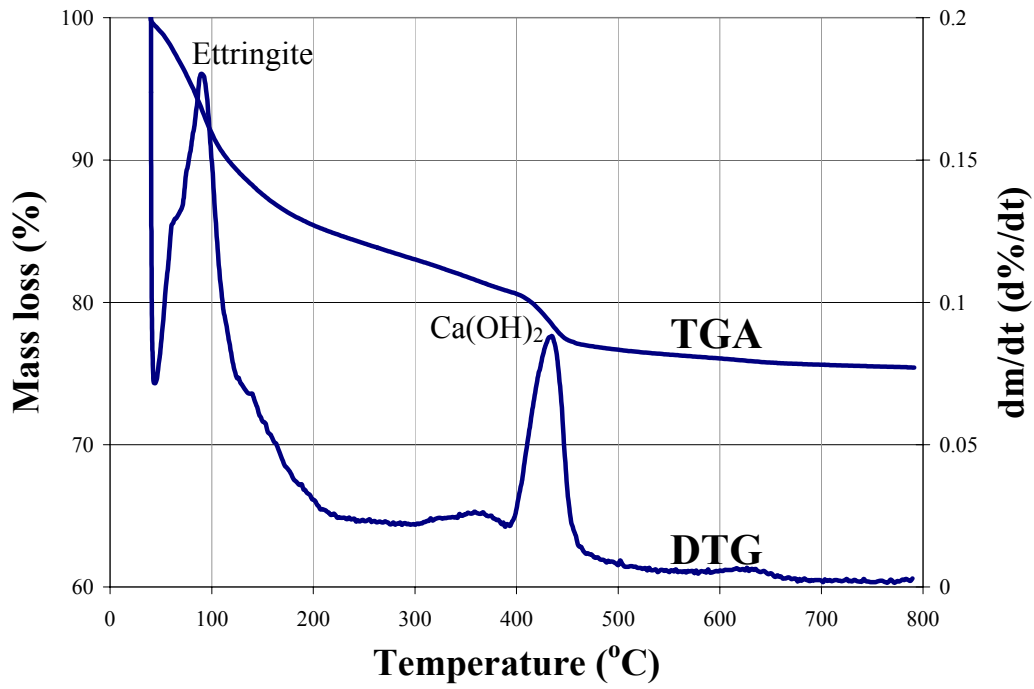
Figure 4.35: TH cement paste thermogravimetric analysis
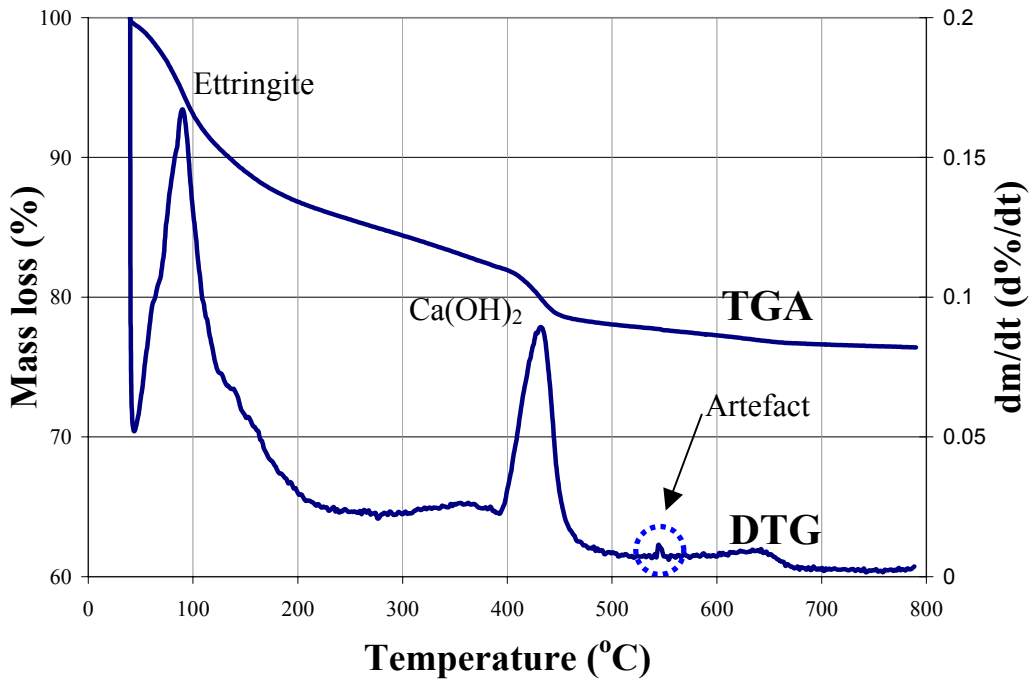
Figure 4.36: WH cement paste thermogravimetric analysis

108

CHAPTER 5
APPLICATION OF FINDINGS

5.1 GENERAL

The main objective of this research program was to evaluate the durability and strengths of concrete using concrete plant wash water and to determine a set of suitable guidelines that could be used to validate the use of wash water in the production of concrete. This chapter presents a recommended procedure for assessing wash water used in durable concrete based on the experiments conducted and the factors that have been found to be critical.

5.2 RECOMMENDED PROCEDURE

Tests indicate that wash water can be used as mixing water for the production of concrete without significant deleterious consequences. This conclusion may not be applicable to all concrete, since the present study only considered two types of concrete. In addition, the wash water used for all tests was obtained from only one source. A recommended approach for assessing the applicability of using wash water is outlined in a set of preliminary procedures, as illustrated by the flow chart in Figure 5.1.

Desire to use wash water in concrete

Step 1 - Yes

Check wash water analysis
within optional limits specified by CSA A23.1-04 cl 4.2.2.4 or ASTM C94

NO →

High concentration
- *Limit use of wash water*

Step 2 - Yes

Check plastic concrete air content
CSA A23.1-04 Table 4 for air content requirements

NO →

Low air content
- *Adjust AEA dosage, or*
- *Limit use of wash water*

Step 3 - Yes

Check set time
within 1 hr. faster or 1.5 hr. slower than the control sample ASTM C94

NO →

Set occurs too quickly or slowly
- *Use set retarder/accelerator, as appropriate, or*
- *Limit use of wash water*

Step 4 - Yes

Check compressive strength
within 90% of the control sample CSA A23.1-04 cl 4.2.2.4 or ASTM C94

NO →

Strength is too low
- *Adjust mixture proportions and use water reducer, if appropriate, or*
- *Limit use of wash water*

Step 5 - Yes

Check hardened air void analysis
- *spacing factor <0.230mm*
- *air content requirement depends on exposure class and aggregate size CSA A23.1-04 cl 4.3.3.2 or ASTM C457*

NO →

Air void system is inadequate
- *Must not be exposed to freezing and thawing conditions, or*
- *Adjust AEA dosage, or*
- *Limit use of wash water*

Step 6 - Yes

Acceptable for use of wash water concrete
- *Exposed to freezing and thawing conditions*
- *Exposed to reactive aggregate (CSA A23.2-27A)*
- *Exposed to chloride environment (CSA A23.1-04 cl 4.1.1.2)*

Figure 5.1: Procedure to assess the use of wash water in concrete

CHAPTER 6

SUMMARY, CONCLUSIONS AND RECOMMENDATIONS

6.1 SUMMARY

Based on the results from the wash water study, the following summaries are made. The analyses of wash water used in the study indicated that the total solids, chloride, and sulphate ions were below the optional limits. The equivalent Na_2O alkali in wash water was greater than the optional limit; however, the equivalent Na_2O is allowed to exceed the limit as long as it can be shown that the alkali contribution from wash water, aggregate, and other sources meet the requirements for protection against alkali-aggregate reactions.

The alkali metals, hydroxyl and sulphate concentrations in pore solution, extracted from wash water cement paste, were found to be similar to the concentrations found in tap water. Therefore, it does not appear that wash water has any significant effect on the hydration chemistry of cement.

The entrained air bubble content in wash water seemed to de-stabilize at a faster rate than in tap water due to the high alkalinity of wash water. This suggests that the effectiveness of using air entraining admixtures in wash water concrete may be compromised.

The cement paste set time test shows that wash water decreased the set time of the paste by as much as 30 minutes; however, it falls within the allowable set time deviation from the control paste.

A comparison of the mortar air content of tap and wash water specimens showed that wash water mortar had 0.5 % less air, but the differences were within the accuracy of the Chace indicator test method. Hence, no difference in air content was detected between the tap water and wash water mortar.

The compressive strength of concrete produced with wash water was comparable to that of tap water. The lower strength mixture using wash water produced a slightly higher compressive strength than that of the equivalent mixture made with tap water, while the higher strength mixture with wash water produced a slightly lower compressive strength than that made with tap water; however, the decrease in compressive strength was within the allowable deviation. The flexural strength of concrete produced with wash water also showed results that were similar to the compressive test, except that the higher strength wash water concrete had a flexural strength that was lower than expected at 28 days. This is thought to be an anomaly, which could not be accounted for. Despite that, compressive and flexural strengths of wash water concrete are within 90 % of those concrete produced with tap water.

The concrete surface resistance to salt scaling test showed that the lower strength concrete without air entraining admixture failed the MTO mass loss evaluation criterion, regardless of the type of water. Meanwhile, the higher strength concretes with air entraining admixture were able to meet this criterion for both types of water. Nevertheless, it is clear that concrete made using tap water has less mass loss than concrete incorporating wash water. This can be attributed to the higher air content in tap water concrete than in wash water concrete, as determined by hardened air void analyses. Based on the differences in air content between wash and tap water concrete, wash water slightly reduces the effectiveness of air entraining admixture in producing entrained air.

Micro-cell corrosion rates of steel bars in tap water concrete were comparable to those in wash water concrete for the lower strength concrete and, after 70 weeks exposure to salt solution, the

steel in both sets of concrete was actively corroding at approximately 10^{-2} A/m^2. Meanwhile, the steel bars in the higher strength wash water concrete showed no sign of active corrosion, with a corrosion rate of 10^{-3} A/m^2, but the same concrete with tap water showed a corrosion rate of 10^{-2} A/m^2 for three out of the five steel bars, indicating active corrosion. Both the macro-cell corrosion rates and half-cell potentials showed good agreement with the micro-cell corrosion rates. Based on the corrosion tests, the wash water does not seem to have a negative effect on corrosion in concrete.

Thermal analyses showed that the major peaks associated with cement hydration were consistent between cement paste prepared using wash water and those prepared using tap water for both types of mixture designs. Other unidentifiable peaks observed at $300^{o}C$, $400^{o}C$, and $460^{o}C$ in the pastes made with wash water were very weak and show an insignificant contribution to the total mass loss. Therefore, using wash water does not have a significant impact on the cement hydration products.

6.2 CONCLUSIONS

On the basis of the results obtained from the comparative study using wash water versus tap water, it appears that wash water can be used as mixing water for the production of concrete without compromising the durability properties related to corrosion and salt scaling performance. In addition, the mechanical and plastic properties of wash water concrete meet all standards pertaining to the use of wash water concrete and are similar to those of tap water concrete. Finally, the pore solution, thermal analyses, and water analyses of wash water and tap water showed comparable results. Overall, with regards to the tests conducted thus far, the use of wash water as mixing water in concrete poses no durability concerns.

6.3 RECOMMENDATIONS FOR FUTURE RESEARCH

There are several other parameters that were not investigated, but should be considered in future studies:

1. Since the water analyses indicated that the alkali content (equivalent Na_2O) was higher than the allowable limit, it is recommended that alkali-silica and alkali-carbonate reaction tests be performed on concrete and mortar prepared with wash water. Recommended tests include a mortar bar expansion test and a concrete prism length change test due to swelling.

2. The effect that wash water may have on the concrete hardened air void system by examining air void systems with varying AEA dosages. Also, it would be useful to determine the relationship between the hardened and plastic air contents, as corrections to the AEA dosage could be based on the plastic air content.

3. The variability in wash water throughout different seasons should be determined, as it is expected that different combinations of chemical admixtures will be used depending on the climate.

4. The effect of wash water should be measured on concrete porosity, as it has been speculated that particulates in wash water act as fine-filler in concrete, thereby influencing ionic movement within concrete.

5. The forms of iron oxide found on the surface of the pickled rebar, responsible for the appearance of darker and lighter grey regions, could be analyzed using Raman Spectroscopy.

6. Variation between batches for concrete should be investigated and in addition examine the characteristics of concrete when diluted wash water is used.

REFERENCES

AASHTO T199, 1999. Air Content of Freshly Mixed Concrete by the Chace Indicator. American Association of State Highway and Transportation Officials, Washington, DC.

Abram, D.A., 1918. Design of Concrete Mixtures. Structural Materials Research Laboratory, Lewis Institute, Chicago, IL.

ACI Committee 116, 2000. Cement and Concrete Terminology. ACI 116R-00, American Concrete Institute, Farmington Hills, MI.

ACI Committee 201, 2001. Guide to Durable Concrete. ACI 201.2R-01 American Concrete Institute, Farmington Hills, MI.

ACI Committee 211, 1997. Standard Practice for Selecting Proportions for Normal Heavyweight, and Mass Concrete. ACI 222.1-91, American Concrete Institute, Farmington Hills, MI.

ACI Committee 212, 2004. Chemical Admixtures for Concrete. ACI 212.3R-04, American Concrete Institute, Farmington Hills, MI.

ACI Committee 221, 1998. State-of-the-Art Report on Alkali-Aggregate Reactivity. ACI 221.1R-98, American Concrete Institute, Farmington Hills, MI.

ACI Committee 225, 1999. Guide to the Selection and Use of Hydraulic Cements. ACI 225R-99, American Concrete Institute, Farmington Hills, MI.

ACI Committee 233, 2003. Slag Cement in Concrete and Mortar. ACI 233R-03, American Concrete Institute, Farmington Hills, MI.

ACI Committee 555, 2001. Removal and Reuse of Hardened Concrete. ACI 555R-01, American Concrete Institute, Farmington Hills, MI.

Alarcon-Ruiz, L., Platret, G., Massieu, E., and Ehrlacher, A., 2005. The use of thermal analysis in assessing the effect of temperature on a cement paste. Cement and Concrete Research, 35(8), pp.609-613.

Andrade, C., and Gonzalez, J.A., 1978. Quantitative measurements of corrosion rate of reinforcing steels embedded in concrete using polarization resistance measurements. Materials and Corrosion, 29(8), pp.515-519.

Andrade, C., Alonso, M.C., and Gonzalez, J.A., 1990. Corrosion Rates of Steel in Concrete. ASTM STP 1065, Philadelphia, PA.

Antao, S.M, Duane, M.J., and Hassan, I., 2002. DTA,TG, and XRD studies of sturmanite and ettringite. The Canadian Mineralogist, Vol. 40, pp.1403-1409.

ASTM C31, 2003. Practice for Making and Curing Concrete Test Specimens in the Field. American Society for Testing and Materials International, West Conshohocken, PA.

ASTM C39, 2003. Standard Test Method for Compressive Strength of Cylindrical Concrete Specimens. American Society for Testing and Materials International, West Conshohocken, PA.

ASTM C78, 2002. Standard Test Method for Flexural Strength of Concrete (Using Simple Beam with Third-Point Loading). American Society for Testing and Materials International, West Conshohocken, PA.

ASTM C94, 2004. Standard Specification for Ready-Mix Concrete. American Society for Testing and Materials International, West Conshohocken, PA, 2004.

ASTM C172, 2004. Standard Practice for Sampling Freshly Mixed Concrete. American Society for Testing and Materials International, West Conshohocken, PA.

ASTM C191, 1992. Standard Test Method for Time of Setting of Hydraulic Cement. American Society for Testing and Materials International, West Conshohocken, PA.

ASTM C293, 2002. Standard Test Method for Flexural Strength of Concrete (Using Simple Beam With Center-Point Loading). American Society for Testing and Materials International, West Conshohocken, PA.

ASTM C457, 1998. Standard Test Method for Microscopical Determination of Parameters of the Air-Void System in Hardened Concrete. American Society for Testing and Materials International, West Conshohocken, PA.

ASTM C496, 2004. Test Method for Splitting Tensile Strength of Cylindrical Concrete Specimen. American Society for Testing and Materials International, West Conshohocken, PA.

ASTM C672, 2003. Concrete Resistance to Surface Scaling due to De-icing Salt. American Society for Testing and Materials International, West Conshohocken, PA.

ASTM C856, 2004. Standard Practice for Spectrographic Examination of Hardened Concrete. American Society for Testing and Materials International, West Conshohocken, PA.

ASTM C876, 1999. Standard Test Method for Half Cell Potentials of Reinforcing Steel in Concrete. American Society for Testing and Materials, West Conshohocken, PA.

ASTM C989, 2006. Standard Specification for Ground Granulated Blast-Furnace Slag for Use in Concrete and Mortars. American Society for Testing and Materials International, West Conshohocken, PA.

ASTM C1202, 2005. Standard Test Method for Electrical Indication of Concrete's Ability to Resist Chloride Ion Penetration. American Society for Testing and Materials International, West Conshohocken, PA.

ASTM G1, 2003. Standard Practice for Preparing, Cleaning, and Evaluating Corrosion Test Specimens. American Society for Testing and Materials International, West Conshohocken, PA.

ASTM G109, 1999. Standard Test Method for Determining the Effects of Chemical Admixtures on the Corrosion of Embedded Steel Reinforcement in Concrete Exposed to Chloride Environments. American Society for Testing and Materials International, West Conshohocken, PA.

Bogue, R.H., 1955. Chemical of Portland Cement, 2nd Edition. Reinhold Publishing, New York, NY.

Bogue, R.H., and Lerch, W., 1934. Hydration of portland cement compounds. Industrial and Engineering Chemistry, 26(8), pp.837-847.

Borger, J, Carrasquillo, R.L., and Fowler, D.W., 1994. Use of Recycled Wash Water and Returned Plastic Concrete in the Production of Fresh Concrete. Advanced Cement Based Materials, 1, pp.267-274.

Brown, P.W., 2006. Hydration. Civ.1299s – Cement Chemistry Course, University of Toronto. Toronto, ON.

Chini, A.R., Muszynski, L.C., Bergin, M., and Ellis, B.S., 2001. Reuse of wastewater generated at concrete plants in Florida in the production of fresh concrete. Magazine of Concrete Research, 55(5), pp.311-319.

Concrete Manual, 8th Edition, 1981. U.S. Bureau of Reclamation.

CSA A23.1/A23.2, 2001. Concrete Materials and Methods of Concrete Construction /Methods of test and Standard Practices for Concrete. Canadian Standard Association, Mississauga, ON.

CSA A23.2-27A, 2004. Standard Practice to Identify Degree of Alkali-Reactivity of Aggregates and to Identify Measures to Avoid Deleterious Expansion in Concrete. Canadian Standard Association, Mississauga, ON.

CSA A23.3-04, 2004. Concrete Design Handbook. Canadian Standard Association, Ottawa, ON.

CSA A3001, 2003. Cementitious Materials for Use in Concrete. Canadian Standard Association, Mississauga, ON.

Diamond, S., 2000. Mercury porosimetry: An inappropriate method for the measurement of pore size distributions in cement-based materials. Cement and Concrete Research, Vol. 30, pp.1517-1525.

Feldman, R.F., and Sereda, P.J., 1968. A model for hydrated portland cement paste as deduced from sorption length change and mechanical Properties. Materiaux et Constructions, 1(6), pp.509-520.

Fontana, M.G., 1986. Corrosion Engineering, 3rd Edition. McGraw-Hill Inc., New York, NY.

FHWA, 1999. Corrosion Costs and Preventive Strategies in the United States. Federal Highway Administration, McLean, VA.

FHWA, 2006. Protocol to Identify Incompatible Combinations of Concrete Materials. Federal Highway Administration, Publication No. FHWA-HRT-06-082, McLean, VA.

Fulton, F.S., 1974. The Properties of Portland Cement Containing Milled Granulated Blast-Furnace Slag. Monograph, Portland Cement Institute, Johannesburg, pp. 4-46.

Gebler, S.H., and Klieger, P., 1986. Effect of Fly Ash on the Durability of Air-Entrained Concrete. Research and Development Bulletin RD090, Portland Cement Association, http://www.portcement.org/pdf_files/RD090.pdf.

Glasser, L.S.D, Lachowski, E.E., Mohan, K., and Taylor, H.F.W., 1978. A Multi-Method Study of C_3S hydration. Cement Concrete Research, 8(6).

Gleick, P.H., 1996. Water resources. Encyclopaedia of Climate and Weather, Oxford University Press, New York, 2, pp.817-823.

Gonnerman, H.F., and Shuman, E.C., 1928. Compression, Flexure and Tension Tests of Plain Concrete. American Society for Testing and Materials, ASTM Proceedings, 28, Part 2, pp.527-564.

Gonzalez, J.A., Andrade, C., Alonso, C., and Feliu, S., 1995. Comparison of rates of general corrosion and maximum pitting penetration on concrete embedded steel reinforcement. Cement and Concrete Research, 25(2), pp.257-264.

Hansson, C.M., 1995. Concrete: The Advanced Industrial Material of the 21st Century. Metallurgical and Materials Transactions A, 26A, pp.1321-1341.

Hansson, C.M., 2000. Discussion of "Corrosion Effects on Bond Strength in Reinforced Concrete" by K. Stanish, R.D. Hooton and V. Pantazopoulou. ACI Structural Journal, Vol. 97.

Hansson, C.M., Poursaee, A., and Laurent, A., 2006. Macrocell and Microcell Corrosion of Steel in Ordinary Portland Cement and High Performance Concretes. Cement and Concrete Research, 36(11), pp.2098-2102.

Helmuth, R.A., 1960. Capillary size restrictions on ice formation in hardened portland cement pastes, 4th International Symposium Proceedings on the Chemistry of Cement. Washington DC, pp.855-869.

Hogan, F.J., and Meusel, J.W., 1981. Evaluation for Durability and Strength Development of a Ground Granulated Blast-Furnace Slag. Cement, Concrete, and Aggregates, 3(1), pp. 40-52.

Jones, D.A., 1996. Principles and Prevention of Corrosion, 2nd Edition. Prentice Hall Inc., Upper Saddle River, NJ.

Klieger, P., 1952. Studies of the Effect of Entrained Air on the Strength and Durability of Concretes Made with Various Maximum Sizes of Aggregate. Proceedings of the Highway Research Board, Chicago, IL, 31.

Larbi, J.A, Fraay, A.L.A, and Bijen, J.M., 1990. The chemistry of the pore fluid of silica fume-blended cement systems. Cement and Concrete Research, 20(4), pp.506-516.

Lea, F.M., 1971. Cement Research: Retrospect and Prospect. Proceeding 4th International Symposium on the Chemistry of Cement, Washington D.C., pp.5-8.

Lea, F.M., 1971. The Chemistry of Cement and Concrete. Chemical Publishing Company Inc., New York, NY.

Locher, F., Richartz, W., and Sprung, S., 1976. Set of cement-Part 1 Reaction and development of structure. Zement-Kalk-Gips.

Kosmatka, S.H., Kerkhoff, B., Panarese, W.C., MacLeod, N.F., and McGrath, R.J., 2002. Design and Control of Concrete Mixtures, 7th Canadian Edition. Cement Association of Canada, Ottawa, ON.

Regional Municipality of Waterloo, 2005. Water Quality Data Report for the Region's Municipal Water Supply System. Waterloo, ON.

Malhotra, V.M., 2005. Global Warming, and Role of Supplementary Cementing Materials and Superplasticizers in Reducing Greenhouse Gas Emissions from the Manufacturing of Portland Cement, CANMET/ACI/JCI Proceedings. International Symposium on Sustainable Development of Cement, Concrete and Concrete Structures, Toronto, ON.

Mammoliti, L., 2007. Wash water concrete. Personal communication, Quality Assurance, Dufferin Concrete, Kitchener, ON.

Mehta, P.K., 2002. Greening of the Concrete Industry for Sustainable Development. Concrete International, 24(7), pp. 23-37.

Mehta, P.K., and Mammohan, D., 2005. Use of Superplasticizers in High-Volume Fly Ash Concrete – U.S. Case Histories, CANMET/ACI/JCI Proceedings. International Symposium on Sustainable Development of Cement, Concrete and Concrete Structures, Toronto, ON.

Mehta, P.K., and Monteiro, P.J., 1993. Concrete: Structure, Properties, and Materials, 2nd Edition. Prentice Hall. Englewood Cliff, NJ.

Meininger, R.C., 1973. Recycling Mixer Wash Water – Its Effect on Ready Mixed Concrete. National Ready Mixed Concrete Association, Silver Spring, MD. Technical Information Letter, No. 298.

Melzer, R., and Eberhard, E., 1989. Phase Identification During Early and Middle Hydration of Tricalciumsilicate (Ca_3SiO_5). Cement and Concrete Research, Vol. 19, pp.411-422.

Meusel, J.W., and Rose, J.H., 1983. Production of Granulated Blast Furnace Slag at Sparrows Point, and the Workability and Strength Potential of Concrete Incorporating the Slag. Fly Ash, Silica Fume, Slag and Other Mineral By-Productions in Concrete, SP-79. American Concrete Institute, Farmington Hills, MI, 1, pp. 867-890.

Miller, F.M., and Tang, F.J., 1996. The distribution of sulfur in present-day clinkers of variable sulfur content". Cement and Concrete Research, 26(12), pp.1821-1829.

Mindess, S., and Young, J.F., "Concrete". Prentice-Hall Inc., Englewood Cliffs, NJ, 1981.

Mindess, S., Young, J.F., and Darwin, D., 2003. Concrete, 2nd Edition. Prentice-Hall Inc., Upper Saddle River, NJ.

MTO LS412, 2006. Methods of Test for Scaling Resistance of Concrete Surfaces Exposed to De-icing Chemicals, Rev. No.23. Ministry of Transportation Laboratory Testing Manual, ON.

Neville, A.M., 1981. Properties of Concrete, 3rd Edition. John Wiley & Sons, New York, NY.

NRMCA Information, 2005. Standard for Mixing Water in Concrete. National Ready Mixed Concrete Association, Silver Spring, MD.

Paolini, M., Khurana, R., 1998. Admixtures for Recycling of Waste Concrete. Cement and Concrete Composites, Vol. 20, pp.221-229.

Ramachandran, V.S., 1979. Differential thermal method of estimating calcium hydroxide in calcium silicate and cement pastes. Cement and Concrete Research, 9, pp.677-684.

Ramachandran, V.S., 1982. Investigation of the role of chemical admixtures in cements − A differential thermal approach. Proceedings of the Seventh International Conference on Thermal Analysis, Vol. 2, pp.1296-1302.

Region of Peel, 2001. Canadian and Water Consumption. Region of Peel: Water Smart. http://www.peelregion.ca/watersmartpeel/involve/involved2.htm, Access 2007.

Perruchot, C., Chehimi, M.M., Vaulay, M.J., and Benzarti, K., 2006. Characterisation of the surface thermodynamic properties of cement components by inverse gas chromatography at infinite dilution. Cement and Concrete Research, Vol. 36, pp.305-319.

Pigeon, M., and Pleau, R., 1995. Durability of Concrete in Cold Climates. E & FN SPON, London.

Pigeon, M., Marchand, J., and Pleau, R., 1996. Frost resistant concrete. Construction and Building Materials, 10(5), pp. 339-348.

Pinto, R.C, and Hover, H.C., 2001. Frost and Scaling Resistance of High-Strength Concrete. Research and Development Bulletin RD122, Portland Cement Association.

Pourbaix, M., 1974. Atlas of electrochemical equilibria in aqueous solutions, 2nd Edition. National Association of Corrosion Engineers, Houston, TX.

Powers, T.C., 1945. Working Hypothesis for Further Studies of Frost Resistance of Concrete. ACI Journal, Proceedings 41(4), pp.245-272.

Powers, T.C., 1949. The air requirement of frost-resistant concrete. Proceedings of the Highway Research Board, 29.

Powers, T.C., 1954. Void spacing as a basis for producing air-entraining concrete. Journal of American Concrete Institute, Vol. 50, pp.741-760.

Powers, T.C., 1956. Resistance to weathering – freezing and thawing. American American Society for Testing and Materials Special Report Technical Publication No. 169, pp. 182-187.

Powers, T.C., 1958. The physical structure and engineering properties of concrete. Portland Cement Association, Bulletin 90.

Powers, T.C., and Brownyard, T.L., 1946. Studies of the physical properties of hardened portland cement paste". Journal of American Concrete Institute, Vol. 43, Nine Parts.

Pressler, E.E., Brunauer, S., Kantro, D.L., and Weise, C.H., 1961. Determination of the Free Calcium Hydroxide Contents of Hydrated Portland Cements and Calcium Silicates. Analytical Chemistry, 33(7), pp.877-889.

Rickert, J., and Grube, H., 2006a. Analysis of recycled water components. http://www.vdz-online.de/fileadmin/gruppen/vdz/3LiteraturRecherche/Betontechnische_Berichte/049-060_Restwasserinhalt.pdf, Access 2006.

Rickert, J., and Grube, H., 2006b. Influence of recycled water from fresh concrete recycling systems on the properties of fresh and hardened concrete. http://www.vdz-online.de/fileadmin/gruppen/vdz/3LiteraturRecherche/Betontechnische_Berichte/059-070_Einfluss_Restwasser.pdf, Access 2006.

Sakai, K., 2005. What Can Concrete Industry do for Sustainable development?. CANMET/ACI/JCI Proceedings, International Symposium on Sustainable Development of Cement, Concrete and Concrete Structures, Toronto, ON.

Sandrolini, F., Franzoni, E., 2001. Waste Wash Water recycling in Ready-Mixed Concrete Plants. Cement and Concrete Research, Vol. 31 pp.485-489.

Selih, J., Milost, E., and Cuznar, A., 2002. Use of recycled rubble-based aggregate and recycled water in concrete. Recycled Aggregate in Concrete, Tomas Telford Ltd., London.

Skalny, J., and Odler, I., 1967. The effect of chlorides upon the hydration of Portland cement and upon some clinker minerals. Magazine of Concrete Research, 19(61), pp.203-210.

Skoog, D.A., Holler, F.J., and Nieman, T.A., 1998. Principles of Instrumental Analysis, 5th Edition. Harcourt Brace College Publishers, Philadelphia, PA.

Soroka, I., 1979. Portland Cement Paste and Concrete. MacMillan Press Limited., Surrey, England.

Stern, M., and Geary, A.L., 1957. Journal of Electrochemistry Society, Vol. 104, pp. 56-63.

Su, N., Miao, B., Liu, F.S., 2002. Effect of wash water and underground water on properties of concrete. Cement and Concrete Research, Vol. 32, pp.777-782.

Taylor, H.F.W., 1990. Cement Chemistry. Academic Press Limited, Harcourt Brace Jovanovich Publishers, London, England.

Taylor, H.F.W., 1999. Distribution of sulfate between phases in Portland cement clinkers. Cement and Concrete Research, 29(8).

Corrosion-club, 2007. Thermodynamic corrosion cycle. http://www.corrosion-club.com/thermocycle.htm, Access 2007.

Ullmann, G.R., 1973. Re-use of Wash Water as Mixing Water. National Ready Mixed Concrete Association, Silver Spring, MD. Technical Information Letter No. 298.

USGS Water Distribution, 2007. Earth water distribution. United States Geological Survey, http://www.ga.water.usgs.gov/edu/earthwherewater.html, Accessed 2007.

USGS, 2006. Explanation of water hardness. United States Geological Survey, http://water.usgs.gov/owq/Explanation.html, Accessed 2006.

Ye, G., Liu, X., De Schutter, G., Poppe, A.M., and Taerwe, L., 2007. Influence of limestone powder used as filler in SCC on hydration and microstructure of cement pastes. Cement and Concrete Composites, Vol. 29, pp.94-102.

Water and Wastewater Report, 2005. Water and Wastewater Report. The Region of Waterloo Transportation & Environmental Services Department, http://www.region.waterloo.on.ca, Accessed 2005.

Winslow, D.N., and Diamond, S., 1970. A mercury porosimetry study of the evolution of porosity in portland cement. Journal of American Society for Testing and Materials (ASTM), Vol. 5.

Wood, K., 1981. Twenty Years of Experience with Slag Cement. Symposium on Slag Cement, University of Alabama, Birmingham.

Wu, X., and Roy, D.M., 1982. Zeta Potential Investigation During Hydration of Slag Cement. Proceedings from M.R.S. Symposium, Boston, MA.

Appendix A:

Wash Water Analyses

	pH	Alkalinity (OH)	Alkalinity (HCO₃)	Alkalinity Total	Turb	F	Cl
		(as mg/L CaCO$_3$)	(as mg/L CaCO$_3$)	(as mg/L CaCO$_3$)	(NTU)	mg/L	mg/L
WH1	12.39	1481.48	370.37	1851.85	782	0.15	167.12
WH2	12.44	1844.66			>1000	0.15	166.72
WL1	12.51	2014.93	74.63	2089.55	>1000	0.36	187.51
WL2	12.20	859.38			>1000	0.26	189.71

(mg/L)	Ca	Cd	Co	Cr	Cu	Fe	Se	SiO2
WH1	764.7	<.0245	<.0450	0.4595	0.0509	0.0627	<1.000	1.451
WH2	871.6	<.0245	<.0450	0.4394	0.0218	0.0268	<1.000	1.012
WL1	1017	<.0245	<.0450	0.3996	0.0199	0.0201	<1.000	0.6883
WL2	499	<.0245	<.0450	0.3840	0.0405	<.0150	<1.000	3.469

(mg/L)	Ni	P	Pb	S	V	NO₃	SO₄	Zn
WH1	<.0700	<.8000	<.3400	485.6	<.0165	21.77	1257.14	0.0989
WH2	<.0700	<.8000	<.3400	498.0	<.0165	21.47	1300.40	<.0445
WL1	<.0700	<.8000	<.3400	497.8	<.0165	36.04	1271.49	<.0445
WL2	<.0700	0.8079	<.3400	484.0	<.0165	40.42	1273.73	<.0445

(mg/L)	Al	As	B	Ba	Mn	Mo	Na	Tl
WH1	<.1850	<.4200	<.0180	0.1433	0.0039	<.1000	165.6	<.3700
WH2	<.1850	<.4200	<.0180	0.241	<.0030	0.1504	163	<.3700
WL1	<.1850	<.4200	<.0180	0.1437	<.0030	0.1921	185.7	<.3700
WL2	<.1850	<.4200	<.0180	0.1832	<.0030	0.1732	182.8	<.3700

(mg/L)	K	Li	Mg	Sn	Sr	Ti
WH1	808.6	0.2009	<.1950	<.2750	11.09	<.0075
WH2	793.1	0.1855	<.1950	<.2750	11.1	<.0075
WL1	837.7	0.3415	<.1950	<.2750	14.98	<.0075
WL2	803.1	0.2565	<.1950	<.2750	11.5	<.0075

Ion Charge Balance Calculations

			WH1	WH2	WL1	WL2
Measured alkali metals	Ca	mg/L	765	872	1017	499
	K	mg/L	809	793	838	803
	Na	mg/L	166	163	186	183
Measured alkali metals	Ca	mmol/L	19.08	21.75	25.37	12.45
	K	mmol/L	21	20	21	21
	Na	mmol/L	7	7	8	8
Calculated OH^- ions	Ca	mmol/L	38.16	43.50	50.74	24.89
	K	mmol/L	21	20	21	21
	Na	mmol/L	7	7	8	8
Total OH^- ions	OH^-	mmol/L	66	71	80	53
Anions subtract from	Cl^-	mmol/L	0.14	0.14	0.14	0.14
OH^-	SO_4^{2-}	mmol/L	26.17	27.06	26.46	26.52
Net OH^- ions	OH^-	mmol/L	39.77	43.67	53.66	26.73
	p(OH)		1.40	1.36	1.27	1.57
	pH		12.60	12.64	12.73	12.43

Notes:
1. pH measurements were made using Orion's low-maintenance Triode ph electrode with several millilitres of unfiltered water.(Electrometric Method 4500-H-B;APHA, 1992)
2. Alkalinity was measured on filtered water samples using standardized H2SO4 and a Hatch digital titration (Titration Method 2320B; American Public Health association (APHA), 1992).
3. Alkalinity-OH was determined by titration with 1.6 N H_2SO_4 to the phenolphthalein end point.
4. Total alkalinity was determined by titration with 1.6 H_2SO_4 to the bromocresol green-methyl red endpoint.
5. Turbidity was measured on 2100 Hach Turbidimeter using 20, 100 and 800 NTU standards. Due to limited sample volume, no dilution was feasible.
6. Analysis for metals and cations has been performed on filtered water using Inductively Coupled Plasma- Optical Emission Spectrometry (ICP-OES) (EPA Method 200.7).
7. Analysis for anions has been performed on filtered water using Ion Chromatography (IC) Dionex 600 (EPA Method 300.0). Samples were diluted 1:10 and 1:50.
8. Water samples for the analysis of alkalinity, anions and cations were filtered with cellulose acetate 0.45 um filters attached to the syringes.

Appendix B:

Pore solution Analyses

SGS *Lakefield Research*

Report No.	**CA10258-FEB07**			
Customer	**University of Waterloo**			
Attention	**Khanh Tran**			
Title	**Final Report**			

				TL	WL	TH	WH
Chloride	mg/L	21-Feb-07		<5	<5	<5	<5
Sulphate	mg/L	21-Feb-07		100	140	1200	1300
Ag	mg/L	21-Feb-07		0.05	< 0.05	< 0.05	< 0.05
Al	mg/L	21-Feb-07		1.90	1.85	3.58	5.13
As	mg/L	21-Feb-07		0.10	< 0.08	< 0.08	< 0.08
Ba	mg/L	21-Feb-07		1.27	1.40	0.476	0.429
Be	mg/L	21-Feb-07		< 0.001	< 0.001	< 0.001	< 0.001
B	mg/L	21-Feb-07		0.025	0.060	0.789	0.736
Bi	mg/L	21-Feb-07		< 0.3	< 0.3	< 0.3	< 0.3
Ca	mg/L	21-Feb-07		85.1	79.9	50.8	47.6
Cd	mg/L	21-Feb-07		< 0.02	< 0.02	< 0.02	< 0.02
Co	mg/L	21-Feb-07		0.078	0.182	0.200	0.208
Cr	mg/L	21-Feb-07		0.066	0.826	5.35	5.41
Cu	mg/L	21-Feb-07		1.32	2.55	1.59	7.43
Fe	mg/L	21-Feb-07		0.30	0.15	0.27	0.48
K	mg/L	21-Feb-07		4870	5540	8840	9580
Li	mg/L	21-Feb-07		7.54	7.48	3.98	4.19
Mg	mg/L	21-Feb-07		< 0.03	< 0.03	< 0.03	< 0.03
Mn	mg/L	21-Feb-07		< 0.01	< 0.01	< 0.01	0.02
Mo	mg/L	21-Feb-07		0.468	0.455	2.73	2.56
Na	mg/L	21-Feb-07		2610	2860	6820	7160

			TL	WL	TH	WH
Ni	mg/L	21-Feb-07	< 0.1	< 0.1	0.3	0.3
P	mg/L	21-Feb-07	0.62	0.50	5.11	12.1
Pb	mg/L	21-Feb-07	0.126	0.208	0.187	0.787
Sb	mg/L	21-Feb-07	< 0.1	< 0.1	< 0.1	< 0.1
Se	mg/L	21-Feb-07	< 0.2	< 0.2	0.2	0.3
Si	mg/L	21-Feb-07	2.08	2.32	11.1	11.3
Sn	mg/L	21-Feb-07	< 0.3	< 0.3	< 0.3	< 0.3
Sr	mg/L	21-Feb-07	3.62	3.78	2.21	2.26
Ti	mg/L	21-Feb-07	< 0.01	< 0.01	< 0.01	< 0.01
Tl	mg/L	21-Feb-07	< 0.1	< 0.1	< 0.1	< 0.1
V	mg/L	21-Feb-07	< 0.01	< 0.01	< 0.01	< 0.01
W	mg/L	21-Feb-07	< 0.1	0.2	< 0.1	< 0.1
Y	mg/L	21-Feb-07	< 0.004	< 0.004	< 0.004	< 0.004
Zn	mg/L	21-Feb-07	15.6	17.1	33.3	52.4

Ion Charge Balance Calculations

			TL	WL	TH	WH
Measured alkali metals	Ca	mg/L	85	80	51	48
	K	mg/L	4870	5540	8840	9580
	Na	mg/L	2610	2860	6820	7160
Measured alkali metals	Ca	mmol/L	2.12	1.99	1.27	1.19
	K	mmol/L	125	142	226	245
	Na	mmol/L	114	124	297	311
Calculated OH^- ions	Ca	mmol/L	4.25	3.99	2.53	2.37
	K	mmol/L	125	142	226	245
	Na	mmol/L	114	124	297	311
Total OH^- ions	OH^-	mmol/L	242	270	525	559
Anions subtract from OH^-	Cl^-	mmol/L	0.14	0.14	0.14	0.14
	SO_4^{2-}	mmol/L	2.08	2.91	24.98	27.06
Net OH^- ions	OH^-	mmol/L	240.10	267.02	500.15	531.62
	p(OH)		0.62	0.57	0.30	0.27
	pH		13.38	13.43	13.70	13.73

Appendix C:

Concrete compressive and four-point bending tests

Compressive Test Results

TL at 3D		
Specimen	Load (kN)	Stress (MPa)
TL1-3D	125	15.9
TL2-3D	123	15.7
TL3-3D	135	17.2
TL4-3D	130	16.6
TL5-3D	142	18.1
AVG	131	16.7

WL at 3D		
Specimen	Load (kN)	Stress (MPa)
WL1-3D	135	17.2
WL2-3D	138	17.6
WL3-3D	143	18.2
WL4-3D	135	17.2
WL5-3D	141	18.0
AVG	138	17.6

TL at 7D		
Specimen	Load (kN)	Stress (MPa)
TL6-7D	159	20.2
TL7-7D	175	22.3
TL8-7D	163	20.8
TL9-7D	173	22.0
TL10-7D	170	21.6
AVG	168	21.4

WL at 7D		
Specimen	Load (kN)	Stress (MPa)
WL6-7D	177	22.5
WL7-7D	178	22.7
WL8-7D	187	23.8
WL9-7D	178	22.7
WL10-7D	195	24.8
AVG	183	23.3

TL at 28D		
Specimen	Load (kN)	Stress (MPa)
TL11-28D	240	30.6
TL12-28D	218	27.8
TL13-28D	226	28.8
TL14-28D	232	29.5
TL15-28D	230	29.3
AVG	229	29.2

WL at 28D		
Specimen	Load (kN)	Stress (MPa)
WL11-28D	261	33.2
WL12-28D	240	30.6
WL13-28D	250	31.8
WL14-28D	237	30.2
WL15-28D	248	31.6
AVG	247	31.5

TL at 56D		
Specimen	Load (kN)	Stress (MPa)
TL16-56D	253	32.2
TL17-56D	248	31.6
TL18-56D	240	30.6
TL19-56D	244	31.1
TL20-56D	245	31.2
AVG	246	31.3

WL at 56D		
Specimen	Load (kN)	Stress (MPa)
WL16-56D	272	34.6
WL17-56D	270	34.4
WL18-56D	269	34.3
WL19-56D	265	33.7
WL20-56D	267	34.0
AVG	269	34.2

*Values excluded from the average, as the cylinder was observed to have improper end caps.

TH at 3D		
Specimen	Load (kN)	Stress (MPa)
TH1-3D	171	21.8
TH2-3D	154	19.6
TH3-3D	195	24.8
TH4-3D	*90	-
TH5-3D	183	23.3
AVG	176	22.4

WH at 3D		
Specimen	Load (kN)	Stress (MPa)
WH1-3D	143	18.2
WH2-3D	154	19.6
WH3-3D	152	19.4
WH4-3D	138	17.6
WH5-3D	145	18.5
AVG	146	18.6

TH at 7D		
Specimen	Load (kN)	Stress (MPa)
TH6-7D	235	29.9
TH7-7D	235	29.9
TH8-7D	228	29.0
TH9-7D	245	31.2
TH10-7D	240	30.6
AVG	237	30.1

WH at 7D		
Specimen	Load (kN)	Stress (MPa)
WH6-7D	*174	-
WH7-7D	203	25.8
WH8-7D	203	25.8
WH9-7D	205	26.1
WH10-7D	205	26.1
AVG	204	26.0

TH at 28D		
Specimen	Load (kN)	Stress (MPa)
TH11-28D	278	35.4
TH12-28D	271	34.5
TH13-28D	288	36.7
TH14-28D	308	39.2
TH15-28D	290	36.9
AVG	287	36.5

WH at 28D		
Specimen	Load (kN)	Stress (MPa)
WH11-28D	267	34.0
WH12-28D	275	35.0
WH13-28D	287	36.5
WH14-28D	264	33.6
WH15-28D	292	37.2
AVG	277	35.3

TH at 56D		
Specimen	Load (kN)	Stress (MPa)
TH16-56D	310	39.5
TH17-56D	316	40.2
TH18-56D	298	37.9
TH19-56D	343	43.7
TH20-56D	324	41.3
AVG	318	40.5

WH at 56D		
Specimen	Load (kN)	Stress (MPa)
WH16-56D	285	36.3
WH17-56D	278	35.4
WH18-56D	295	37.6
WH19-56D	292	37.2
WH20-56D	303	38.6
AVG	291	37.0

Four-point Bending Test Results

TL at 7D				
Specimen	b (mm)	d (mm)	Load (kN)	R (MPa)
TL1-7D	150	155	20.1	2.5
TL2-7D	150	155	17.5	2.2
TL3-7D	150	154	20.8	2.6
Avg.	-	-	19.5	2.4

WL at 7D				
Specimen	b (mm)	d (mm)	Load (kN)	R (MPa)
WL1-7D	150	151	24.7	3.2
WL2-7D	150	155	24.1	3.0
WL3-7D	150	150	23.4	3.1
Avg.	-	-	24.1	3.1

TL at 28D				
Specimen	b (mm)	d (mm)	Load (kN)	R (MPa)
TL4-28D	150	150	24.3	3.2
TL5-28D	149	153	24.8	3.2
TL6-28D	150	150	28.9	3.9
Avg.	-	-	26.0	3.4

WL at 28D				
Specimen	b (mm)	d (mm)	Load (kN)	R (MPa)
WL4-28D	153	155	25.6	3.1
WL5-28D	152	155	30.5	3.8
WL6-28D	151	156	32.9	4.0
Avg.	-	-	29.7	3.6

TL at 56D				
Specimen	b (mm)	d (mm)	Load (kN)	R (MPa)
TL7-56D	150	157	34.1	4.2
TL8-56D	150	156	34.9	4.3
TL9-56D	150	157	37.9	4.6
Avg.	-	-	35.6	4.4

WL at 56D				
Specimen	b (mm)	d (mm)	Load (kN)	R (MPa)
WL7-56D	150	154	34.9	4.4
WL8-56D	151	154	34.9	4.4
WL9-56D	150	150	**27	-
Avg.	-	-	34.9	4.4

**Values were excluded from the average, as the flexural strengths were more than 10% deviation from the mean and were treated as a statistical outlier.

TH at 7D				
Specimen	b (mm)	d (mm)	Load (kN)	R (MPa)
TH1-7D	150	151	33.6	4.4
TH2-7D	151	152	**25.9	-
TH3-7D	151	155	30.4	3.8
Avg.	-	-	32.0	4.1

WH at 7D				
Specimen	b (mm)	d (mm)	Load (kN)	R (MPa)
WH1-7D	150	155	31.8	4.0
WH2-7D	150	155	33.4	4.2
WH3-7D	150	150	**26.6	-
Avg.	-	-	32.6	4.1

TH at 28D				
Specimen	b (mm)	d (mm)	Load (kN)	R (MPa)
TH4-28D	151	153	36.9	4.7
TH5-28D	150	154	*39.3	-
TH6-28D	150	155	33.8	4.2
Avg.	-	-	35.4	4.5

WH at 28D				
Specimen	b (mm)	d (mm)	Load (kN)	R (MPa)
WH4-28D	152	157	26.3	3.2
WH5-28D	150	153	27.5	3.5
WH6-28D	150	150	27.3	3.6
Avg.	-	-	27.0	3.6

TH at 56D				
Specimen	b (mm)	d (mm)	Load (kN)	R (MPa)
TH7-56D	150	154	32.4	4.1
TH8-56D	150	154	37.7	4.8
TH9-56D	150	154	41.7	5.3
Avg.	-	-	37.3	4.7

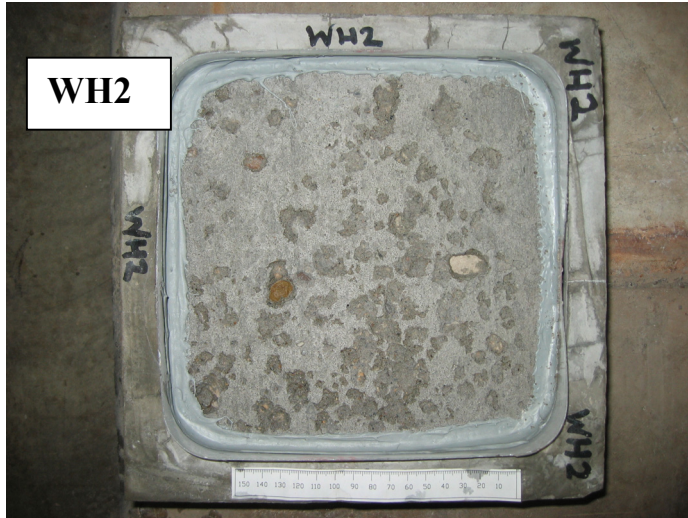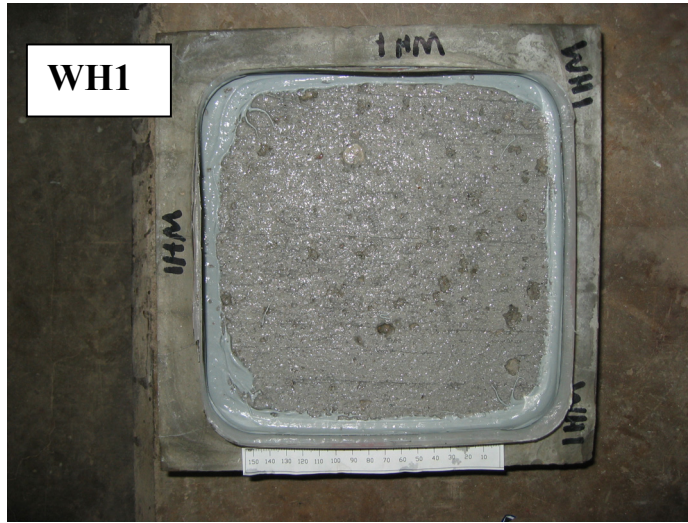| WH at 56D				
Specimen	b (mm)	d (mm)	Load (kN)	R (MPa)
WH7-56D	150	153	30.3	3.9
WH8-56D	150	157	31.8	3.9
WH9-56D	150	153	34.1	4.4
Avg.	-	-	32.1	4.0

136

Appendix D:

Concrete surface condition after

salt scaling test
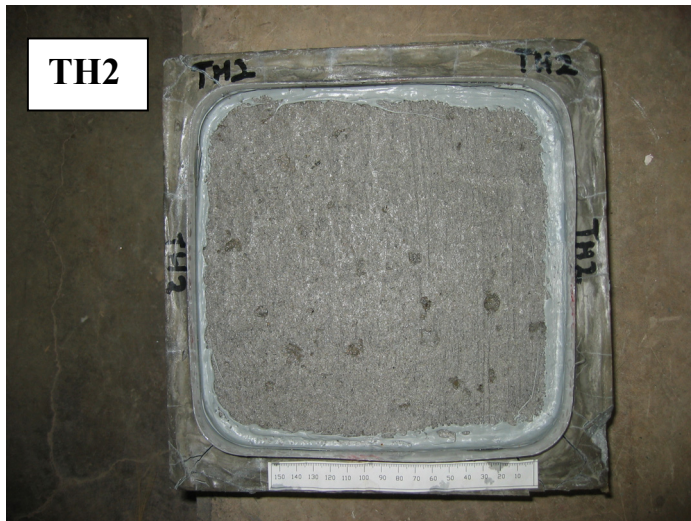
Appendix E:

Adjusted micro-cell corrosion rates

Adjusted micro-cell corrosion rates are calculated by using the last measured corrosion current and divide by the corroded area determined from visual examination of the top rebar after breaking open the G109 concrete specimen.

		Micro-cell: TL		
	Icorr (A)	Length (m)	Area (m^2)	Icorr (A/m^2)
1	8.5E-06	0.03	9.4E-04	9.0E-03
*2	1.3E-05	0.03	9.4E-04	1.4E-02
*3	1.9E-05	0.03	9.4E-04	2.0E-02
4	2.0E-05	0.03	9.4E-04	2.1E-02
5	1.2E-05	0.03	9.4E-04	1.3E-02

* Top steel bar that has been removed from the G109 concrete specimen.
Note: The length of the corroded area found on the steel bar of TL2 and TL3 concrete specimens was approximately 30 mm. It is assumed that all the steel bars in this series have the same corroded length.

		Micro-cell: WL		
	Icorr (A)	Length (m)	Area (m^2)	Icorr (A/m^2)
1	7.1E-07	0.03	9.4E-04	7.5E-04
*2	2.6E-05	0.03	9.4E-04	2.8E-02
*3	2.4E-05	0.03	9.4E-04	2.5E-02
4	1.9E-05	0.03	9.4E-04	2.0E-02
5	3.4E-05	0.03	9.4E-04	3.6E-02

* Top steel bar that has been removed from the G109 concrete specimen.
Note: The length of the corroded area found on the steel bar of WL2 and WL3 concrete specimens was approximately 30 mm. It is assumed that all the steel bars in this series have the same corroded length.

Micro-cell: TH			
	Icorr (A)	Length (m)	Area (m^2)	Icorr (A/m^2)
---	---	---	---	---
1	1.2E-06	0.01	3.1E-04	3.8E-03
*2	1.0E-06	0.01	3.1E-04	3.2E-03
*3	1.4E-05	0.02	6.3E-04	2.2E-02
4	1.1E-05	0.02	6.3E-04	1.8E-02
5	2.5E-05	0.02	6.3E-04	4.0E-02

* Top steel bar that has been removed from the G109 concrete specimen.
Note: The length of the corroded area found on the steel bar of TH2 and TH3 concrete specimens were approximately 10 mm and 20 mm, respectively. It is assumed that the steel bar in TH1 has the same corroded area as TH2 and TH4 and TH5 have the same corroded area as TH3.

Micro-cell: WH			
	Icorr (A)	Length (m)	Area (m^2)	Icorr (A/m^2)
---	---	---	---	---
1	1.1E-06	0.01	3.1E-04	3.5E-03
2	1.2E-06	0.01	3.1E-04	3.8E-03
3	1.4E-06	0.01	3.1E-04	4.5E-03
*4	1.6E-06	0.01	3.1E-04	5.1E-03
*5	1.5E-06	0.01	3.1E-04	4.8E-03

* Top steel bar that has been removed from the G109 concrete specimen.
Note: The length of the corroded area found on the steel bar of WH4 and WH5 concrete specimens was approximately 10 mm. It is assumed that all the steel bars in this series have the same corroded length.